Investigation into the failure mechanism of masonry under uniaxial compression based on fracture mechanics and nonlinear finite element modelling

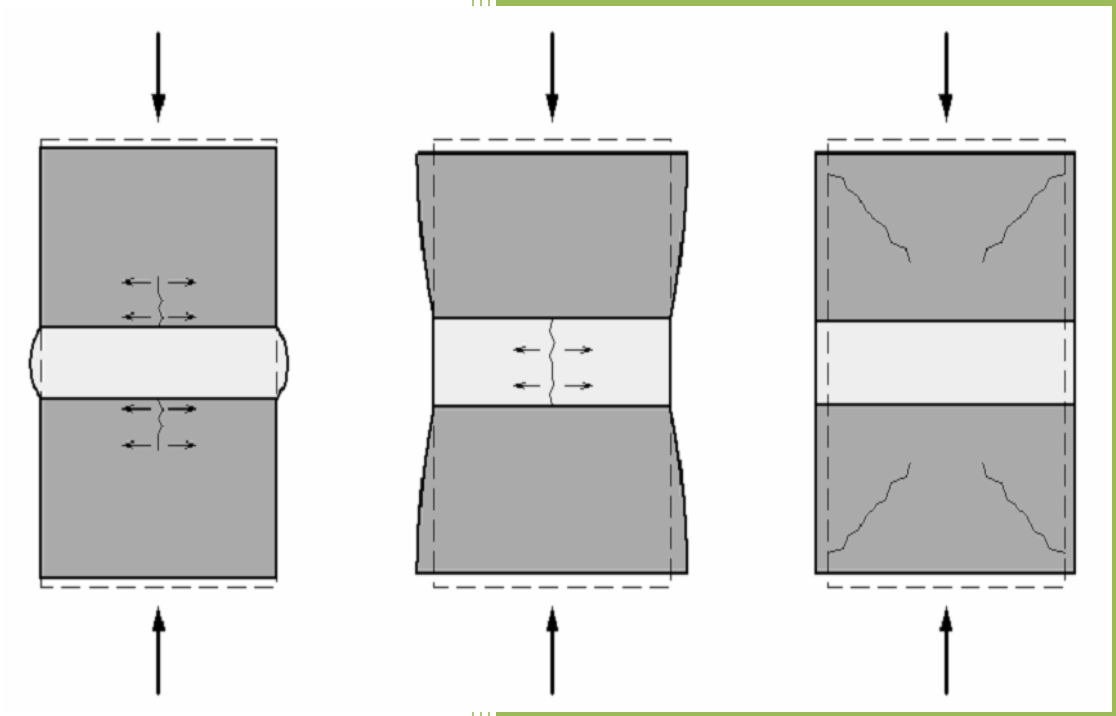

Mathew, Christian

Publication Partner:
International Journal of Scientific and Research Publications (ISSN: 2250-3153)

Investigation into the failure mechanism of masonry under uniaxial compression based on fracture mechanics and nonlinear finite element modelling

Master Thesis

Christian Chukwudi Mathew

Publishing Partner:

IJSRP Inc.

www.ijsrp.org

ISSN 2250-3153

9 772250 315302

Preface

Since the work of Hilsdorf, several theoretical and experimental studies have been carried out to describe the behaviour of masonry under a complex state of stresses and most of these studies described the nonlinearity of masonry through plasticity models, damage models or a combination thereof. In contrast, structural masonry is considered anisotropic and has not received the same attention as its concrete counterpart. Only a few studies have been conducted on the failure mechanism of masonry under a complex state of stresses and these studies have focused on the testing of the components.

The aim of this master thesis is to estimate the compressive strength of short masonry walls (without flexural buckling) based on fracture mechanics, depending on the mechanical and geometrical properties of its components. The triaxial material behaviour of mortar and unit under compression should be considered. The developed models and the applied assumptions should be verified by test results and finite element analysis with ANSYS.

Copyright and Trademarks

Authors

Christian Chukwudi Mathew.

Institute of structural analysis, Faculty of civil engineering, technical university of Dresden, Germany

Dedication

In memory of my sister MATHEW, MELODY CHIBUZOR, and my father MATHEW PIUS, may their souls continue to rest in peace.

Acknowledgements

I would like to thank all those who have contributed to my understanding of masonry, ANSYS software and specifically the completion of this thesis. I owe a debt of gratitude to my supervisor Prof. Dr.-Ing. habil. Michael Kaliske, at the Institute of Structural Analysis, Technical University of Dresden, for his numerous hours of help throughout my graduate thesis studies and to make sure that my master thesis is successfully brought to the end in appropriate manner.

I want to, in a special way, acknowledge all my lecturers who taught me for their guidance, knowledge, understanding throughout my stay in TU Dresden.

I would like to thank my family and my friends for their support, encouragement and understanding. Without them this accomplishment to the work would not have been possible.

Notation

Abbreviations and Symbols

General scheme of notation

Roman and italic letters	**Scalars**
Lower-case bold letters	**Vectors and tensors**
Upper-case bold letters	**Tensors**
Calligraphic upper-case letters	**Vector Spaces**

α bed joint inclination angle < 90;

A_b the area of the unit;

β constant equal to $\frac{E_{br}}{E_{br}}$;

γ density of sandstone brick;

δ normalizing factor taken from DIN 772-1;

δ_{ij} Kronecker delta =1 for i = j = 1, 2, 3 and = 0 for i ≠ j;

η constant equal to $\frac{h_{br}}{h_{mo}}$;

μ_{br} Poisson's ratio of the brick (unit);

μ_{mo} Poisson's ratio of the mortar;

$\bar{\mu}_{mo}$ plastic ratio of Poisson;

ρ the angle of internal friction of mortar;

σ_c compressive stress of material at the time of

σ_{xx} vertical stress in the brick (compression);

$\sigma_{yy,br}$ lateral y stress in the brick (tension);

$\sigma_{zz,br}$ lateral z stress in the brick (tension);

σ_L the lateral tensile stress

ε_{ii} principal strains;

$\varepsilon_{yy\ br}$ lateral y strain in the brick;

$\varepsilon_{zz,br}$ lateral z strain in the brick;

$\varepsilon_{yy,mo}$ lateral y strain in the mortar;

$\varepsilon_{zz,mo}$ lateral z strain in the mortar;

σ_{ii} Principal stresses;

$\sigma_{st,br}$ splitting tensile stress in the brick

A the area of masonry;

α form factor of Mann;

c cohesion of the mortar;

d diameter of transfer area or diameter of brick;

d_{br} the width of unit;

d_{min} smallest brick width d, the sum of spalling parts of the mortar;

E_{br} modulus of elasticity of the unit;

E_{mo} modulus of elasticity of the mortar;

f_b normalized mean compressive strength of a masonry unit;

E_{mo} elasticity modulus of brick

E_{br} elasticity modulus of the unit

E_{Ma} elasticity modulus of the masonry

$\ddot{u}$ transmission factor

$f_{c,br}$ compression strength of the brick;

$f_{c,ma}$ compression strength of masonry;

$f_{c,ma\ all}$ cracking stress of masonry;

$f_{c,mo}$ compression strength of mortar;

$f_{t,br}$ strength of the unit under biaxial tension;

$F_{xx,Ma}$ total force of the masonry

h_v thickness of the vertical joint;

h_{mo} thickness of the bed joint;

h_{br} height of the unit;

b smaller diameter of ellipse;

σ_o stress needed for crack to propagate;

σ_c critical compressive cracking stress strength;

τ_0 the shear stress

Y the stress intensity modification factor

K_1 stress intensity factor in mode 1;

K_{11} stress intensity factors in mode 11;

K_{111} stress intensity factors in mode 111;

K_{1c} critical stress intensity factor or fracture toughness in mode 1;

U_d elastic energy density;

2a crack length;

t thickness;

U_E elastic strain energy per unit thickness;

γ_s specific Surface energy per Area;

γ_p specific Surface energy per Area

U_S crack surface energy

V_E total potential of the external forces;

G strain energy release rate;

G_C the critical value of G;

G_F fracture energy

$v_{f,br}$ volume fractions of the brick

$v_{f,mo}$ volume fractions of the mortar

l_{ch} characteristic length

ABSTRACT

An understanding of mortar behaviour in a multi-axial stress state is important and necessary to determine its influence on the strength, deformation, and failure mode of masonry. When masonry is subjected to vertical loads, mechanical interactions between blocks and mortar at the joints induce lateral tension and compression stresses. This phenomenon may affect the capacity and the failure mode of masonry structures. An analytical research program, therefore, was designed with the objective to expand the knowledge on the behavior of mortar subjected to triaxial stresses. This thesis presents the results of that analysis of the mechanical behaviour of mortar samples under triaxial loading. In addition to compressive strength values, elastic modulus and Poisson's ratio values were obtained and are presented. Meaningful differences were observed between the triaxial, and uniaxial tests and these differences are also discussed. In addition, the analytical results of masonry behavior under different levels of confinement are compared to those made by other researchers. Most commonly the mechanical behaviour of the masonry composite is derived from the complex mechanical interaction in between the masonry units such as stone and/or brick, and the mortar joint. Prediction of failure mechanisms in concrete is a fairly complex task due to heterogeneous concrete microstructure, localization process triggered by cracks, multiple crack interactions during their growth and coalescence, different dissipative mechanisms in fracture process zone prior to localized failure and in a localization zone during the failure. While mortars generally are described by means of their mechanical properties in standardized uniaxial compression, equilibrium within the masonry composite most often results in the presence of horizontal confinement within the mortar joint. A series of tests on mortar samples in a state of triaxial compression evidence a clear change in mechanical behaviour and failure mechanism compared to the mechanical behaviour of the mortar in uniaxial compression. Depending upon the importance of the horizontal confining pressure, within the mortar joint, the mechanical behaviour of the mortar can shift from a very brittle material to highly elasto-plastic, while in the meantime a pore collapse mechanism is induced. In order to describe the mechanical behaviour of the masonry composite from the individual materials, an adequate modelling of the mechanical behaviour in triaxial compression of the mortar becomes necessary. The work gives an overview of the mechanical behaviour and failure mechanism of masonry in uniaxial and triaxial states of stress.

Lastly, a new proposal to calculate the cracking strength of masonry using the energy balance criteria is presented. The proposal can represent unreinforced, reinforced, and confined masonry, considering different configurations. Additionally, the model can consider different bricks, mortar, and interface brick-mortar material properties. The most important point in the proposal is the implementation of the equation which can be used to estimate the compressive and tensile strength of masonry. Additionally, the Representative volume element for porous masonry is introduced.

Table of Contents

1. INTRODUCTION

Several theoretical and experimental studies have been conducted to describe the behaviour of masonry under a complex state of stresses and most of these studies depicted the nonlinearity of masonry through plasticity models, damage models or a combination thereof. In contrast, structural masonry is considered anisotropic and has not received the same attention as its concrete counterpart. Only a few studies have been conducted on the failure mechanism of masonry under a complex state of stresses and these studies have focused on the testing of the components. For concrete block masonry mortar is usually the soft component due to its high water-cement ratio and may control the deformation of the masonry. Therefore, the primary goal of this research is to evaluate the mechanical properties of bedding mortar by assessing its damage onset, stiffness plasticity degradation and apparent Poisson´s ratio under compression for different diameter/height (d/h) ratios, focusing on the material strain behaviour under loading until failure. Masonry walls are widely used in building constructions around the world for their low-cost material and broad availability, and their sound insulation properties and energy efficiency. Unreinforced masonry is a heterogeneous, inelastic, and anisotropic material made of two components, brick units and mortar joints exhibiting very different stiffness, strength, and ductility properties. When these two constituents are assembled in form of a masonry prism, a stack of bricks bonded by mortar bed joints, axial splitting of the prism is observed under compressive loading due to the mismatch conditions of the masonry composite. This mismatch results from the different response behavior of the stiff brick units and the soft mortar layers generating triaxial stress and deformation conditions in the brick unit and the mortar joint. This means that during axial compression of the masonry prism the softer mortar joints are restrained by the brick units from Structures. Lateral expansion and hence experience triaxial confinement, while the stiffer brick units are subjected to lateral tension besides far-field axial compression.

A brick masonry wall is not elastic, homogeneous, nor isotropic. It is much more subject to crack propagation, especially from impact loads, and so it is much less adequately analyzed by the relationships used most often to calculate load bearing capacity. Simple formulas are used in construction, but they contain a safety factor based upon an assumed range of brick-and-mortar properties and of brick laying skills. The compressive strength of a masonry wall depends on the strength of the units used, the bricks or blocks, and the mortar. The assessment of the combined strength of the elements will also be affected by the degree of quality control exercised in

manufacture and construction. The slenderness ratio, in turn, depends upon the effective height (or length) and the effective thickness of the wall or column.

1.1. STATEMENT OF PURPOSE

Masonry is one of the oldest building materials, which is used in many parts of the world. Although it has a long-term tradition of building, its behaviour is still in many aspects unclear and estimating its strength depends mainly on approximations with extremely high reserve factors rather than precise equations. The main objective for the presented study is to understand the mechanical behaviour of masonry its failure mechanism under uniaxial and triaxial loading and to understand the differences in material behaviour of the composite masonry constructed with different mortar types, e.g., putty lime, hydraulic lime, and cement or lime-cement mortars. While lime mortars generally obtain a lower uniaxial compressive strength, determined in a standardized way, than nowadays cement- based mortars, its influence on the overall strength of the masonry structure is minimal and the possibility of the former to adapt to settlements is extraordinary and still not understood. Masonry is a composite material, built up of brick or natural stone units and a mortar as binder matrix. Both composing materials are different in nature. Both brick and natural stone can be considered as an elastic brittle material with a certain compressive strength and some tensile strength, which is often considered only one tenth of its compressive strength. Mortar is generally also considered an elastic brittle material, however, with a much higher deformability regarding the brick or natural stone units. Due the composite nature of masonry and the crucial difference in deformability of the composing materials, the stresses and strains will be divided in a complex manner between the brick units and mortar matrix, if masonry is subjected to an external loading. Most common masonry is loaded by the dead load of the structures it bears. The vertical loads result in a horizontal confining pressure on the mortar inside the horizontal joint, as the mortar tries to move out horizontally from between both bricks due to its elevated deformability. Equilibrium in the composite masonry results in horizontal tensile stresses in the brick. The code approaches used to estimate compression strength of masonry are a statistically evaluation of test data, without considering the mechanical and geometrical properties of masonry components, mortar, and units. This requires new statistically evaluations of full data when new brick-mortar combination is to be introduced in the market. Available research projects cover one case of masonry, namely when the deformation properties of mortar are greater than those of the unit. The other case, when deformation properties of unit are greater, is not covered yet, but plays a significant role e.g., in case of lightweight concrete unit.

The aim of this research is to define the compressive strength of masonry depending on the mechanical and geometrical properties of its components. Furthermore, the three-axial material behaviour of mortar and unit in masonry under compression should be considered and studied and advanced models which describe the three-axial material behaviour will be used. The developed formulas and applied assumptions should be verified by test results and finite element calculations. Unfortunately, for masonry there is still no clear model to describe the nonlinear behaviour of this material, because of its complexity and wide variety of forms and, therefore, it is not easy to determine the "pushover curve" of a masonry structure. Some efforts have been made to solve this situation, but the results are still not conclusive. To contribute to this research field, an analytical formula to characterize the in-plane behaviour of masonry under compression, tension, and lateral loads (seismic loads) is developed and numerical simulation also done.

1.2. OBJECTIVES

The objectives are listed as follows:

- Failure mechanism of masonry structure.
- Determine mechanical properties of the contact between brick and mortar.
- Investigate the behaviour of masonry under uniaxial and multiaxial stress.
- Develop a general formula for calculating the cracking strength of masonry structures using energy balance criteria.
- Implementation of the results with ASYS software.

1.3 SCOPE OF WORKS

- The objectives are achieved using extensive research method. The following were the activities compared under the scope of this work.
- Conduct a detailed literature review on masonry compressive behaviour under loading and failure mechanism.
- Derive several equations from the first principle to calculate the cracking strength of masonry using conservation of energy principle which has done been done before. Modelling of masonry prism with ANSYS software.

1.4 METHODOLOGY

Starting with reviewing available code and research approaches to define the compression strength of masonry depending on the mechanical and geometrical properties of its components when deformation properties of mortar are greater than those of the unit, an analytical formula was developed to cover the other case, when the deformation properties of units are greater than those of mortar.

In order to estimate the compressive strength of masonry, first we tried to resolve all the nine components of stress acting on a masonry cube and taking some assumptions. In addition, we developed a formula for calculating the elastic modulus of the masonry from elastic modulus of its components connected in series. We now proved from the first principle of conservation of energy principle the cracking strength of masonry structures and finally the masonry prism is simulated with FEM software.

1.5 ORGANISATION OF THESIS

The materials in this thesis are organized as follows:

Chapter 2 contains a detailed literature review of previous studies that relate to the current study. Meticulous descriptions of test results and figures are also provided in this chapter.

Chapter 3 deals with the formulae for calculating the compressive strength of masonry.

Chapter 4 introduced the estimation of stiffness of masonry matrix from stiffness masonry components.

Chapter 5 describes the cracking strength of masonry both in tensile, compressive and shear loading.

Chapter 6 describes cohesive model, crack length and interface model.

Chapter 7 is about numerical solution of Compressive strength of masonry with extended Drucker Prager yield cap and Menetery-William constants.

Chapter 8 provides the summary, conclusions, and recommendations for this study.

2. STATE OF ARTS

As already stated, masonry is a complex material that shows different properties depending on the geometrical disposition and the quality of the constituents (bricks and mortar). Usually, the properties of bricks and mortar are independently defined through experimental tests. These tests are widely described in literature and codes. There are also experimental tests to determine the properties of masonry, considering a special geometric configuration and quality of materials. These tests are also widely reported in literature and codes (DIN 1053-100, 2007) and (DIN EN 1996-1-1, Eurocode 6:1-1, 2013).

The compression strength of masonry usually lies between the compression strength of mortar as a lower limit and the compression strength of brick as an upper limit. Rarely reaches the compression strength of masonry that of the single brick.

The effect of mortar geometry and mechanical properties on masonry mechanical property is as follows: when using the same brick, the masonry strength increases with increased mortar quality, thinner mortar joints, and when increasing the quality of handwork during building (Hilsdorf, 1965)

If the mortar strength is much less than that of the brick, then the masonry strength is only a small percent of the brick strength; however, it is many times higher than the strength of the mortar alone. Only if the mortar strength is much higher than that of the brick, then the strength of the masonry reaches the strength of the brick (Hilsdorf, 1965). Increasing the thickness of the brick, which is the thickness of the masonry wall in case single-leaf ones, increases the strength of the masonry wall (Huster, 2000). The same trend appears in case of increasing the brick height (Huster, 2000).

2.1. MASONRY UNIT

Concrete masonry products are versatile in shapes and sizes. Briefly, block units can be categorized as solid, semi-solid, and hollow. Concrete block units are classified by physical properties such as: solid content, compressive strength, density, and moisture content.

Depending on the quality of clay (or concrete in the case of blocks) or manufacture, the properties of bricks and blocks vary in a wide range of values. Additionally, the mechanical behaviour of bricks is not necessarily homogeneous and isotropic (especially for hollow or perforated bricks). This means that the properties are not the same in different directions and are also not the same in tension or compression. Normally, the behaviour of bricks is described as elastic brittle. (Campbell & Durán, 2017).

To describe the mechanical behaviour of bricks or blocks, usually a simple compression test is made. To have a complete characterization of bricks, normally these tests are made considering different directions

(the three orthogonal directions of the block, parallel or perpendicular to holes, for example). From this test the stress-strain curve of the brick is obtained, associated with the direction of the applied load and measured deformation, and characteristic compression strength. To determine the traction strength of bricks, there are tests like the "uniaxial tensile strength test," the "splitting tensile test," the "flexural tensile strength" and the "uniaxial tensile strength of bone-shaped specimens" (only for solid blocks). A typical stress-strain curve for compression in bricks is shown in Figure 1. Types "B," "M," "O" and "S" correspond to different brick manufacturers, as indicated by Kaushik (Kaushik et al., 2007).

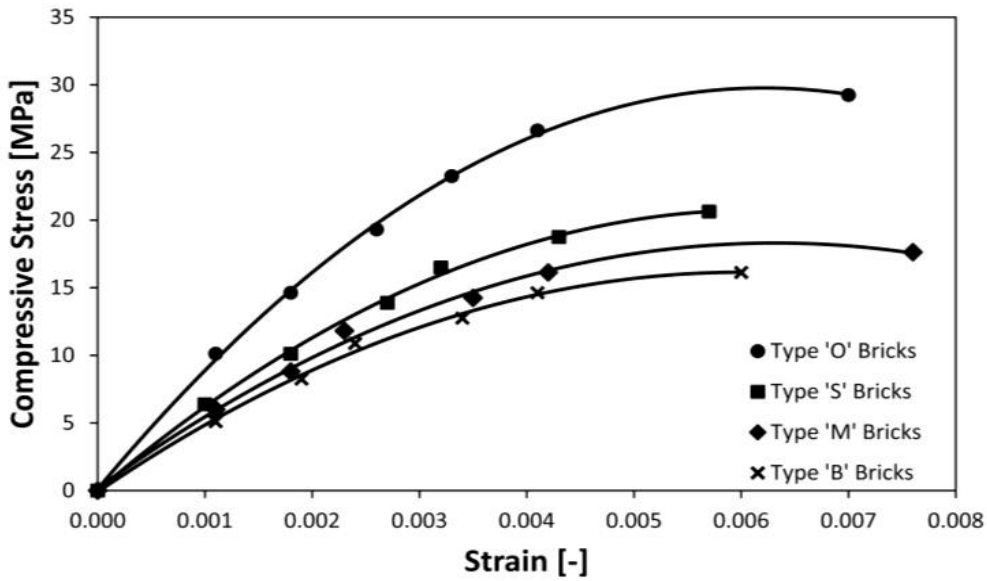

Figure 2.1; A typical stress-strain curve for compression in bricks according to Kaushik et al. (2007).

To estimate the elasticity module E_b of clay bricks, (Basha & Kaushik, 2014) recommends a range of values depending on the compression strength of the brick F_b. These values are estimated to be between 150 and 500 times the compression strength of the brick.

2.1.1. EFFECT OF MASONRY UNIT STRENGTH

For a given mortar, the ratio of wall strength to unit compressive strength is often recognized as the "efficiency" of the wall. Tests by (Kreuger (C.21) showed an "efficiency factor" of about 20% for brick (25 x 12 x 6.5 cm) masonry prisms 78 to 86 cm (30 in.) high laid in lime mortar with bricks of six different strengths ranging from 135 kg/cm2 (1900 psi) to 606 kg/cm2 (8500 psi).

Considering the strong influence of capping, test machine bearing platens, and the method of testing on brick strength and also considering the different types of tests for masonry strength.

Despite these disturbing facts about test results, there does exist a correlation between tested brick strength and masonry strength.

2.2. MORTAR

Mortar has many similarities with concrete, but difficulties arise from the different proportion of the components (cement, sand, lime, and gypsum), which is the key point in order to determine its mechanical properties. In many cases, it is better to have a good bond between mortar and brick than a high resistance mortar. In masonry construction, mortar performs as a key portion which is used to bond individual units into a composite assemblage and provide uniform bearing between units. Mortar can be made by two different methods: proportion specification and property specification. Only one method is available at a time. For proportion specification, mortar is defined by volume ratio of the materials that are used to constitute mortar. This method is acceptable in most cases.

When mixing mortar with new and innovative material, property specification which classifies mortar by performance (compressive strength, water retention, and air content) is preferable. Mortar is generally evaluated by two properties: workability and compressive strength. On-site workability is not possible due to variability in site environment, mortar mixing methods, and so on. It can only be measured by flow test. Mortar compressive strength is obtained by testing 50 mm cube under loading until failure at the ages of either 7th day or 28th day (CSA A179, 2004c). The detailed effect of various mortar properties on masonry prisms studied by previous research are discussed in the subsequent section. To describe the mechanical behaviour of mortar, different tests can be used. The first, and maybe the most typical and important one, is the simple compression test. From this test the stress-strain curve of the mortar is obtained and a characteristic compression strength. To determine the tensile strength of mortar, different tests can be used. Some of these tests are the “uniaxial tensile strength test”, the “splitting tensile test” and the “flexural tensile strength”. A typical stress-strain curve for compression in bricks is shown in Figure 2.1, where three different dosages in terms of cement: lime: sand by volume are presented.

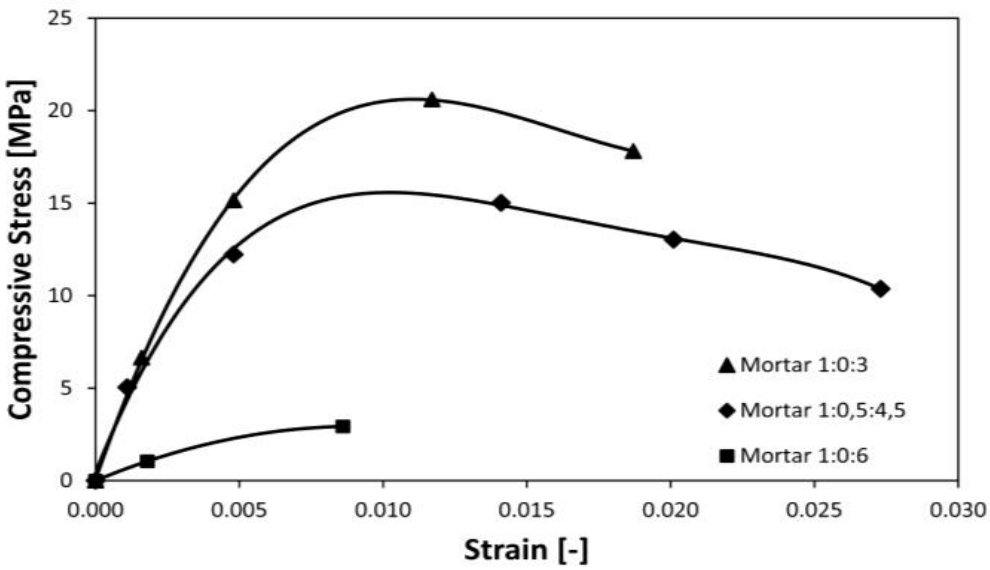

Figure 2.2; Typical stress-strain curves for compression in mortar according (Kaushik et al., 2007)

2.2.1. EFFECT OF MORTAR STRENGTH

Masonry strength is strongly correlated to the strength of the mortar, a fact which can be clearly noticed after construction work. The influence of the mortar strength on the masonry strength was also tested by Kreliger on piers about 80 cm (30 in.) high, laid in different mortars but of one single brick strength (284 kg/cm^2 or 4000 psi). The bricks were 25 × 12 × 6.5 cm, and thus the cross section of the piers was about 25 × 12 cm. Numerous studies, which have attempted to establish a relationship between mortar strength and masonry strength, have produced a wide range of results. It appears that masonry strength may vary as the one-third power or the two-third power of mortar strength.

2.2.2. EFFECT OF MORTAR JOINT THICKNESS

Since the mortar is usually the weaker part of the masonry composite, the highest strengths are obtained with thin bed joints and a low ratio of bed joint thickness to unit height (Sahlin, 1971). The mortar joint thickness has a significant effect on masonry strength (Maurenbrecher, 1978). (Khalaf 1996) conducted tests to investigate the effect of mortar thickness on the compressive strength of the masonry prisms. For both grouted and hollow prisms, an increase in the mortar thickness from 5cm to 20cm reduced the compressive strength of the prisms. The reduction strength was larger in hollow prisms. (Drysdale and Hamid 1979) also studied the effect of joint thickness through prism tests. This study found that an increase in the mortar joint thickness from 9.5 mm to 19 mm for both grouted and hollow prism the compressive

strength for prism decreased by 3% and 16%, respectively. This study concluded that the mortar joint thickness has certain influence on hollow prisms and nearly no influence on grouted prisms.

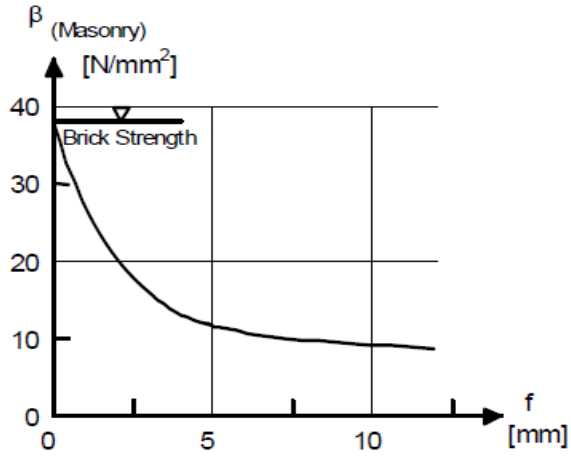

Figure 2.3; Strength of masonry in dependence of joint height f or h_{mo}

2.2.3. INFLUENCE OF VARIATIONS IN DIMENSIONS

If the dimensions of the masonry units vary, the dimensions of the mortar joints will also vary. The result is nonuniform joint thicknesses, which create bending moments and stress concentrations in the bricks. In order to obtain a high masonry strength, it is advisable to use units of well-controlled dimensions, with a maximum tolerance, say, of the order of a few percent of the nominal dimensions. In addition, careful control of unit dimensions markedly increases the speed of brick laying, according to (Sahlin, 1971).

2.2.4. EFFECT OF PATTERNS AND METHODS OF BONDING

Masonry units can be laid in numerous different patterns by overlapping (displacing in the plane of the wall) the units more or less from one course to another. Stretchers and headers can be mixed in different ways, and certain patterns can be repeated in every second, third, or fourth course, and so on. Such differences do not seem to affect the strength of the masonry. If different heights of units are mixed, for example, a course of low units following a course of higher units, etc., it would be safe to assume, for the purpose of calculation, that the whole wall consisted of low units. The higher joint thickness to unit height ratio of the lower units would be considered this way. If a masonry wall is several wythes thick without cavity, the individual wythes are bonded together with bricks (headers) or metal reinforcement bars (ties) between the wythes. These binders will of course be more highly stressed the higher the shear force in the wall is. Tests on walls with metal ties and regular brick bonding, as well as tests with different configurations

and numbers of binders show little or no difference in wall strength (concentric axial compression) within reasonable sizes of bricks or blocks and with reasonable arrangements of the bonding. This statement holds only if the stress is calculated based on the net area, the vertical joints between the wythes excluded. The unit strength, however, of single-wythe walls seems to be somewhat higher than multiwythe walls.

2.2.5. THE INFLUENCE OF WORKMANSHIP

Workmanship has a strong influence on the compressive strength of masonry-especially on low strength brick and mortar, for example. For brick strengths up to approximately 200 kg/cm^2 (approximately 3000 psi), an increase of up to 1 00% can be obtained by improving the workmanship over the ordinary. For higher brick strengths, Monk reports the gain to be 10 to 70%. The detrimental effect of poor workmanship is due to improper filling of joints and furrowing, as well as to other malpractices, which contribute to uneven and incomplete filling of all joints.

2.2.6. EFFECT OF AGING

The curing time of the mortar in the joints affects masonry wall strength in the same way as it affects the strength of poured concrete. The mortar strength increases with time. (Silen) studied the increase in masonry strength with time and found that brick walls continue to gain strength long after they have been built.

2.2.7. MORTAR BEDDING

Two bedding methods, namely full bedding and face shell bedding can be applied during masonry prism fabrication. The full bedding shall be used for prisms built with solid unit and face shell bedding shall be used for prisms made with hollow and semi-solid unit.

Hamid and Chukwunenye (1986) analyzed the lateral tensile stress in the webs for three course hollow prims built with two different mortar types. This study used three-dimensional finite element analysis. Due to deep beam action produced by the gap that exists between webs, a larger lateral tensile stress in web was found in the face shell bedding prisms. This induces web cracking at a relatively lower load level for face shell bedded prisms as compared to full bedded prisms. Furthermore, web cracking can cause the failure of the prisms as long as the cracks at the webs propagate through the entire height of the prisms. Also, they studied the stress distribution at the face shell along the height of the prisms. The stress distribution for face shell bedded prisms is highly nonuniform. However, for full bedded prisms the stress distribution is fairly

uniform. Consequently, the mechanical behavior for these two prisms is significantly different. Ganesan and Ramamurthy (1992) made an additional confirmatory study on five course high hollow concrete prisms. High lateral tensile stress and highly nonuniform axial stress were also found in web shells and face shells, respectively.

2.2.8. GROUT

In masonry construction, grout is a mixture of cementations material, aggregate, and water. Grout is used to fill cells for hollow or semi-hollow concrete units. Grout can enhance the load carrying capacity and bonds with the reinforcement in the masonry structure. High slump (200-250 mm) must be guaranteed so as to ensure flow ability and fill voids completely. Two types of grouts are used, and they are fine grout and coarse grout. The fine grout does not contain coarse aggregate. The use of fine or coarse grout is prescribed by grout space. According to CSA A179 (2004c) if the minimum dimension for grout space is 50mm or coarser grout shall be applied. In previous several studies, the effects of grout property (compressive strength, deformation capacity) on prism compressive strength were determined.

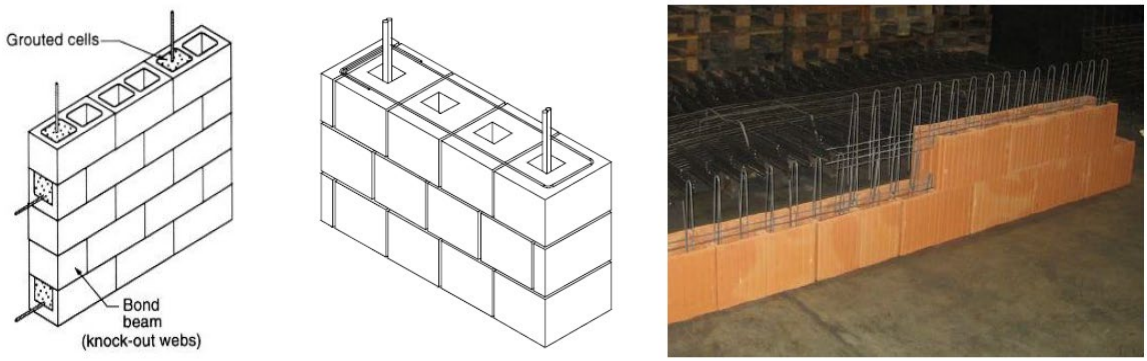

Figure 2.4; Examples of modern masonry (a) confined masonry in areas of moderate to high seismicity, again with thick blocks; (b) different reinforced masonry solutions, adopted in the US, Italy and Switzerland, respectively (Lourenco, 2004).

2.3. CONTACT (INTERFACE) BETWEEN BRICK AND MORTAR

The bond between the unit and mortar is often the weakest link in masonry assemblages. The nonlinear response of the joints, which is then controlled by the unit-mortar interface, is one of the most relevant

features of masonry behaviour. Two different phenomena occur in the unit-mortar interface, one associated with tensile failure (mode I) and the other associated with shear failure (mode II).

The mechanical properties of the contact between brick and mortar can also be estimated from laboratory tests. To determine the tensile behaviour of the interface between brick and mortar, the "tensile bond test" may be used. On the other hand, the estimation of the shear-behaviour of the interface between brick and mortar is made using the "shear bond test". In this test the failure can occur either on the interface or in the mortar.

2.4. MASONRY (COMPOSITE MATERIAL)

It is important to consider the properties of masonry as a whole sometimes. The important thing in these cases is that the interaction between bricks and mortar and the geometrical disposition of the units is considered. In this case, many tests can be carried out. One of these tests is the compression test for masonry prisms, from which a stress-strain curve can be obtained (INN, 2003). Another test to estimate some properties of masonry is the diagonal compression test on wallettes (INN, 1997).

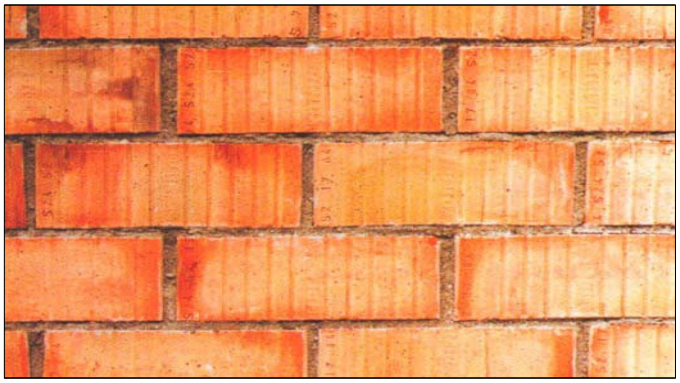

Figure 2.5; Masonry assembly.

Concrete and reinforcing bars: In the case of reinforced and/or confined masonry it is also necessary to consider the quality of concrete and steel. Both materials have been widely studied and there is enough information on their properties in codes and literature. In the case of concrete, the compression strength (fc) is needed, which is also used to determine the elasticity module (E). For steel reinforcing bars, the tensile strength f_y is needed, and the elasticity module E_s is 210000 N/mm^2.

Disposition of bricks: Another important factor to consider for the determination of the behavior of masonry is the disposition of bricks or type of bond. Masonry is an organized disposition of bricks bonded with mortar and the way the bricks are organized may determine the structural response of the wall.

2.4.1. TYPES OF MASONRY

Depending on the regions of the world, and the building traditions of the country, masonry has different configurations as a structural element. These configurations vary from unreinforced masonry to reinforced and confined masonry. The type of masonry used is related to the amount of seismicity, for example in countries with very low seismic activity, unreinforced masonry is used. On the other hand, in countries with mid to high seismic activity, reinforced or confined masonry is used.

Reinforced masonry is a type of masonry that considers reinforcement by steel bars embedded in the mortar. This reinforcement is placed in the horizontal joints and/or in the brick holes and then filled with grout. The horizontal reinforcement helps to improve the resistance to horizontal loads (shear failure) and the vertical reinforcement helps to improve the flexural resistance. In seismic countries, this type of masonry is widely used and, sometimes, obligatory.

Confined masonry is a special type of masonry which considers the confinement of the masonry within a reinforced concrete frame. This confinement is materialized with vertical tie columns and a horizontal bond beam. Normally, the codes define the requirements for the maximum area to be confined in order to have a good structural performance. In seismic countries, this type of masonry is widely used and, sometimes, obligatory (Tensile or shear).

2.5. PROPERTIES OF THE COMPOSITE MATERIAL

The uniaxial behaviour of the composite material is described next regarding the material axes, namely the directions parallel and normal to the bed joints.

2.5.1. BEHAVIOR OF MASONRY UNDER UNIAXIAL STRESS

Masonry is typically a nonelastic, nonhomogeneous, and anisotropic material composed of two materials of quite different properties: stiffer bricks and relatively softer mortar. Under lateral loads, masonry does not behave elastically even in the range of small deformations. Masonry is said to be very weak in tension because it is composed of two different materials distributed at regular intervals and the bond between them is weak. Therefore, masonry is normally provided and expected to resist only compressive forces. As shown in Figs. 2.6a and b, during compression of masonry prisms constructed with stronger and stiffer bricks, mortar of the bed joint tends to expand laterally more than the bricks because of lesser stiffness. However, mortar is confined laterally at the brick–mortar interface by the bricks because of the bond between them; therefore, shear stresses at the brick-mortar interface result in an internal state of stress which consists of

triaxial compression in mortar and bilateral tension coupled with axial compression in bricks. This state of stress initiates vertical splitting cracks in bricks that lead to the failure of the prisms.

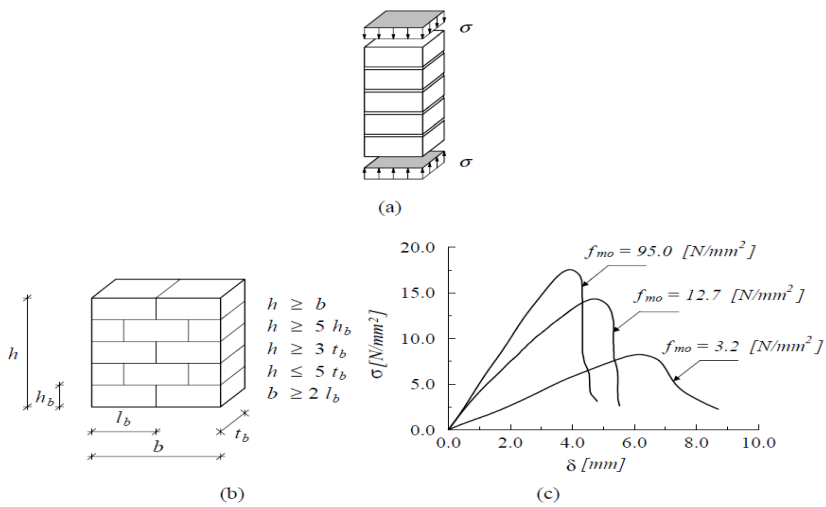

Figure 2.6; Uniaxial behaviour of masonry upon loading normal to the bed joints: (a) stacked bond prism; (b) schematic representation of RILEM test specimen; (c) typical experimental stress-displacement diagrams for 500 ×250 ×600 [mm3] prisms of solid soft mud brick, (Binda, Fontana, & Frigerio, 1988).

Here, f_{mo} is the mortar compressive strength. Since masonry is an assemblage of bricks and mortar, it is generally believed that the strength and stiffness of masonry would lie somewhere between that of bricks and mortar.

2.5.2. UNIAXIAL TENSILE BEHAVIOUR OF MASONRY

For tensile loading perpendicular to the bed joints, failure is generally caused by failure of the relatively low tensile bond strength between the bed joint and the unit. As a rough approximation, the masonry tensile strength can be equated to the tensile bond strength between the joint and the unit, in masonry with low strength units and greater tensile bond strength between the bed joint and the unit, e.g., high-strength mortar and units with numerous small perforations, which produce a dowel effect, failure may occur because of stresses exceeding the unit tensile strength. As a rough approximation, the masonry tensile strength in this case can be equated to the tensile strength of the unit.

For tensile loading parallel to the bed joints a complete test program was set-up by, (Backes, 1985)The specimen consists of four courses, initially laid down in the usual manner, see Figure 2.6a. A special device attached to the specimen turns it 90° in the intended direction of testing shortly before the test time, see

Figure 2.6. The load is applied via steel plates attached to the top and bottom of the specimen by a special glue. The entire load-displacement diagram is traced upon displacement control.

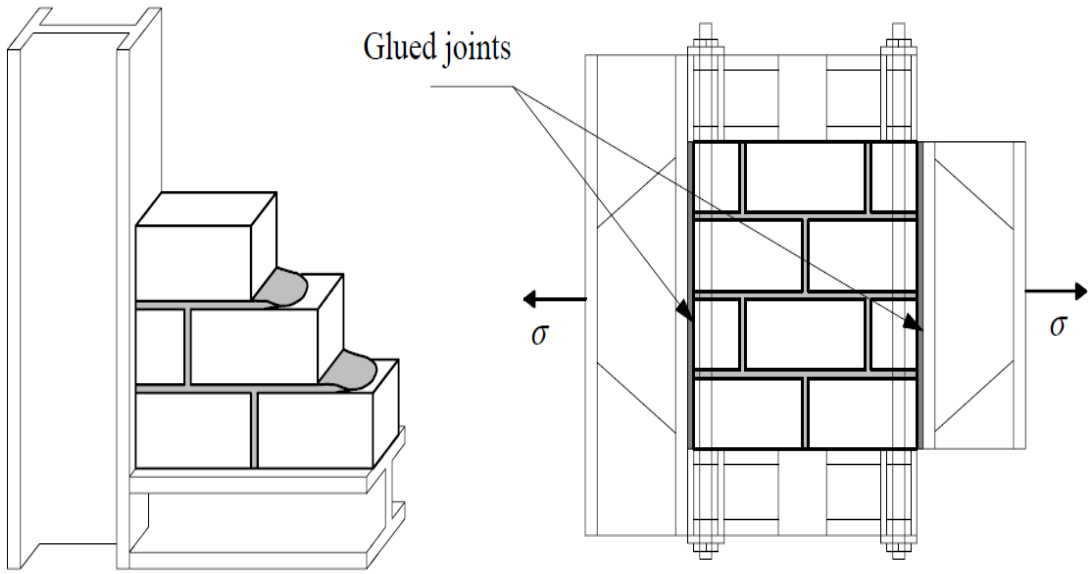

Figure 2.7; Test set-up for tensile strength of masonry parallel to the bed joints, (Backes, 1985), (a) building of the test specimen; (b) test specimen before 90º rotation and testing.

Two distinct types of failure are possible, depending on the relative strength of joints and units, see Figure 2.7. In the first type of failure cracks zigzag through head and bed joints. A typical stress-displacement diagram shows some residual plateau upon increasing deformation. The post-peak response of the specimen is governed by the fracture energy of the head joints and the post-peak mode II behaviour of bed joints. In the second type of failure cracks run almost vertically through the units and head joints.

A typical stress-displacement diagram shows progressive softening until zero. The post peak response is governed by the fracture energy of the units and head joints.

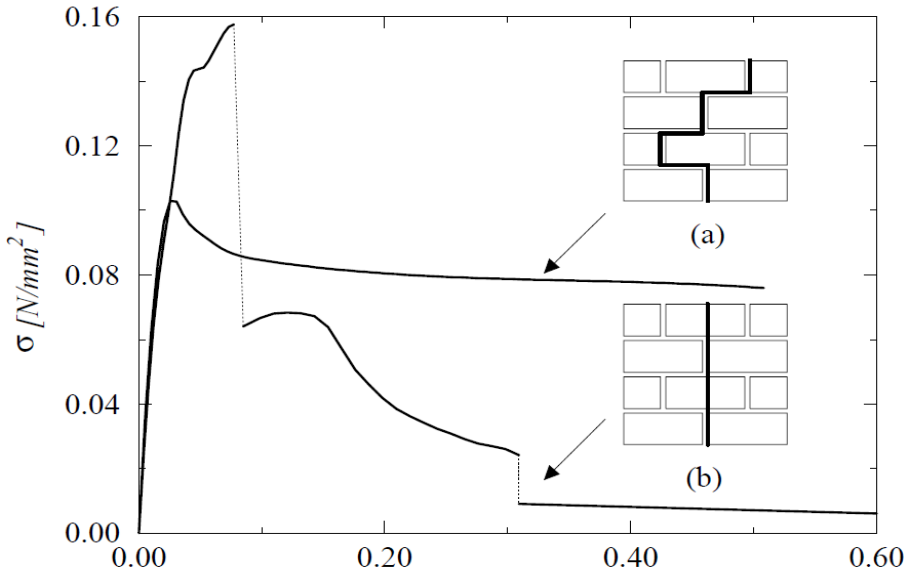

Figure 2.8; Typical experimental stress-displacement diagrams for tension in the direction parallel to the bed joints, (Backes, 1985)(a) failure occurs with a stepped crack through head and bed joints; (b) failure occurs vertically through head joints and units.

2.5.3. BEHAVIOR OF MASONRY UNDER BIAXIAL AND MULTIAXIAL STRESS

When masonry is submitted to vertical loads, several joint phenomena occur between the units and the mortar inducing compression as well as lateral tension in the system. Experimental tests of blocks under compression show a stress-strain behavior that is essentially linear. However, the mortar under the same conditions of stress and strain has a nonlinear behavior. Such behavior must be considered in any numerical simulation to predict the capacity of masonry strength. The understanding of such nonlinear behavior is important to correctly define the failure criterion of the assembly caused by the crushing of the mortar and it is essential for accurate constitutive modelling of masonry.

The constitutive behaviour of masonry under biaxial states of stress cannot be completely described from the constitutive behaviour under uniaxial loading conditions. We investigate the influence of the biaxial stress state up to peak stress to provide a biaxial strength envelope, which cannot be described solely in terms of principal stresses because masonry is an anisotropic material. Hence, the biaxial strength envelope of masonry must be either described in terms of the full stress vector in a fixed set of material axes or, in terms of principal stresses and the rotation angle between the principal stresses and the material axes. The different modes of failure are illustrated in Figure 2.9.

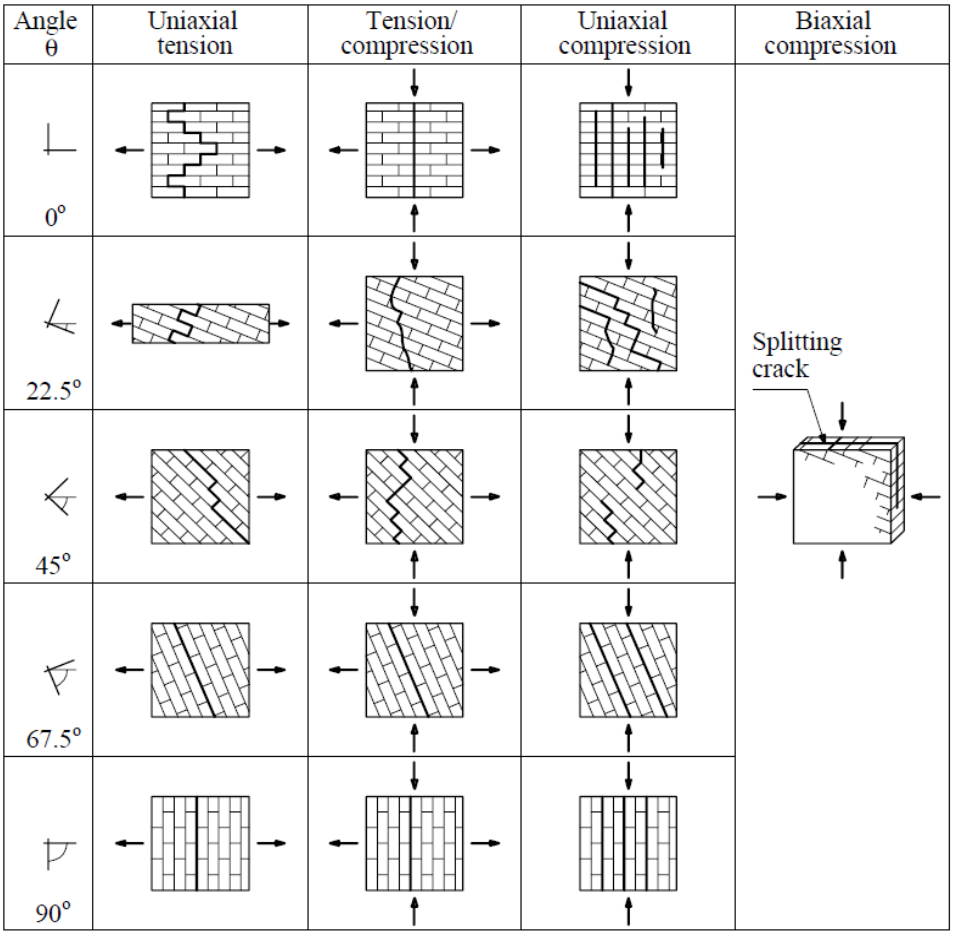

Figure 2.9; Modes of failure of solid clay units masonry under biaxial loading, (Lourenco, 1996).

For uniaxial tension, failure occurred by cracking and sliding of the head and bed joints. The influence of the lateral tensile stress in the tensile strength is not known because no experimental results are available. A lateral compressive stress decreases the tensile strength, which can be explained by the damage induced in the composite material, by micro slip of the joints and micro cracking of the units. In the tension-compression loading cases failure occurred either by cracking and sliding of the joints alone or in a combined mechanism involving both units and joints. Similar types of failure occurred for uniaxial compression, but a smooth transition is found to other type of failure mode in biaxial compression. In biaxial compression failure typically occurred by splitting of the specimen at mid-thickness, in a plane parallel to its free surface, regardless of the orientation of the principal stresses. For principal stress ratios << 1 and >> 1, the orientation played a significant role and failure occurred in a combined mechanism involving both joint failure and lateral splitting. The increase of compressive strength under biaxial compression can be explained by friction in the joints and internal friction in the units and mortar. For concrete, the failure

envelope seems to be largely independent of the loading path, (NELISSEN, 1972), which confirms the presence of a single failure mode, i.e. continuous crack growth at the micro level.

Summary

- The difference between the strength of prisms constructed with the stronger mortar and that of the prisms constructed with the weaker mortar prisms was less than 8%.
- Mortar controls the prism's failure mode. Prisms with stronger mortar behaved as a homogeneous material, with a conical-break cracking pattern. In contrast, prisms with weaker mortar experienced mortar crushing and complete degradation of the bond between the mortar and blocks. This behavior was observed at stresses close to 50% of the strength.
- The measurement of the compressive strength of prism is not a reliable parameter without analysis of the failure mode; the compressive strength of prisms built with strong and weak mortars were similar. However, the failure mode of the prisms with weak mortar starts by crushing at half of the final strength.

3. FAILURE MECHANISM OF MASONRY

Several theoretical and experimental studies have been conducted to describe the behavior of concrete under a complex state of stresses and most of these studies depicted the nonlinearity of concrete through plasticity models, damage models or a combination thereof. In contrast, structural masonry is considered anisotropic and has not received the same attention as its concrete counterpart. Only a few studies have been conducted on the failure mechanism of masonry under a complex state of stresses and these studies have focused on the testing of the components. For concrete block masonry mortar is usually the soft component due to its high water-cement ratio and may control the deformation of the masonry. Therefore, the primary goal of this chapter is to evaluate the failure mechanism of masonry structure and mechanical properties of bedding mortar by assessing its damage onset, stiffness plasticity degradation and apparent Poisson´s ratio under compression for different diameter/height (d/h) ratios, focusing on the material strain behavior under loading until failure. The results of the pilot testing presented herein are preliminary and require further validation.

The failure of masonry is related to the interaction of unit (brick, stone etc.) and mortar. It is also related to the difference in the mechanical properties of unit and mortar (stiffness and poison ratios. Masonry fails under three categories as follows.

- Masonry with stronger unit: if the stiffness of the unit is higher than the stiffness of the mortar, the mortar will tend to expand laterally and three axial compression-tension in mortar and tensile stress is developed in the unit as shown below in Fig 2.18a.
- Masonry with stronger mortar: when the stiffness of mortar is higher than the stiffness of the unit, the unit tends to expand laterally, which causes tensile stress in the mortar. Hence no deformation in the mortar as shown in Fig 2.18b
- Masonry with equal stiffness of mortar and unit: Here a homogeneous behavior is expected. Both the mortar and the unit expand laterally. Fig.2.18c

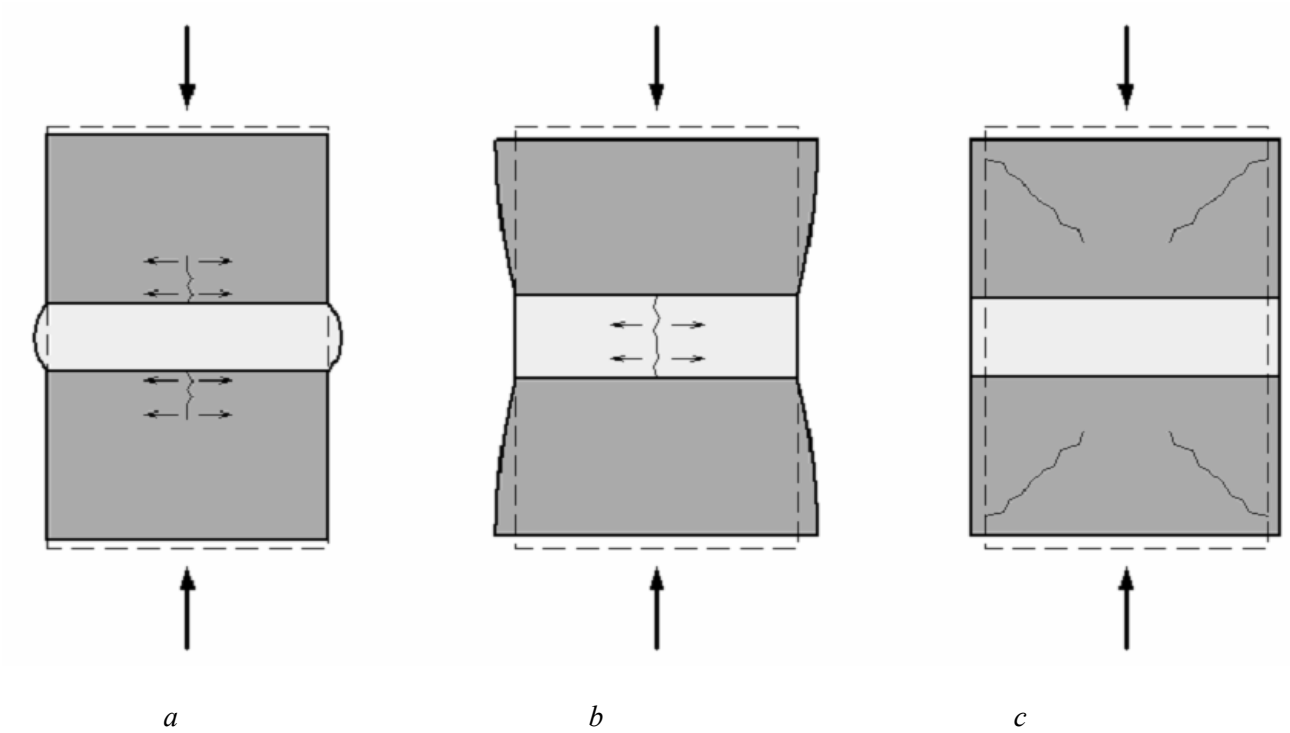

Figure 3.1; Hypothesis for deformation and crack initiation for different stiffness ratios between mortar and unit. (a) unit stiffness is higher than the mortar stiffness, (b) the mortar stiffness is higher than the unit stiffness, (c) the stiffness of unit and the stiffness of mortar are equal, (Hendrickx, 2010).

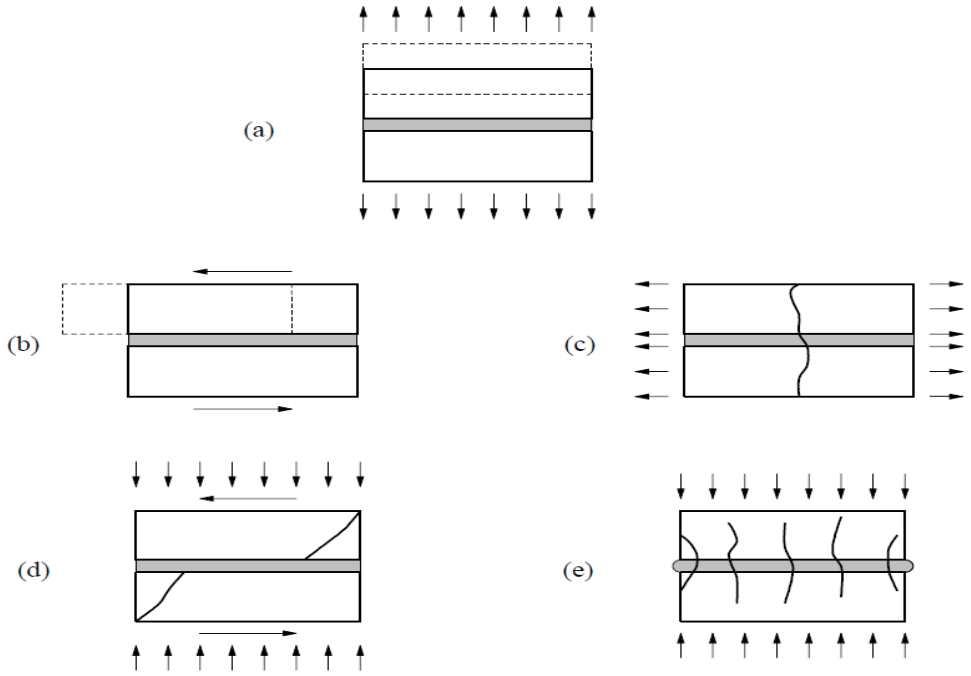

Figure 3.2; Masonry failure mechanisms: (a) joint tensile cracking; (b) joint slipping.

(c) unit direct tensile cracking; (d) unit diagonal tensile cracking; (e) masonry crushing.

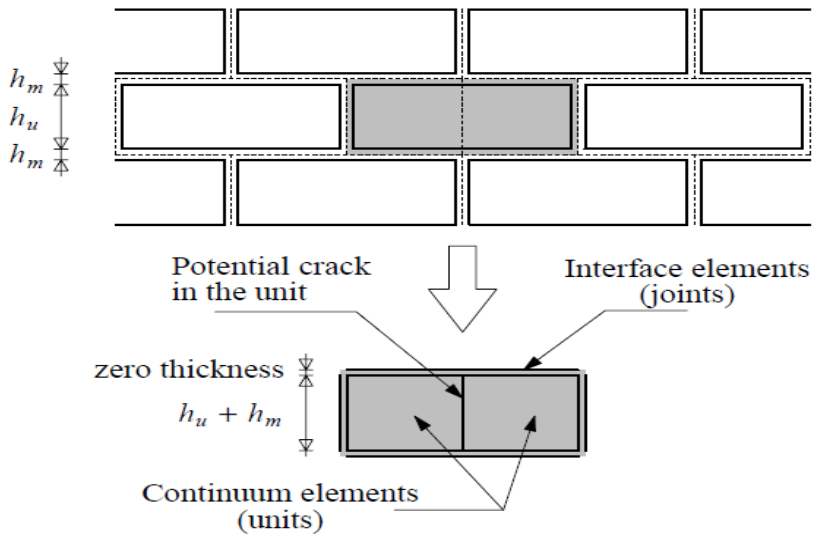

Figure 3.3; Suggested modelling strategy. Units (u), which are expanded in both directions by the mortar thickness, are modelled with continuum elements. Mortar joints (m) and potential cracks in the units are modelled with zero-thickness interface elements.

3.1. SHEAR FAILURE AT THE MORTAR EDGE

Masonry is a heterogeneous material created by the combination of mortar and units. The main features of masonry are a rather large compressive strength and very low tensile strength. This has led to buildings that are not very good at resisting earthquakes which is one the main reasons of collapse of ancient structures and was a determining factor for the way that ancient buildings were constructed (Zucchini & Lourenço, 2007). Masonry is an anisotropic material, even though its constituent parts may be isotropic, with the two components having different elastic properties (Zimmermann T., 2010). The joints between mortar and unit are acting as planes of weakness, therefore, the unit-mortar interface is one of the most sensitive parts of the material and where we are finding the modes of failure. Mode I am the tensile failure, where we have the unit detaching from the mortar, as shown in Figure 2.12, and Mode II is the shear failure that can occur

when we have either sliding between the units or the failing in shear of the joint as shown in Figure 2.21

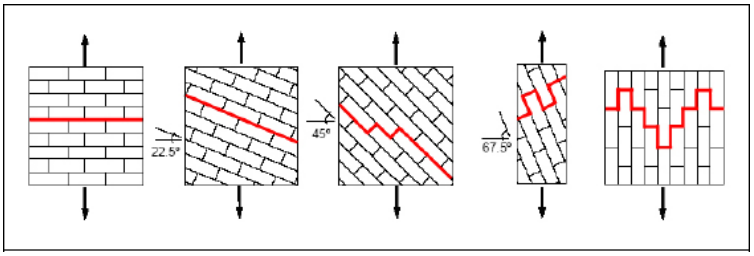

(Augenti & Parisi, 2011).

Figure 3.4; (a) Modes of failure of solid clay unit's masonry under uniaxial tension (Sotirios & Dimitris, n.d.)

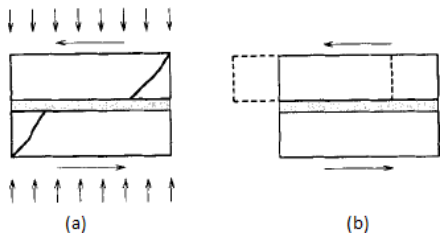

(b): Failure mechanisms of masonry in shear: (a) joint slip and (b) unit diagonal tension crack

When dealing with historic masonry one of the problems is identifying the material that was used for its construction or its reparation, which may change throughout the element, something that must be done while bearing in mind that we should not use any destructive methods (Kohees et al., 2019). Another difficulty is figuring out the parts that need strengthening since many times there is no difference between load bearing and ornamental elements, we need to locate the existing weaknesses and damage, again in the least obtrusive way possible (Lourenco, 1996).

3.2. MORTAR STRENGTH VERSUS MASONRY FAILURE MECHANISMS

Masonry is a composite material built with units and mortar that almost certainly have different strengths, and the interaction between the individual materials produce a complex stress state under loading. The mortar in concrete block masonry appears to experience changes in its mechanical properties under loading. Two factors may be responsible for the observed effects: the confinement produced by the small thickness of the mortar between the blocks and the required high porosity level to produce proper mortar workability. An example of changes in mortar mechanical properties is presented in Figure 1, which shows the vertical stress and strain for three-unit high prisms under compression, constructed with the same block type but with mortars with different strengths.

One prism was assembled with a high strength mortar of 19.8 MPa (type I), another prism was assembled with a medium strength mortar of 7.2 MPa (type II) and a third prism was assembled with a low strength mortar of 4.4 MPa (type III). Hollow concrete blocks were used with dimensions 390mm x 14 0mm x 190mm (length x thickness x height), having a net area compressive strength of 23.1Mpa. The response of the prism with mortar type I was almost linear, with a slight release of strain when the prism developed a sudden crack at a stress/strength ratio of approximately 60%. The response is almost linear both before and after the occurrence of the crack. The crack propagated through the block, but visual inspection detected no crushing or crumbling of the mortar. The prism finally split into two halves due to propagation of the crack in the vertical direction. Differently, the prisms with mortar types II and III experienced a gradual non-linear increase in vertical strains with an increase in stress. Although the prism with mortar type II also experienced a sudden crack at a stress/strength ratio of approximately 60%, the observed non-linear behavior following initial loading is an indication of the change in stress state of the mortar, the propagation of micro cracks inside the mortar or a combination thereof. The failure of the prisms with mortar types II and III was due to localized crushing and crumbling of mortar joint, as shown in Figure 2. After mortar crumbling, localized spalling of the mortar and sometimes even of the blocks were observed, and vertical cracks began to propagate towards the top and bottom surfaces of the prism.

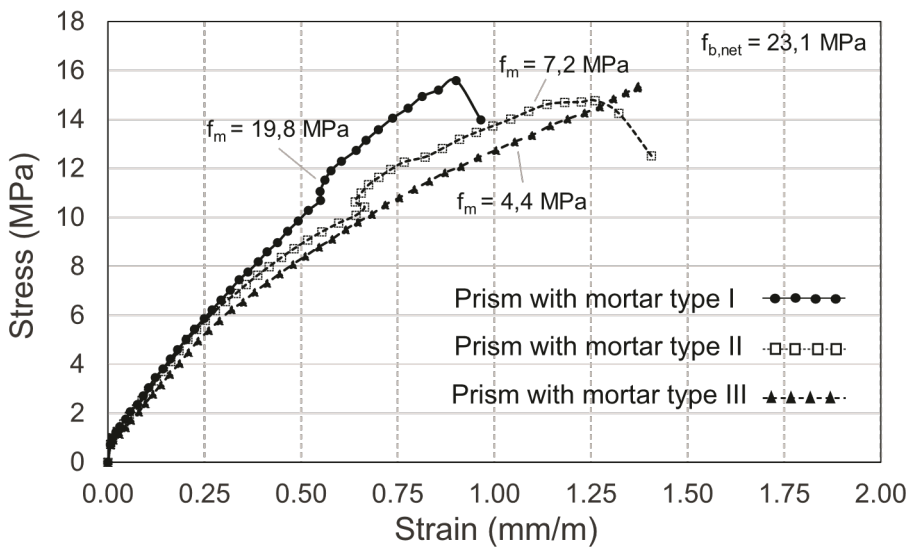

Figure 3.5; Masonry stress-strain for three mortar types (Mohamad et al., 2018)

3.2.1. LATERAL ELASTIC EXPANSION OF MORTAR.

The results shown in Figure 1 indicate that the mortar, in some cases mortar, in some cases, governs the failure characteristic of the prisms and that such failure depends on the f_{mo}/f_{br} ratio. For example, for a

prism constructed with mortar almost as strong as the block f_{mo}/f_{br} ratio of approximately 0.85), and compressed axially, the mortar expands laterally due to their different Poisson's ratios. As a result, the mortar induces tensile stresses in the block. Because the mortar is strong, its compressive and shear strengths are greater than the tensile strength of the block; thus, the block cracks vertically and the prism fails. For prisms constructed with medium and weak mortars f_{mo}/f_{br}= 0.31 and 0.19, respectively) and subjected to axially compressive loading, the mortar will expand laterally, similar to the case of prisms with strong mortar. Because the mortar, however, is significantly weaker than the block, any increase in load causes crushing of the mortar. The mortar essentially cracks internally and starts to crumble and spall. As the load continues to increase, the mortar continues to expand laterally, and vertical cracks develop in the mortar. With further increase in load, more lateral expansion occurs and the cracks in the mortar propagate vertically through the blocks causing failure of the prism. Such a failure evolution is depicted in Figure 3.6.

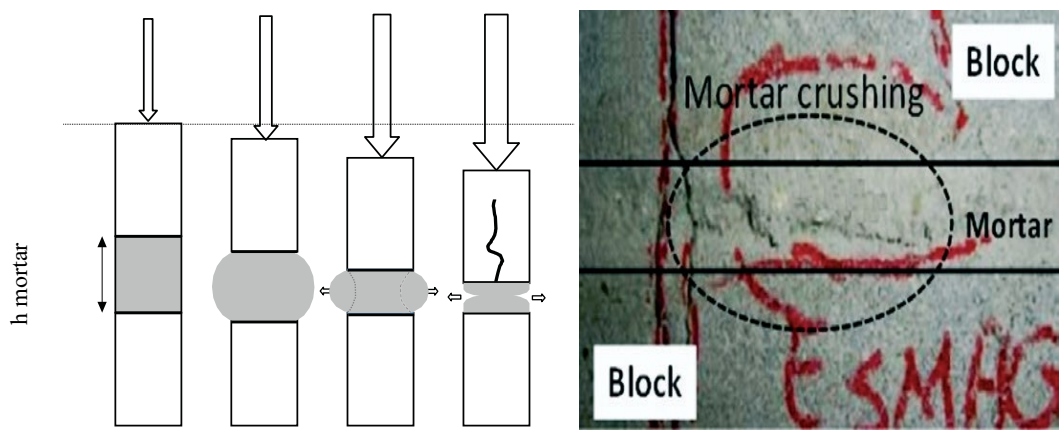

Figure 3.6; (a) Failure mechanism of prism; (b) Weak mortar failure model evolution under loading with weak mortar

(Mohamad et al., 2018) compiled the results of several experimental investigations to develop a model to predict the compressive strength of ungrouted hollow concrete block masonry. With respect to the mortar effect on the masonry compressive strength, a considerable scatter in data was determined, as shown in Figure 4. For example, for a mortar strength of 5MPa, the masonry strength ranges from 7.5MPa to approximately 25MPa. Although tests results indicate that mortar strength has no appreciable effect on the strength of hollow prisms, such a scatter may indicate that it is not reliable to evaluate only the ultimate load obtained from compression tests without determining the masonry failure mode for the same compressive strength of concrete block; i.e., either the block is failing in tension (due to the relative low block tensile strength) or the mortar is failing by crushing (due to the relative low mortar compressive strength). If the mortar crushes before the block tensile strength is reached, the ultimate measured load is an inflated value, portraying the block strength rather than the masonry strength.

Researchers believe that much of the observed scatter in Figure 3.6b occurs because the masonry strength, defined as the maximum applied load on tested prisms, does not capture the changes on the mechanical properties and consequently the failure of the mortar confined between the blocks. As currently defined, the strength of masonry is governed by the strength of the blocks, i.e., the effects of mortar are underestimated, which explains why many authors have stated that the mortar does not significantly affect the strength of masonry.

3.2.2. COMPATIBILITY OF DISPLACEMENTS AT THE CONTACT SURFACE OF UNIT AND MORTAR.

(Zucchini & Lourenço, 2007) described the behavior of joints and bricks in their interaction. The model described can be divided into one component cell (Figure 2.24), where the vertical union is presented between two bricks (vertical joint), the horizontal union between two bricks (horizontal joint), and the brick itself. The general deformation of the mechanism can be explained in the following way, before a top horizontal displacement:

- It begins to deform sideways, and joints begin to interact with the masonry, through mechanisms of friction material.
- The vertical joints have lateral displacements since the lower masonry tries to keep to its initial position and the brick on the top moves depending on the load and/or displacement applied.
- Since the upper masonry moves laterally in the direction of the applied load, Joint 1A experiences a tension force and thus making adjacent masonry move together with a differential deformation on the horizontal axis due to joint driven expansion.
- Joint 1B is compressed, and it allows the movement of the masonry.

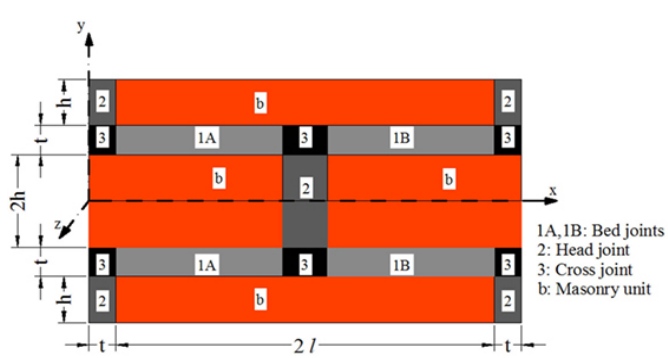

Figure 3.7; Definition of masonry axes and masonry components considered in the adopted formulation: unit, head joint, bed joint and cross joint.

3.2.3. SPALLING OF MORTAR EDGES FOR CASE $E_{mo} < E_{br}$

In masonry '**spalling**' refers to the flaking, cracking, peeling, crumbling, or chipping of mortar from the stone or bricks, particularly where areas of the surface are said to have blown. This can occur as a result of weaker mortar, water penetration, freezing, heating (such as during a fire) or by mechanical processes. Prisms constructed with weaker mortar experienced larger deformation than those of the prisms with stronger mortar.

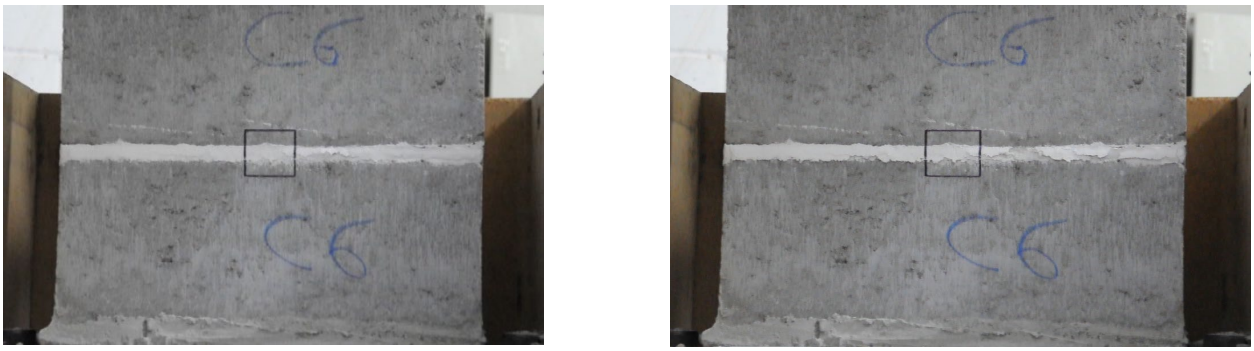

Figure 3.8; Failure sequence of the prism (weak mortar).

Figure 3.8 shows the mortar crushing started at maximum stress and the rupture started with the mortar joint crushing and after that, vertical cracks appeared on the blocks.

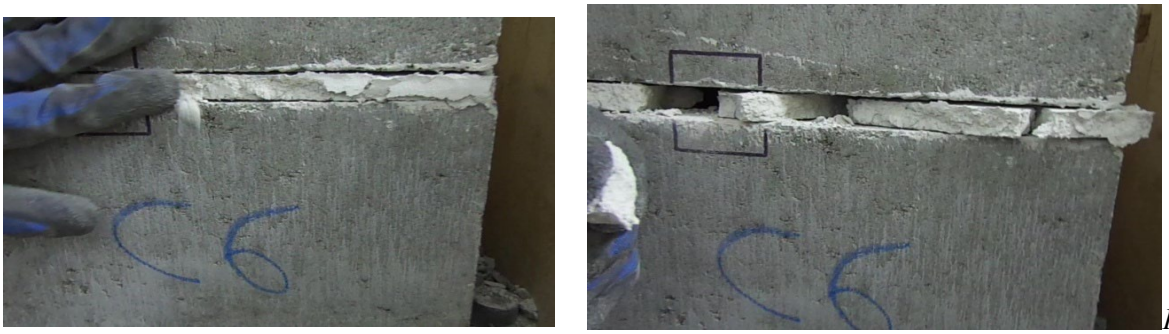

Figure 3.9; Failure mode – Weak Mortar Prisms.

The block-mortar bond was completely broken, and the mortar porous structure completely destroyed in prisms with weaker mortar.

3.2.4. CRACKING OF UNITS FOR CASE $E_{mo} > E_{br}$

Prisms with stronger mortar had conical-break post-failure cracking. In turn, prisms with weaker mortar experienced **joint crushing** at stress levels between 30 and 50% of the prism strength, see Figure below.

Figure 3.10; Cracking pattern of Unit (strong mortar).

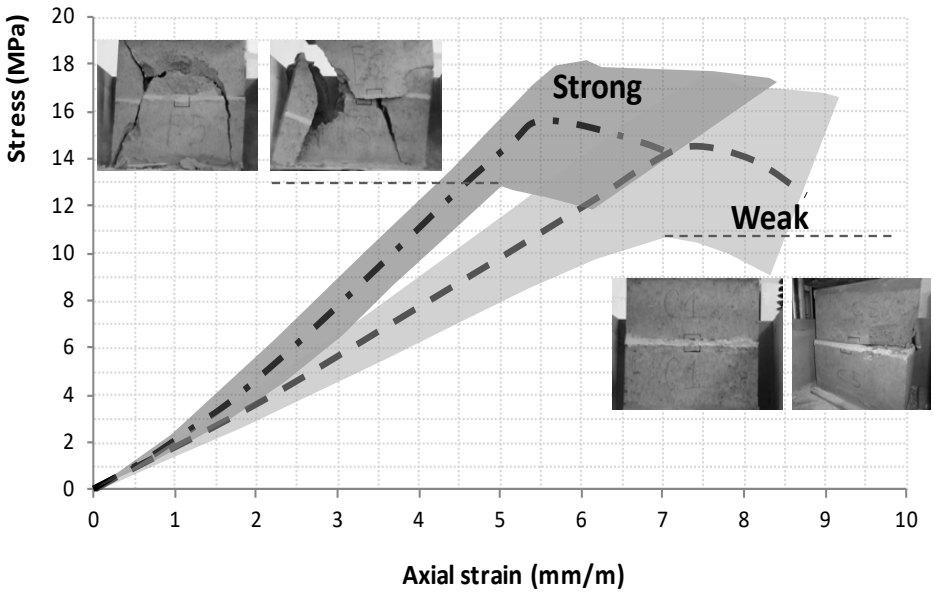

Figure 3.11; Stress-strain curves under multiaxial loading

3.3. CURVES UNDER MULTIAXIAL LOADING. MECHANICAL BEHAVIOR OF MASONRY UNDER COMPLEX LOADING CONDITIONS

Looking at the results of the triaxial analysis, the difference in material behavior of the masonry can neither be attributed to a difference in material behavior of the mortars (Tammam, 2012). There is a difference in actual deformation of the mortars upon triaxial loading, however not to such an extent that it can account for the large difference in deformability of the masonry. Since the difference in deformability for the different types of masonry apparently cannot be attributed to the material behavior of the mortar, the explanation has necessarily to be found in the composite nature of the masonry where the triaxial interaction occurs as a result of the brick-mortar interaction. As said before, the ultimate state of the masonry upon

failure is determined by the tensile strength of the brick or natural stone and/or the shear strength on the brick/stone-mortar interface. The development of the stresses and strains upon loading a masonry wall can, for the moment being, not be explained. However, based on the present analysis of the triaxial behavior of the mortar, the ultimate state of the masonry at the moment of failure of the brick can be examined.

When the masonry fails, the lime mortar, therefore, behaves as an elasto-plastic material with an activated pore collapse mechanism. Hence, large deformations of the mortar, and consequently the masonry, can be observed. The lime-cement mortar, on the other hand, is situated at a κ-value of around 0.15 on the verge of the plastic-viscous material behavior. Around peak stress already to some extent an increased plastic deformation of the mortar occurs, however without the initiation of the pore collapse mechanism. No cement mortars were tested, due to the high strength of the mortar in respect to the attainable confining pressure within the triaxial test apparatus. From the knowledge gained in the study of the three other mortar types and the ultimate strength of the cement mortar in uniaxial compression (15 MPa), an imaginary envelope in the triaxial yield criterion can be imagined, intersecting both axes at $\sigma_h = \sigma_v$ = 15 MPa. The ultimate state of the masonry will in such a case be defined by a triaxial state of compression with κ around 0.05 to 0.10, where the cement mortar is thus a more or less brittle material with only the elastic deformation being addressed. This agrees with earlier test results on masonry walls, where for lime-based bedding mortars important plastic deformations were recorded, before collapse of the masonry structure, and none for the masonry structures based on pure cement bedding mortars. The increase in deformability of the different types of masonry is thus not explained by the difference in elastic properties of the mortar, but rather by a difference in material behavior when applied in the composite masonry. The issue of mechanical compatibility, upon applying new materials in historic masonry, therefore, should not focus on maximizing the strength characteristics of the new material, but instead turn to the evocation of the plastic material behavior in triaxial compression. Weaker mortars will be able to address their plastic deformation much more, compared to stronger mortars, before subjecting the bricks to tensile stresses, which will break the latter. As such the restored masonry will fully employ its ability to adapt to the imposed settlements.

3.3.1. TRIAXIAL FAILURE OF MORTAR (FROM BRITTLE TO ELASTO-PLASTIC DEFORMATION)

There exists a change in material behavior upon triaxial loading. This material is very clear to observe, and it is demonstrated in Figure 5.1 below. The deformations of the mortar are represented in both uniaxial and triaxial loading conditions. From the analysis of the development of the stress strain relationship with an increasing $\frac{\sigma_L}{\sigma_{xx}}$ - ratio – this ratio was denoted as κ. (Hayen, R.; Van Balen, K. & Van Gemert, D.:, 2004).

$$\sigma_L = \frac{\frac{E_{br}}{E_{mo}}\mu_{mo} - \mu_{br}}{(1-\mu_{br}) + (1-\mu_{mo})\frac{E_{br}}{E_{mo}}\frac{h_{br}}{h_{mo}}}\sigma_{xx} \qquad 3.1$$

$$K = \frac{\sigma_L}{\sigma_{xx}} = \frac{\frac{E_{br}}{E_{mo}}\mu_{mo} - \mu_{br}}{(1-\mu_{br}) + (1-\mu_{mo})\frac{E_{br}}{E_{mo}}\frac{h_{br}}{h_{mo}}} \qquad 3.2$$

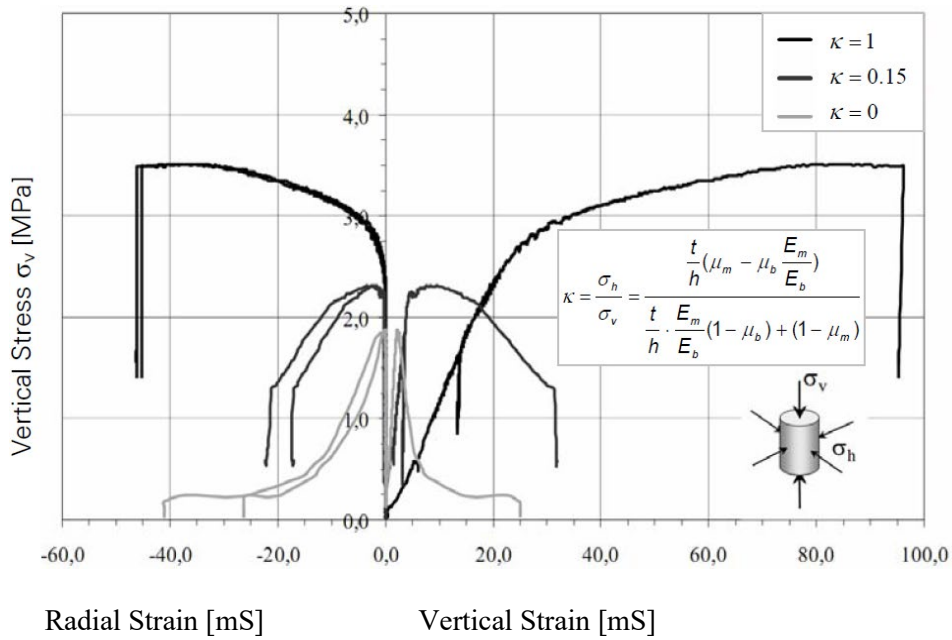

Figure 3.12; Vertical and horizontal deformations in uniaxial and triaxial loading conditions for putty lime mortar, (Hayen et al., 2003).

From equation 3.1 and 3.2, a change in material behavior is observed from brittle in uniaxial loading to a combined elastic and plastic behavior in triaxial loading, from rather low confining pressures up to hydrostatic compression. From κ as low as 0.15 the influence of the rather limited confining pressure is important, resulting initially in some post-peak plastic behavior and gradually, as increases, altering the mechanical behavior to an elasto-plastic material. A similar change in material behavior has been recorded for several other materials such as, e.g., porous chalk, porous sandstone, and concrete.

• an important increase in strength is observed with only a slight increase in the contribution of the horizontal confining pressure on the overall loading condition. This is fairly evident in the graphical representation of the corresponding horizontal and vertical loading conditions at failure, the triaxial yield criterion in the $\sigma_{11} = \sigma_{111} = \sigma_h$ plane, in figure 2.9.

• a tendency towards an increase in deformability in the elastic region at higher κ-values. The collected data is however rather limited and too scattered to formulate a relationship between the change in modulus of elasticity and κ.

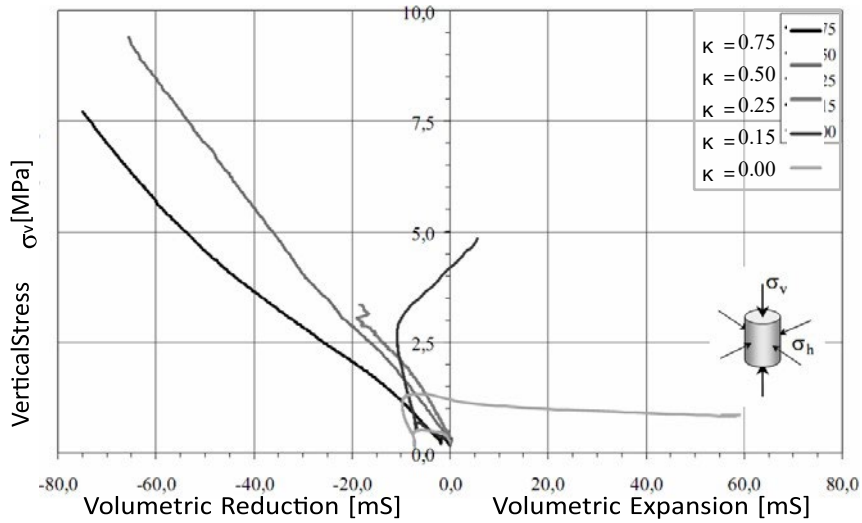

Figure 3.13; Volumetric deformations in uniaxial and triaxial loading conditions for hydraulic lime mortar. (Hayen et al., 2003).

In addition to the traditional tensile-shear failure, the hypothesis of a pore collapse mechanism has been formulated which may be dominant in low-strength mortars. Hayen found that based on the value of k, two modes of failure can be recognized:

when k < 0.25 the tensile-shear mechanism is dominant. This mode is characterized by increasing in volume due to the growth of vertical cracks. The mortar sample collapses along diagonal shear bands.

When k > 0.25 the pore collapse, mechanism was dominant. This mode is characterized by decreasing in volume up to the end of the test. Pore collapse can be understood as multiple internal fractures that lead to compaction of the material in the same way as a granular material. It is characterized by a general loss of cohesion. For many mortar unit combinations, the failure under compression occurs as vertical tensile cracks in the units near the center of the specimen. The major failure of the mortar occurs due to shear-tensile failure but in some cases, pore collapse failure could occur. If the tensile strength of the unit is about 2MPa, this means σ_L = 2Mpa in the mortar just before the failure near the interface. The line σ_b= 2Mpa has been plotted in Figure 16 which intersects the triaxial yield curves for three types of mortars at points A, B, and C.

- The triaxial yield curve for lime-cement mortar at point A has stress coefficient

  k = 0.15, this means the mortar fails due to shear-tensile failure because κ<0.25.

- The triaxial yield curve for hydraulic lime mortar at point B has stress coefficient

K = 0.35, this means the mortar fails due to pore collapse mechanism because

K >0.25.

- The triaxial yield curve for lime putty mortar at point C has stress coefficient k = 0.50,

This means the mortar fails due to pore collapse mechanism because k > 0.25.

The mortar at the edges, where not enough lateral stresses exist, squeezes out of the joints while pore collapse failure occurs for mortar at middle.

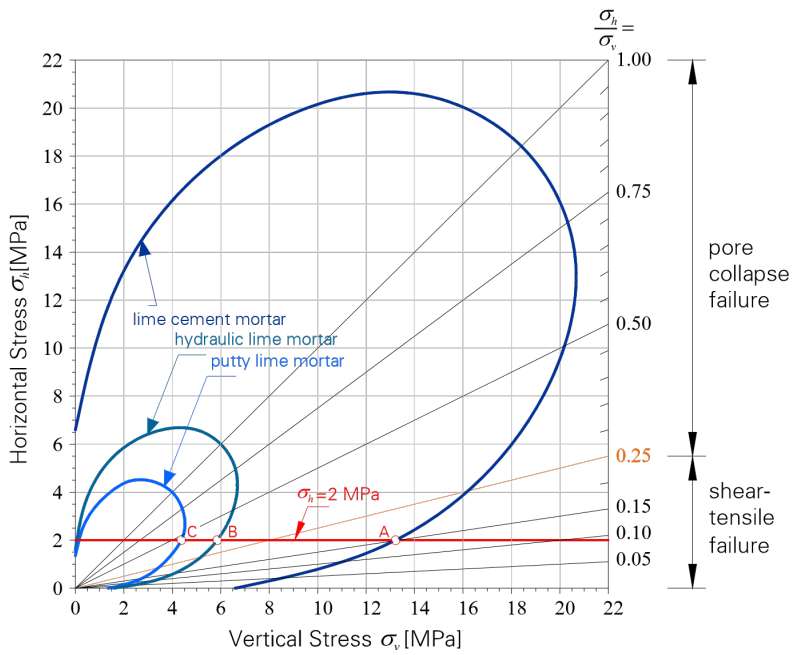

Figure 3.14; Triaxial yield criterion for mortar. Drawn according to (Hayen et al., n.d.)

3.3.2. FAILURE MECHANISM IN CIRCULAR HOLE INFINITE PLATE

The occurrence of intersecting diagonal shear bands in uniaxial vertical compression is generally attributed to the formation of a network of interacting vertical cracks, which are induced by the stress concentrations occurring around pores, anomalies, or existing flaws within the internal structure of the mortar upon compression (figure 2.32). The analytical solution for the 2-dimensional stress distribution surrounding a circular hole in an infinite plate is well known. The structural discontinuity of the hole leads to the occurrence of both compressive and tensile stress concentrations at its edge. In uniaxial compression, a compressive stress, 3 times the applied uniaxial stress, appears at the holes' edges in a direction perpendicular to the externally applied stress, while tensile stresses, in absolute value equal to the applied stress, occur at the holes' edges parallel to the loading direction. The occurrence of such tensile stresses in

a low tensile strength material leads gradually, as the external loads increase, to the formation of an increasing number of cracks parallel to the applied load at pores, anomalies, and existing flaws within the mortar structure. The mechanical interaction of these individual cracks finally leads to the occurrence of diagonal shear bands, inducing failure of the mortar sample.

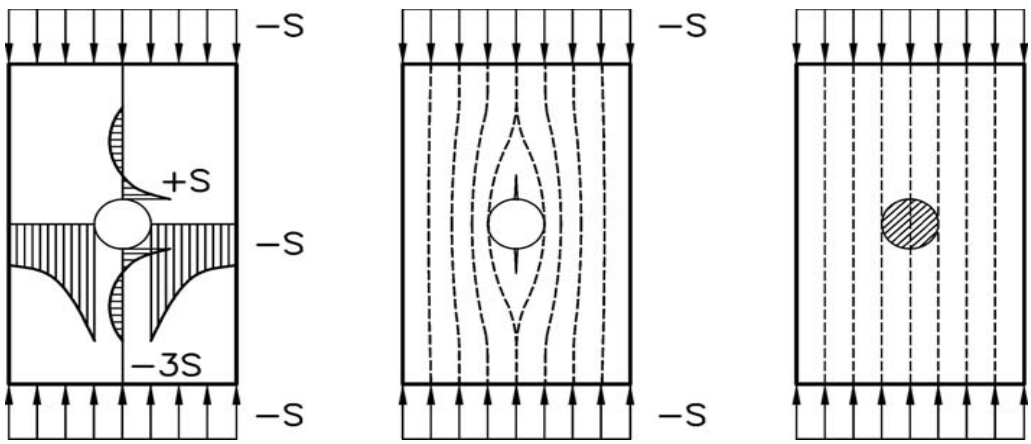

Figure 3.15; Stress distribution and the onset of crack formation for a circular hole in an infinite plate in uniaxial compression

In the case of a triaxial loading condition, the horizontal confinement will of course counteract the horizontal tensile stresses induced by the main 'vertical' load. Returning to the analytical solution of the stress distribution around a hole, one can determine that at a kappa value of 0.25 the maximum tensile stress at the holes' edge has already diminished considerably. For a crack to form and the adhered shear band to develop, the main 'vertical' load must increase accordingly. At a kappa value of 1/3, the tensile stresses within the holes' neighborhood even disappear completely. Hence, failure along shear bands becomes impossible. Regarding the fact that the internal structure of a material always presents at least some tensile strength, the formation of shear bands will practically be already inhibited at a somewhat earlier stage.

3.4. GENERALIZED FAILURE MODEL (NUMERICAL MODEL)

Masonry is also usually described as a material exhibiting distinct directional properties due to the mortar joints, which act as planes of weakness. This description of material is associated mostly with the material, whereas a different material description can be given at structural level. These descriptions are briefly reviewed below.

In general, the approach towards the numerical representation of masonry can address the micro modelling of the individual components, namely. unit (brick, block, etc.) and mortar, or the macro modelling of masonry as a composite, (Rots, 1988). Depending on the level of accuracy and the simplicity desired, it is possible to use the following modelling strategies, see Figure 2.33: Detailed micro-modelling - units and mortar in the joints are represented by continuum elements whereas the unit-mortar interface is represented by discontinuum elements.

Simplified micro-modelling - expanded units are represented by continuum elements whereas the behavior of the mortar joints and unit-mortar interface is lumped in discontinuum elements; Macro-modelling - units, mortar and unit-mortar interface are smeared out in a homogeneous continuum. In fact, the term "micro-modelling" is probably not the most adequate and the term "meso-modelling" would be more reasonable, leaving the former designation for approaches at a lower scale. But the terms macro and micro-modelling are now widely accepted by the masonry community (Kenan, 2012).

The state of art knowledge on the failure models of masonry under compression shows the following lacking points:

- The failure models consider the shear-tension failure in mortar to define the failure model of mortar but not the pore collapse case.

- The failure models are developed for the case when the stiffness of the unit higher than the stiffness of the mortar, e.g., in the failure model of Berndt, it is assumed that E_{br}/μ- The failure models don't consider hollow or vertical perforated units.

The above-mentioned points need to be implemented in a generalized failure model. Based on the current state of mortar triaxial behavior such generalized model is possible to be established with minimum number of experiments by using the advanced numerical tools. After appropriate modelling of the mortar, unit, and interface materials, parametric study can be performed to study the influence of different parameters on the compression strength of masonry.

In the following a sample model is calculated to check the capabilities of available numerical tools to capture all post failure behaviors under compression. The model consists of two hollow clay bricks with thin layer mortar. The compressive strength of the unit is $f_{c,br}$*=10 N/mm2*, and for the mortar f_{mo}*=7 N/mm2*. The upper and lower surfaces of the units are restrained. The crack formation and spalling of the brick sides fit to the known behavior in compression tests of this type of unit. *b*> E_{mo}/μ_{mo}.

3.4.1. TYPES OF NUMERICAL MODELS

According to many authors, there are different possibilities to solve the problem of modeling masonry. These alternatives depend on how detailed is the modeling, and, as a consequence of that, if the model is able to describe accurately different types of failure (Barbosa et al., 2007). Usually, the alternatives are classified as: detailed micro model, simplified micro model and macro model.

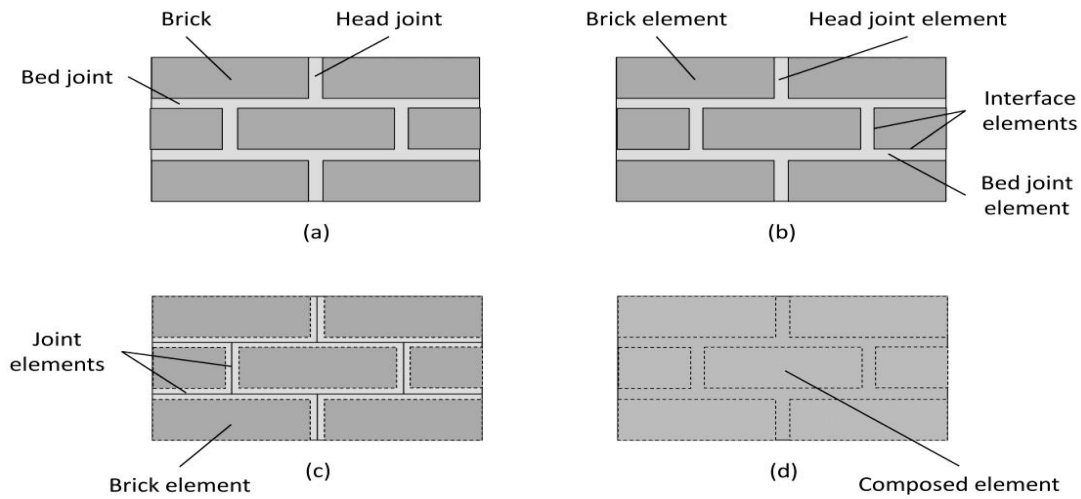

Figure 3.16; (a) Masonry sample and types of models for masonry in (b) detailed micro-modelling, (c) simplified micro-modelling (d) macro modelling (Lourenco, 1996)

The first alternative in describing a masonry model is the "detailed micro model" (Figure 2.33 b). This type of modeling considers bricks and mortar as continuum elements with defined failure criteria. The interface between bricks and mortar is modeled by special elements that represent the discontinuities. In this case, the geometry of the wall is completely reproduced. Because of the level of detail of this model, it is supposed that it can represent most failure mechanisms in masonry.

In the second alternative, the "simplified micro model" (Figure 2.33 c), the bricks are kept as in the "detailed micro model", but the mortar joints and interface elements are re-defined as individual elements to represent a contact area. This means that the general geometry is maintained, but the individual elements that represent joints and interface are not able to describe Poisson's effect of mortar over bricks. Because of this last example, some types of failure mechanisms cannot be reproduced in this type of model.

The last alternative is the "macro model" (Figure 2.33 d). In this case, the masonry panel (or a part of it) is considered as a homogeneous element. Because of its characteristics, this type of model should be able to

reproduce the general structural behavior of a masonry panel, but it is not able to reproduce all the types of failure mechanisms.

3.4.2. CONTINUITY AND DISCONTINUUM MODELING

Numerical methods could be either by using continuum or discontinuum models. Standard non-linear continuum models, based on plasticity and cracking, are widely available but such models overestimate the experimental strength of masonry prisms under (Zucchini & Lourenço, 2007)Many parameters and complex microstructure influence these models making it difficult to reproduce test results. Some authors indicate that standard continuum finite element micro-models, based on plasticity and cracking, are capable of obtaining an adequate response of the masonry composite, e.g. (Brencich, A & Gambarotta, 2005) and (Roman & Gomes, 2004)But similar simulations carried out by ((Lourenco, 1996)demonstrated otherwise. Homogenization macro approach overestimates the test results (Zucchini & Lourenço, 2007).

Discontinuum modeling approaches that consider the micro-structure of quasi-brittle materials are therefore needed; available approaches include Finite Element Method with interface elements, discrete element methods and lattice models. For simple geometries under symmetric loading or when the crack path is known in advance from experiments, interface elements can be embedded in the finite element mesh along expected crack paths, (Rots, 1988). If the crack pattern is not known in advance, expensive remeshing techniques, (Ingraffea & Saouma, 1985), or approaches where a sufficient number of interface elements are included in the mesh to account for potential crack paths, (Carol et al., 2001), may be adopted. Typical applications of interface elements in the finite element analysis of masonry structures are the modeling of cracking, slipping or crushing planes, like unit-mortar interfaces or potential cracks in the units, see (Lotfi & Shing, 1994) and (Lourenco, P.B. & Rots, 1997). It should be distinguished between the distinct element method pioneered by (Cundall, 1971)and the discontinuous deformation analysis originally developed by (Shi, 1988). Recently, a lattice-type model has been proposed by (Bazant, 2014) aiming at a correct simulation of both tensile and compressive fracture processes, as well as three-dimensional effects.

3.5. ESTIMATION OF ELASTICITY MODULUS AND SHEAR MODULUS OF MASONRY

To proceed the derivation of tensile/compressive cracking strength of masonry using energy criterion, we will first estimate the modulus of elasticity of masonry composite from the elastic modulus of its components and as well its shear modulus.

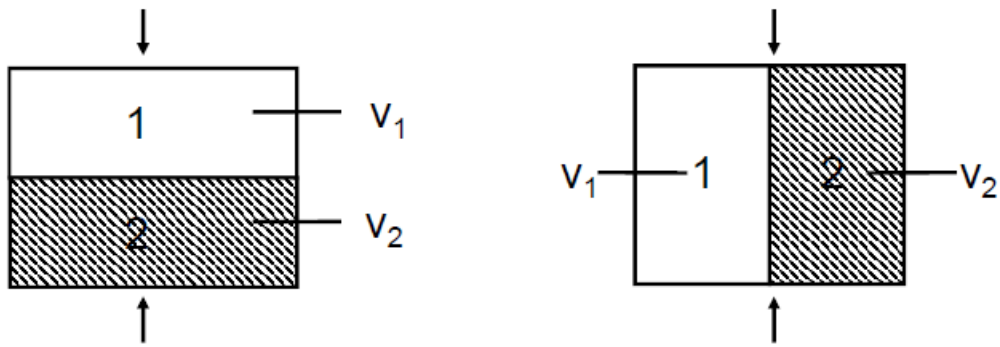

Figure 3.17a; Serial arrangement ('soft'). *3.17b; Parallel arrangement ('stiff').*

Basic models of the theory of composite materials: masonry composite elastic modulus can be computed using either serial or parallel arrangement of its constituents. Or longitudinal and transverse loading orientation.

3.5.1. ESTIMATION OF ELASTIC MODULUS OF MASONRY IN SERIES ARRANGEMENT

First, we introduce volume fraction for the two components, $v_{f,br}$, $v_{f,mo}$

$$v_{f,br} = \frac{V_{br}}{V_{ma}} = \frac{A_{br}}{A_{Ma}} = \frac{h_{br}}{h_{ma}} \qquad 3.3$$

and

$$v_{f,mo} = \frac{V_{mo}}{V_{Ma}} = \frac{A_{mo}}{A_{Ma}} = \frac{h_{mo}}{h_{Ma}} \qquad 3.4$$

$$v_{f,br} + v_{f,mo} = 1 \qquad 3.5$$

Serial arrangement ('soft') loaded in the longitudinal direction (Reuss model)

When a unidirectional masonry composite is loaded longitudinal, the stress in the masonry direction is given as, $\sigma_{yy,Ma}$. The strain $\varepsilon_{yy,Ma}$ will be proportional to the applied stress $\sigma_{yy,Ma}$.

To estimate the transverse modulus, we use a block model with constraints i.e., well bounded components with similar Poisson ratios, and no visco-elastic response from the composite. The simplest model assumes that the mortar and the brick carry the same stress, this is iso – stress model.

$$\sigma_{yy,Ma} = \sigma_{yy,br} = \sigma_{yy,mo} \qquad 3.6$$

And the extension of the model is the sum of the extensions of the two components.

$$\Delta h_{Ma} = \Delta h_{br} + \Delta h_{mo} \qquad 3.7$$

Recall from hook's law that $\varepsilon = \frac{\Delta h}{h}$, and substituting $\Delta h = \varepsilon.h$ into equation 3.7

$$\varepsilon_{yy,Ma} h_{Ma} = \varepsilon_{yy,br} h_{br} + \varepsilon_{yy,mo} h_{mo} \quad 3.8$$

$$\varepsilon_{yy,Ma} = \varepsilon_{yy,br} \frac{h_{br}}{h_{Ma}} + \varepsilon_{yy,mo} \frac{h_{mo}}{h_{Ma}} \quad 3.9$$

$$\varepsilon_{yy,Ma} = \varepsilon_{yy,br}.\ v_{f,br} + \varepsilon_{yy,mo}.\ v_{f,mo}$$

And $\varepsilon = \frac{\sigma}{E}$, then we have

$$\frac{\sigma_{yy,Ma}}{E_{Ma}} = \frac{\sigma_{yy,br}}{E_{br}} \frac{h_{br}}{h_{Ma}} + \frac{\sigma_{yy,mo}}{E_{mo}} \frac{h_{mo}}{h_{Ma}} \quad 3.10$$

But $\sigma_{yy,Ma} = \sigma_{yy,br} = \sigma_{yy,mo}$ and $h_{Ma} = h_{br} + h_{mo}$

$$\frac{1}{E_{Ma}} = \frac{1}{E_{br}} \frac{h_{br}}{(h_{br}+h_{mo})} + \frac{1}{E_{mo}} \frac{h_{mo}}{(h_{br}+h_{mo})} \quad 3.11$$

$$\frac{1}{E_{Ma}} = \frac{E_{mo} h_{br} + E_{yy,br} h_{mo}}{E_{br}.E_{mo}.(h_{br}+h_{mo})}$$

$$E_{Ma} = \frac{E_{br}.E_{mo}.(h_{br}+h_{mo})}{E_{mo} h_{br} + E_{br} h_{mo}} \quad 3.12$$

where.

h_{br} = height of the brick

h_{mo} = height of the mortar

h_{Ma} = height of the masonry

A_{br} = area of the brick

A_{mo} = area of the mortar

A_{Ma} = area of the masonry

$V_{br} = v_1$ = volume of the brick

$V_{ma} = v_2$ = volume of the mortar

V_{Ma} = volume of the masonry

$v_{f,br}$ = volume fractions of the brick

$v_{f,mo}$ = volume fractions of the mortar

$\sigma_{yy,br}$ = longitudinal stress in the brick in the series arrangement

$\sigma_{yy,mo}$ = longitudinal stress in the mortar in the series arrangement

$\sigma_{yy,Ma}$ = longitudinal stress in the masonry in the series arrangement

Δh_{br}= deformation in the brick

Δh_{mo} = deformation in the unit

Δh_{Ma} = total deformation of the masonry

$\varepsilon_{yy,br}$= longitudinal strain in the brick in the series arrangement

$\varepsilon_{yy,mo}$ = longitudinal strain in the mortar in the series arrangement

$\varepsilon_{yy,Ma}$ = longitudinal strain in the masonry in the series arrangement

E_{mo} = elasticity modulus of brick

E_{br} = elasticity modulus of the unit

E_{Ma} = elasticity modulus of the masonry

3.5.2. ESTIMATION OF ELASTICITY MODULUS OF MASONRY IN PARALLEL ARRANGEMENT

Parallel arrangement ('stiff') loaded in longitudinal direction (Voigt model), or serial arrangement loaded transversely i.e., either x-direction or out of plane normal stress z-direction

To estimate the transverse modulus, we use a block model with constraints i.e., well bounded components with similar Poisson ratios, and no visco-elastic response from the composite. This is iso – strain model such that,

$$\varepsilon_{xx,Ma} = \varepsilon_{xx,br} = \varepsilon_{xx,mo} \qquad 3.13$$

But the force carried by the individual component are not the same and the total force is the sum of the force carried by components.

$$F_{Ma} = F_{br} + F_{mo} \qquad 3.14$$

From $\sigma = \frac{F}{A}$ and putting $F = \sigma A$ into equation 3.14

$$\sigma_{xx,Ma} A_{Ma} = \sigma_{xx,br} A_{br} + \sigma_{xx,mo} A_{mo} \qquad 3.15$$

$$\sigma_{xx,Ma} = \sigma_{xx,br}\frac{A_{br}}{A_{Ma}} + \sigma_{mo}\frac{A_{mo}}{A_{Ma}} \quad 3.16$$

$$\sigma_{xx,Ma} = \sigma_{xx,br}.\ v_{f,br} + \sigma_{xx,mo}.\ v_{f,mo}$$

From Hook's law, $\sigma = \varepsilon.E$, we have

$$E_{Ma}\varepsilon_{xx,Ma} = E_{br}\varepsilon_{br}\ v_{f,br} + E_{mo}\varepsilon_{xx,mo}\ v_{f,mo} \quad 3.17$$

$$E_{Ma}\varepsilon_{xx,Ma} = E_{br}\varepsilon_{xx,br}.\frac{h_{br}}{h_{Ma}} + E_{mo}\varepsilon_{xx,mo}.\frac{h_{mo}}{h_{Ma}} \quad 3.18$$

But $\varepsilon_{Ma} = \varepsilon_{xx,br} = \varepsilon_{xx,mo}$ and $h_{Ma} = h_{br} + h_{mo}$

$$E_{Ma} = E_{br}.\frac{h_{br}}{(h_{br}+h_{mo})} + E_{xx,mo}.\frac{h_{mo}}{(h_{br}+h_{mo})}$$

$$E_{Ma} = \frac{E_{br}\ h_{br} + E_{mo}\ h_{mo}.}{(h_{br}+h_{mo})} \quad 3.19$$

where.

$F_{xx,br}$ = force carried by the brick

$F_{xx,mo}$ = force carried by the mortar

$F_{xx,Ma}$ = total force of the masonry

$\sigma_{xx,br}$ = transverse stress in the brick in parallel arrangement

σ_{xxmo} = transverse stress in the mortar in parallel arrangement

$\sigma_{xx,Ma}$ = transverse stress in the masonry in parallel arrangement

$\varepsilon_{xx,br}$= transverse strain in the brick in parallel arrangement

$\varepsilon_{xx,mo}$ = transverse strain in the mortar in parallel arrangement

$\varepsilon_{xx,Ma}$ = transverse strain in the masonry in parallel arrangement

E_{mo} = elasticity modulus of brick

E_{br} = elasticity modulus of the unit

E_{Ma} = elasticity modulus of the masonry

Note: For out of plane normal stress, z-z axis

$$E_{Ma} = .\frac{E_{br}\ h_{br} + E_{mo}\ h_{mo}}{(h_{br}+h_{mo})} \quad 3.20$$

3.5.3. ESTIMATION OF IN PLANE SHEAR MODULUS OF MASONRY G_{xy} IN SERIES

When a unidirectional masonry composite is loaded by in plane shear force, it distorts to a parallelogram. The shear stress in the masonry direction, τ_{xy}. The simplest model assumes that the mortar and the brick carry the same shear stress. The shear strain γ will be proportional to the applied shear stress τ_{xy}.

Serial arrangement ('soft') or loading in transverse direction; to estimate the transverse modulus, we use a block model with constraints i.e., well bounded components with similar Poisson ratios, and no visco-elastic response from the composite. This is iso – stress model such that.

$$\tau_{xy,Ma} = \tau_{xy,br} = \tau_{xy,mo} \qquad 3.21$$

And the shear deformations in the individual component are not the same and the total shear deformation is the sum of the components' deformations.

$$\Delta_{xy,Ma} = \Delta_{xy,br} + \Delta_{xy,mo} \qquad 3.22$$

Recall that $\gamma = \frac{\Delta}{h} = \tan\emptyset$, and substituting $\Delta = \gamma.h$, into equation 2.4

$$\gamma_{xy,Ma} h_{Ma} = \gamma_{xy,br}\, h_{br} + \gamma_{xy,mo} h_{br} \qquad 3.23$$

$$\gamma_{xy,Ma} = \gamma_{xy,br} \frac{h_{br}}{h_{Ma}} + \gamma_{xy,mo} \frac{h_{mo}}{h_{Ma}} \qquad 3.24$$

$$\gamma_{xy,Ma} = \varepsilon_{xy,br}.\, v_{f,br} + \varepsilon_{xy,mo}.\, v_{f,mo}$$

Also $\gamma_{xy} = \frac{\tau_{xy}}{G_{xy}}$, then we have

$$\frac{\tau_{xy,Ma}}{G_{xy,Ma}} = \frac{\tau_{xy,br}}{G_{xy,br}} \frac{h_{br}}{h_{Ma}} + \frac{\tau_{xy,mo}}{G_{xy,mo}} \frac{h_{mo}}{h_{Ma}} \qquad 3.25$$

But $\tau_{xy,Ma} = \tau_{xy,br} = \tau_{xy,mo}$ and $h_{Ma} = h_{br} + h_{mo}$

$$\frac{1}{G_{xy,Ma}} = \frac{1}{G_{xy,br}} \frac{h_{br}}{(h_{br}+h_{mo})} + \frac{1}{G_{xy,mo}} \frac{h_{mo}}{(h_{br}+h_{mo})} \qquad 3.26$$

$$\frac{1}{G_{xy,Ma}} = \frac{G_{xy,mo} h_{br} + G_{xy,br} h_{mo}}{G_{xy,br}.G_{xy,mo}.(h_{br}+h_{mo})}$$

$$G_{xy,Ma} = \frac{G_{xy,br}.G_{xy,mo}.(h_{br}+h_{mo})}{G_{xy,mo} h_{br} + G_{xy,br} h_{mo}} \qquad 3.27$$

3.5.4. ESTIMATION OF IN PLANE SHEAR MODULUS OF MASONRY G_{xy} IN PARALLEL

Parallel arrangement ('stiff') loaded in longitudinal direction,

Here the loading is longitudinal, the strains in the two volume fractions are equal i.e., Iso-strain,

$$\gamma_{xy,Ma} = \gamma_{xy,br} = \gamma_{xy,mo} \qquad 3.28$$

But the shear force carried by the individual components is not the same i.e., the total force is the sum of the force carried by components.

$$F_{xy,Ma} = F_{xy,br} + F_{xy,mo} \qquad 3.29$$

From $\tau_{xy} = \frac{F_{xy}}{A}$ and putting $F_{xy} = \tau_{xy}A$ into equation 5.27

$$\tau_{xy,Ma}A_{Ma} = \tau_{xy,br}A_{br} + \tau_{xy,mo}A_{mo} \qquad 3.30$$

$$\tau_{xy,Ma} = \tau_{xy,br}\frac{A_{br}}{A_{Ma}} + \tau_{xy,mo}\frac{A_{mo}}{A_{Ma}} \qquad 3.31$$

$$\tau_{xy,Ma} = \tau_{xy,br}.\ v_{f,br} + \tau_{xy,mo}.\ v_{f,mo}$$

From Hook's law $\tau_{xy} = \gamma_{xy}.G_{xy}$, we have

$$G_{xy,Ma}\gamma_{xy,Ma} = G_{xy,br}\gamma_{br}\ v_{f,br} + G_{xy,mo}\gamma_{xy,mo}\ v_{f,mo}$$

$$G_{xy,Ma}\gamma_{xy,Ma} = G_{xy,br}\gamma_{xy,br}.\frac{h_{br}}{h_{Ma}} + G_{xy,mo}\gamma_{xy,mo}.\frac{h_{mo}}{h_{Ma}} \qquad 3.32$$

But $\gamma_{xy,Ma} = \gamma_{xy,br} = \gamma_{xy,mo}$ and $h_{Ma} = h_{br} + h_{mo}$

$$G_{xy,Ma} = G_{xy,br}.\frac{h_{br}}{(h_{br}+h_{mo})} + G_{xy,mo}.\frac{h_{mo}}{(h_{br}+h_{mo})}$$

$$G_{xy,Ma} = \frac{G_{xy,br}\ h_{br} + G_{xy,mo}\ h_{mo}.}{(h_{br}+h_{mo})} \qquad 3.33$$

where.

$F_{xy,Ma}$= transverse loading (in series) or longitudinal (in parallel) in plane shear force in the masonry

$F_{xy,br}$ = transverse loading (in series) or longitudinal (in parallel) in plane shear force in the brick

$F_{xy,mo}$ = transverse loading (in series) or longitudinal (in parallel) in plane shear force in the mortar

$\tau_{xy,br}$ = transverse loading (in series) or longitudinal (in parallel) in plane shear stress in the brick

$\tau_{xy,mo}$ = transverse loading (in series) or longitudinal (in parallel) in plane shear stress in the mortar

$\tau_{xy,Ma}$ = transverse loading (in series) or longitudinal (in parallel) in plane shear stress in the masonry

$\Delta_{xy,br}$ = in plane shear deformation in the brick

$\Delta_{xy,mo}$ = in plane shear deformation in the unit

$\Delta_{xy,Ma}$ = total in plane shear deformation of the masonry

$\gamma_{xy,br}$= transverse loading (in series) or longitudinal (in parallel) in plane shear strain in the brick

$\gamma_{xy,br}$ = transverse loading (in series) or longitudinal (in parallel) in plane shear strain in the mortar

$\gamma_{xy,br}$ = transverse loading (in series) or longitudinal (in parallel) in plane shear strain in the masonry

$G_{xy,br}$ = transverse loading (in series) or longitudinal (in parallel) in plane shear elastic modulus of the brick

$G_{xy,mo}$ = transverse loading (in series) or longitudinal (in parallel) in plane shear elasticity modulus of the unit

$G_{xy,Ma}$ = transverse loading (in series) or longitudinal (in parallel) in plane shear elastic modulus of the masonry

Note: for out of plane shear (y-z or z-x direction), we use out of plane shear stress and out of plane loading in a similar approach to estimate the shear modulus of masonry, we will have,

$\tau_{yz,Ma} = \tau_{yz,br} = \tau_{yz,mo}$ and $\gamma_{yz,Ma} = \gamma_{yz,br}\frac{h_{br}}{h_{Ma}} + \gamma_{yz,mo}\frac{h_{mo}}{h_{Ma}}$

$$G_{yz,Ma} = \frac{G_{yz,br}.G_{yz,mo}.(h_{br}+h_{mo})}{G_{yz,mo}h_{br} + G_{yz,br}h_{mo}} \quad 3.34$$

Out of plane in z-x direction

$\tau_{zx,Ma} = \tau_{zx,br} = \tau_{zx,mo}$ and $\gamma_{zx,Ma} = \gamma_{zx,br}\frac{h_{br}}{h_{Ma}} + \gamma_{zx,mo}\frac{h_{mo}}{h_{Ma}}$

$$G_{zx,Ma} = \frac{G_{zx,br}.G_{zx,mo}.(h_{br}+h_{mo})}{G_{zx,mo}h_{br} + G_{zx,br}h_{mo}} \quad 3.35$$

where.

$\tau_{yz,mo}$ and $\tau_{zx,mo}$= longitudinal and transverse out of plane shear stress in the brick

$\tau_{yz,br}$ and $\tau_{zx,br}$ longitudinal and transverse out of plane shear stress in the mortar

$\tau_{yz,Ma}$ and $\tau_{zx,Ma}$= longitudinal and transverse out of plane shear stress in the masonry

$\Delta_{yz,br}$ and $\Delta_{zx,Ma}$= longitudinal and transverse out of plane shear deformation in the brick

$\Delta_{yz,mo}$ and $\Delta_{zx,Ma}$= longitudinal and transverse out of plane shear deformation in the unit

Δ_{yzMa} and $\Delta_{zx,Ma}$= total longitudinal and transverse out of plane shear deformation of the masonry

$\gamma_{yz,br}$ and $\gamma_{zx,br}$ = longitudinal and transverse out of plane strain in the brick

$\gamma_{yz,br}$ and $\gamma_{zx,br}$= longitudinal and transverse out of plane shear strain in the mortar

$\gamma_{yz,br}$ and $\gamma_{zx,br}$= longitudinal and transverse out of plane shear strain in the masonry

$G_{yz,br}$ and $G_{zx,Ma}$= longitudinal and transverse out of plane elasticity modulus of brick

$G_{yz,mo}$ and $G_{zx,Ma}$ = longitudinal and transverse out of plane elasticity modulus of the unit

$G_{yz,Ma}$ and $G_{zx,Ma}$= longitudinal and transverse out of plane elasticity modulus of the masonry

4. EMPIRICAL ESTIMATION OF COMPRESSIVE STRENGTH OF MASONRY

A concentrically loaded masonry wall shows considerable vertical cracking before failure. The first cracks appear at a load of roughly half the ultimate load. High strength mortar seems to delay the cracking. At failure the wall exhibits numerous cracks and is often divided into several separate "columns" at mid height. The reason for the vertical cracking is well agreed upon. When the masonry is loaded, the bricks and the mortar expand laterally; but since the mortar expands more than the bricks, the bricks are tensioned laterally. The mortar has usually also been "crushed" before the wall fails, and it is prevented from squeezing out of the bed joints by the bricks. This induces a triaxial state of stress in the bricks: vertical compression and bidirectional tension. Many attempts have been made to formulate the relationship between the strength of the masonry and the unit and mortar strengths. Most of these formulas are, however, not fully based on the fundamental triaxial state of stress in both the bricks and the mortar. Compression strength of masonry in the direction normal to the bed joints is the most relevant structural material property of masonry structures. Here the approaches of codes, numerical and analytical methods are briefly presented and evaluated.

4.1. CODES APPROACH (EC6 (DIN EN 1996-1-1, EC 6:1-1, 2013)

The present approach in codes, e.g., European code Eurocode 6 (DIN EN 1996-1-1, Eurocode 6:1-1, 2013)and American code (ACI 530.1-02, 2004), is to make the compressive strength of the masonry composite dependent of the compressive strength of the masonry components (units and mortar). These empirical approaches depending on many experimental tests under-estimate the compressive strength of masonry since it is resulted from the lower envelope of the failure database, representing the decisive subgroup of units in the group defined according to table 3.3 of Eurocode 6. Comparing the results of these codes with test results showed in some cases conservative results up to 40% of test results (Zucchini & Lourenço, 2007). Carrying out tests according to DIN EN 1052-1 (DIN EN 1052-1:1998, 1998) to get the compressive strength of masonry then following the formulas given in Eurocode 6 is expensive and requires many specimens.

EC6 (DIN EN 1996-1-1, Eurocode 6:1-1, 2013): The recognized norm to calculate the masonry strength is (DIN EN 1996-1-1, Eurocode 6:1-1, 2013). This German/European norm is a substitute of (DIN 1053-1, 1996)(DIN 1053-3, 1990) and (DIN 1053-2, 1996), which was foreseen to estimate masonry strength based on tests is cancelled without a substitute. This norm estimates the characteristic masonry compression strength, which is later reduced by using the material safety factor. The material safety factor ranges between 1.5 and 3.0 (chapter 2.4.3 of the EC6).

The characteristic masonry compression strength is estimated based on the mechanical properties of its components. The characteristic compression strength can be determined using possibility (ii) of clause (2) in chapter 3.6.1.2 in EC6 (DIN EN 1996-1-1) for masonry with general purpose mortar and light weight mortar equation (3.1a), for masonry with thin layer mortar and clay units of Group 1 and 4 equation (3.1b), and for masonry with thin layer mortar and clay units of Group 2 and 3 equation (3.1c).

$$f_{k,Ma} = K . f_{c,br}^{0.7} . f_{c,mo}^{0.3} \quad 4.1a$$

$$f_{k,Ma} = K . f_{c,br}^{0.85} \quad 4.1b$$

$$f_{k,Ma} = K . f_{c,br}^{0.7} \quad 4.1c$$

where.

$f_{k,Ma}$ = is the characteristic masonry compression strength in N/mm2

K = is constant; it is taken from Table 4.1 below for general purpose mortar, thin bed mortar and light weight mortar.

$f_{c,br}$ = is normalized brick compression strength in the load direction in N/mm2 ≤ 75N/mm^2 in case of general-purpose mortar, and ≤ 50 N/mm^2 in case of thin bed mortar. To get the normalized brick compression strength $f_{k,Ma}$ the compression strength of the brick $f_{c,Br}$ must be multiplied by a normalizing factor δ taken from DIN EN 772-1.

$f_{c,mo}$ = is mortar compression strength in N/mm^2 ≤ 20 N/mm^2 or 2 in case general purpose mortar, and ≤ 10 N/mm^2 in case of light weight mortar.

Alternative, 'I' can also be chosen in the National Annex to calculate the characteristic strength with variable exponents α and β of $f_{c,br}$ and $f_{c,mo}$ where the exponents should be given nationally.

Table 4.1; Values of K

Type of brick		General purpose mortar	Thin bed mortar (0,5-3mm)	Light weight mortar with dry density	
Clay brick	Group 1	0,55	0,75	0,30	0,40
	Group 2	0,45	0,70	0,25	0,30
	Group 3	0,35	0,50	0,20	0,25
	Group 4	0,35	0,35	0,20	0,25
Lime sand brick	Group 1	0,55	0,80	ł	ł
	Group 2	0,45	0,65	ł	ł
Concrete	Group 1	0,55	0,80	0,45	0,45
	Group 2	0,45	0,65	0,45	0,45
	Group 3	0,40	0,50	ł	ł
	Group 4	0,35	ł	ł	ł
porous concrete	Group 1	0,55	0,80	0,45	0,45
artificial stone	Group 1	0,45	0,75	ł	ł
Size controlled natural brick	Group 1	0,45	ł	ł	ł
ł no value available because this brick-mortar combination is not used.					

Note: Type and thickness of mortar influence the result of the equation (4.1.a) through the value of the factor K. Mortar compression strength is considered as a factor $f_{c,mo}$ with exponent 0.3 in case of general-purpose mortar.

4.2. ANALYTICAL APPROACH

The basic work on failure model of masonry under compression has been defined by (Hilsdorf, 1969) who introduced in his formulae the friction between mortar and units during compression failure due to the mortar deformation.

Later on, (Hilsdorf, 1969) Berndt developed this fact further and described the strength of masonry on the basis of the cohesion and the angle of inner friction of the mortar as well as of the tensile (splitting) strength of the units. This was done exemplarily for masonry made of Saxon sandstone and lime or lime-cement mortar. The formulae allowed considering different mechanical characteristics based on a failure model.

4.2.1. ANALYTICAL FORMULAE

Different lateral strains of both materials lead to tri-axial compression in mortar and compression - tension in brick. These tensile stresses in the unit are the main reason for cracking and failure of the masonry structure.

In this chapter, the engineering model for the case when deformation properties of mortar are greater than those of the unit will be presented. This model has been developed by a series of research projects starting from (Hilsdorf, H.K. 1965) through (Berndt, 1996) until the final formula of (Huster, 2000)

In a similar way, depending on finite element calculations and test observation, an analytical formula was developed to cover the case when deformation properties of unit are greater than those of the mortar. Comparing test results with the calculated results shows the feasibility of the extracted analytical formula.

The general relation between stresses and strains in matrix form is given by:

The specimen of both unit and mortar are assumed to be anisotropic with symmetry in which only two independent elastic parameters exist.

Let σ = stress and ε = strain and E =Elastic modulus, C is 6×6 matrix containing elastic modulus and μ = Poisson's ratio. The distribution of stress and strain in matrix notation is shown below.

$$\sigma = \begin{bmatrix} \sigma_{xx} & \sigma_{xy} & \sigma_{xz} \\ \sigma_{yx} & \sigma_{yy} & \sigma_{yz} \\ \sigma_{zx} & \sigma_{zy} & \sigma_{zz} \end{bmatrix} \qquad 4.2$$

Due to symmetry, $\sigma_{yx} = \sigma_{xy}$, $\sigma_{yz} = \sigma_{yz}$, $\sigma_{zy} = \sigma_{yz}$, the matrix reduces to

$$\sigma = \begin{bmatrix} \sigma_{xx} & \sigma_{xy} & \sigma_{xz} \\ \sigma_{xy} & \sigma_{yy} & \sigma_{yz} \\ \sigma_{xz} & \sigma_{yz} & \sigma_{zz} \end{bmatrix}$$

Transforming into a column matrix, we obtain

$$\sigma = \begin{bmatrix} \sigma_{xx} \\ \sigma_{yy} \\ \sigma_{zz} \\ \sigma_{yz} = \sigma_{zy} \\ \sigma_{zx} = \sigma_{xz} \\ \sigma_{xy} = \sigma_{yx} \end{bmatrix} = \begin{bmatrix} \sigma_{xx} \\ \sigma_{yy} \\ \sigma_{zz} \\ \sigma_{yz} \\ \sigma_{xz} \\ \sigma_{xy} \end{bmatrix} \quad 4.3$$

Subsequently, the strain distribution in the matrix notation is given by.

$$\varepsilon = \begin{bmatrix} \varepsilon_{xx} & 2\varepsilon_{xy} & 2\varepsilon_{xz} \\ 2\varepsilon_{yx} & \varepsilon_{yy} & 2\varepsilon_{yz} \\ 2\varepsilon_{zx} & 2\varepsilon_{zy} & \varepsilon_{zz} \end{bmatrix} \quad 4.4$$

Due to symmetry, $\varepsilon_{yx} = \varepsilon_{xy}$, $\varepsilon_{yz} = \varepsilon_{yz}$, $\varepsilon_{zy} = \varepsilon_{yz}$, the matrix reduces to

$$\varepsilon = \begin{bmatrix} \varepsilon_{xx} & 2\varepsilon_{xy} & 2\varepsilon_{xz} \\ 2\varepsilon_{yx} & \varepsilon_{yy} & 2\varepsilon_{yz} \\ 2\varepsilon_{zx} & 2\varepsilon_{zy} & \varepsilon_{zz} \end{bmatrix}$$

Transforming into a column matrix, we obtain,

$$\sigma = \begin{bmatrix} \varepsilon_{xx} \\ \varepsilon_{yy} \\ \varepsilon_{zz} \\ \varepsilon_{yz} + \varepsilon_{zy} \\ \varepsilon_{zx} + \varepsilon_{xz} \\ \varepsilon_{xy} + \varepsilon_{yx} \end{bmatrix} = \begin{bmatrix} \varepsilon_{xx} \\ \varepsilon_{yy} \\ \varepsilon_{zz} \\ 2\varepsilon_{yz} \\ 2\varepsilon_{zx} \\ 2\varepsilon_{xy} \end{bmatrix} = \begin{bmatrix} \varepsilon_{xx} \\ \varepsilon_{yy} \\ \varepsilon_{zz} \\ \gamma_{yz} \\ \gamma_{zx} \\ \gamma_{xy} \end{bmatrix} \quad 4.5$$

where $2\varepsilon = \gamma$ and γ is Engineering strain.

Reduced C, Elasticity in 6×6 matrix

$$C = \frac{1}{E} \begin{bmatrix} 1 & -\mu & -\mu & 0 & 0 & 0 \\ -\mu & 1 & -\mu & 0 & 0 & 0 \\ -\mu & -\mu & 1 & 0 & 0 & 0 \\ 0 & 0 & 0 & (1+\mu) & 0 & 0 \\ 0 & 0 & 0 & 0 & (1+\mu) & 0 \\ 0 & 0 & 0 & 0 & 0 & (1+\mu) \end{bmatrix} \quad 4.6$$

4.2.2. COMPRESSION STRENGTH IN CASE $E_{br} > E_{mo}$

In this case, we have masonry with stronger unit than mortar. ((Hilsdorf, 1969) and (Hilsdorf, 1965)showed that different lateral strains of brick-and-mortar lead to three-axial compression in mortar, and compression

tension in brick. These tensile stresses in the brick are the main factor in the cracking and failure of the masonry structure.

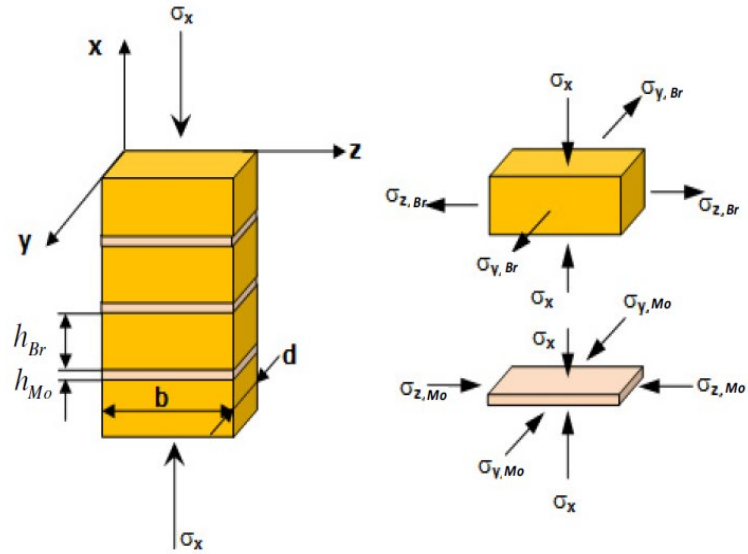

Figure 4.1; Stress state in the masonry components: brick and mortar (Hilsdorf, 1965)

From Hook's law of elasticity, $\varepsilon = \frac{1}{E}\,\sigma$, incorporation of equation (4.2), (4.4) and (4.5), we obtain

$$\begin{bmatrix} \varepsilon_{xx} \\ \varepsilon_{yy} \\ \varepsilon_{zz} \\ \gamma_{yz} \\ \gamma_{zx} \\ \gamma_{xy} \end{bmatrix} = \frac{1}{E}\begin{bmatrix} 1 & -\mu & -\mu & 0 & 0 & 0 \\ -\mu & 1 & -\mu & 0 & 0 & 0 \\ -\mu & -\mu & 1 & 0 & 0 & 0 \\ 0 & 0 & 0 & (1+\mu) & 0 & 0 \\ 0 & 0 & 0 & 0 & (1+\mu) & 0 \\ 0 & 0 & 0 & 0 & 0 & (1+\mu) \end{bmatrix}\begin{bmatrix} \sigma_{xx} \\ \sigma_{yy} \\ \sigma_{zz} \\ \sigma_{yz} \\ \sigma_{xz} \\ \sigma_{xy} \end{bmatrix} \qquad 4.7$$

Solving for first second and third boundaries

$$\varepsilon_{xx} = \frac{1}{E}(\sigma_{xx} - \mu\sigma_{yy} - \mu\sigma_{zz} + 0\sigma_{xy} + 0\sigma_{yz} + 0\sigma_{xz})$$

For x-direction, $\varepsilon_{xx} = \frac{1}{E}\left[\sigma_{xx} - \mu(\sigma_{yy} + \sigma_{zz})\right]$

For y-direction, $\varepsilon_{yy} = \frac{1}{E}\left[\sigma_{yy} - \mu(\sigma_{xx} + \sigma_{zz})\right]$

For z-direction, $\varepsilon_{zz} = \frac{1}{E}\left[\sigma_{zz} - \mu(\sigma_{xx} + \sigma_{yy})\right]$

Parameters for unit (brick).

$$\varepsilon_{yy,br} = \frac{1}{E_{br}}\left[\sigma_{yy,br} - \mu_{br}(\sigma_{xx} + \sigma_{zz,br})\right] \qquad 4.8$$

$$\varepsilon_{zz,br} = \frac{1}{E_{br}}\left[\sigma_{zz,br} - \mu_{br}(\sigma_{xx} + \sigma_{yy,br})\right] \quad 4.9$$

Parameter for mortar.

$$\varepsilon_{yy,mo} = \frac{1}{E_{mo}}\left[\sigma_{yy.mo} - \mu_{mo}(\sigma_{xx} + \sigma_{zz,mo})\right] \quad 4.10$$

$$\varepsilon_{zz,mo} = \frac{1}{E_{mo}}\left[\sigma_{zz,mo} - \mu_{mo}(\sigma_{xx} + \sigma_{yy,mo})\right] \quad 4.11$$

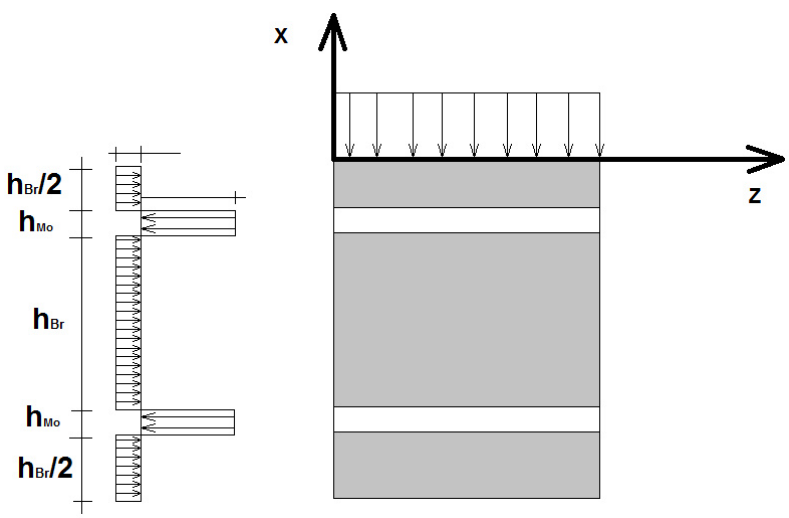

Figure 4.2; Stress distribution in brick and mortar due to compression in masonry

Due to equilibrium, the total results are in the following below.

Lateral compression force in the mortar in y direction equals lateral tensile force in the unit in y direction.

$$f_{yy} = -\sigma_{yy,mo} \cdot h_{mo} = \sigma_{yy,br} \cdot h_{br} \quad 4.12a$$

Lateral compression force in the mortar in z direction equals lateral tensile force in the unit in z direction.

$$f_{zz} = -\sigma_{zz,mo} \cdot h_{mo} = \sigma_{zz,br} \cdot h_{br} \quad 4.12b$$

From the Figure 3.2 below and with considering the different signs $\sigma_{yy,br}$ of and $\sigma_{yy,mo}$ it can be written

$$\sigma_{yy,mo} = -\sigma_{yy,br}\frac{h_{br}}{h_{mo}} \quad 4.13$$

And in a similar way $\sigma_{zz,Br}$ of and $\sigma_{zz,Mo}$, it can be written.

$$\sigma_{zz,mo} = -\sigma_{zz,br}\frac{h_{br}}{h_{mo}} \quad 4.14$$

$$\Rightarrow \sigma_{yy,mo} = \sigma_{zz,mo} = -\sigma_{yy,br}\frac{.h_{br}}{h_{mo}} = -\sigma_{zz,Br}\frac{h_{br}}{h_{mo}}$$

$$\sigma_{yy,br} = \sigma_{zz,br} \text{ and } \sigma_{yy,mo} = \sigma_{zz,mo} \qquad 4.15$$

The compatibility condition implies that transversal strains in brick and mortar are the same:

$$\varepsilon_{yy,br} = \varepsilon_{yy,mo} \qquad 4.16a$$

And

$$\varepsilon_{zz,br} = \varepsilon_{zz,mo} \qquad 4.16b$$

From equation (4.16a), (4.8) and (4.10)

$$\therefore \ \frac{1}{E_{br}}\left[\sigma_{yy,br} - \mu_{br}(\sigma_{xx} + \sigma_{zz,br})\right] = \frac{1}{E_{mo}}\left[\sigma_{yy,mo} - \mu_{mo}(\sigma_{xx} + \sigma_{zz,mo})\right]$$

$$\left[\sigma_{yy,br} - \mu_{br}(\sigma_{xx} + \sigma_{zz,br})\right] = \frac{E_{br}}{E_{mo}}\left[\sigma_{yy,mo} - \mu_{mo}(\sigma_{xx} + \sigma_{zz,mo})\right]$$

$$\sigma_{yy,br} = \frac{E_{br}}{E_{mo}}\left[\sigma_{yy,mo} - \mu_{mo}(\sigma_{xx} + \sigma_{zz,mo})\right] + \mu_{br}(\sigma_{xx} + \sigma_{zz,br}) \qquad 4.17$$

Substituting equation (4.13 and 4.14) in equation (4.17) gives:

$$\sigma_{yy,br} = \frac{E_{br}}{E_{mo}}\left[-\sigma_{yy,br}\frac{h_{br}}{h_{mo}} - \mu_{mo}(\sigma_{xx} - \sigma_{zz,br}\frac{h_{br}}{h_{mo}})\right] + \mu_{br}(\sigma_{xx} + \sigma_{yy,br}) \qquad 4.18$$

By setting,

$$\beta = \frac{E_{br}}{E_{mo}} \text{ and } \eta = \frac{h_{br}}{h_{mo}} \qquad 4.19$$

$$\therefore \ \sigma_{yy,br} = \beta\left[-\sigma_{yy,br}\eta - \mu_{mo}(\sigma_{xx} - \sigma_{zz,br}\eta)\right] + \mu_{br}(\sigma_{xx} + \sigma_{yy,br})$$

$$\sigma_{yy,br} = -\sigma_{yy,br}\beta\eta - \mu_{mo}\sigma_{xx}\beta + \mu_{mo}\sigma_{zz,br}\beta\eta + \mu_{br}\sigma_{xx} + \mu_{br}\sigma_{yy,br}$$

$$\sigma_{yy,br} + \sigma_{yy,br}\beta\eta - \mu_{mo}\sigma_{yy,Br}\beta\eta - \mu_{Br}\sigma_{yy,br} = -\mu_{mo}\sigma_{xx}\beta + \mu_{br}\sigma_{xx}$$

$$\sigma_{yy,br}\ (1 + \beta\eta - \mu_{mo}\beta\eta - \mu_{br}) = (-\mu_{Mo}\beta + \mu_{br})\sigma_{xx}$$

$$\sigma_{yy,br} = \frac{(-\mu_{mo}\beta + \mu_{br})\,\sigma_{xx}}{(1 + \beta\eta - \mu_{mo}\beta\eta - \mu_{br})}$$

$$\sigma_{yy,br} = \frac{(-\mu_{mo}\beta + \mu_{br})}{(1 - \mu_{br} + \beta\eta - \mu_{mo}\beta\eta)}\ \sigma_{xx}$$

$$\sigma_{yy,br} = \frac{-(\mu_{mo}\beta - \mu_{br})}{(1 - \mu_{br}) + (1 - \mu_{mo})\beta\eta)}\sigma_{xx} \qquad 4.20$$

The same for z direction, we already proved that $\sigma_{yy,br} = \sigma_{zz,br}$

$$\sigma_{yy,br} = \sigma_{zz,br} = -\frac{(\mu_{mo}\beta - \mu_{br})}{(1-\mu_{br}) + (1-\mu_{mo})\beta\eta)}\sigma_{xx} \qquad 4.21$$

Hence in summary

$$\sigma_{yy,br} = \sigma_{zz,br} = \sigma_{L1} = -\frac{(\mu_{mo}\frac{E_{br}}{E_{mo}} - \mu_{br})}{\frac{E_{br}}{E_{mo}}\frac{h_{br}}{h_{mo}}(1-\mu_{br}) + (1-\mu_{mo})}\sigma_{xx} \qquad 4.22$$

where

μ_{br} = Poisson's ratio of the brick

μ_{mo} = Poisson's ratio of the mortar

σ_{xx} = vertical stress in the brick (compression)

$\sigma_{yy,br}$ = lateral y stress in the brick (tension)

$\sigma_{zz,br}$ = lateral z stress in the brick (tension)

σ_{L1} =1st lateral stress in the brick (tension) due to different elasticity

E_{br} = E-modulus of the brick,

E_{mo} = E-modulus of the Mortar

h_{mo} = height of the bed joint

h_{br} = height of the brick

Note this equation gives the stresses in the brick, in the case, $E_{br} > E_{mo}$. When $E_{br} < E_{mo}$ we get the same equations. However, with compression stresses instead of tensile stresses in the brick, and tensile stresses in the mortar.

When $E_{br} >> E_{mo}$ or $\frac{E_{br}}{E_{mo}}\mu_{mo} \gg \mu_{br}$, equation (4.22) can be written as (Berndt, 1996):

$$\sigma_{yy,br} = \sigma_{zz,br} = \sigma_{L1} = -\frac{1 - \frac{\mu_{br}}{\frac{E_{br}}{E_{mo}}\mu_{mo}}}{\frac{(1-\mu_{br})}{\frac{E_{br}}{E_{mo}}\mu_{mo}} + (1-\mu_{mo})\frac{1}{\mu_{mo}}\frac{h_{br}}{h_{mo}})}\sigma_{xx}$$

$$\sigma_{yy,br} = \sigma_{zz,br} = \sigma_{L1} = -\frac{1 - \frac{\mu_{br}}{\to\infty}}{\frac{(1-\mu_{br})}{\infty} + (1+\mu_{mo})\frac{1}{\mu_{mo}}\frac{h_{br}}{h_{mo}})}\sigma_{xx}$$

$$\sigma_{yy,br} = \sigma_{zz,br} = \sigma_{L1} = -\frac{1 - 0}{0 + (1-\mu_{mo})\frac{1}{\mu_{mo}}\frac{h_{br}}{h_{mo}})}\sigma_{xx}$$

$$\sigma_{yy,br} = \sigma_{zz,br} = \sigma_{L1} = -\frac{\mu_{mo}}{(1-\mu_{mo})\frac{h_{br}}{h_{mo}}}\sigma_{xx} \qquad 4.23$$

Crumbling away of the bed joint edges leads to additional transverse stresses at the middle of the brick height. The so-called splitting tensile forces are induced by redirecting the vertical forces in the brick and lead to cracking in the middle of the brick (Berndt, 1996) See Figure 4.4 below.

Extracting this force/stress depends on many assumptions; it is assumed that it appears in the middle of the brick height. Where the height of the brick is less than the wall width 2 x d (or 2 x w). From Figure 4.3c, the tangent inclination of the force is:

$$2\alpha = \frac{h'/2}{d} \Rightarrow \alpha = \frac{1}{4}\frac{h'}{d} \qquad 4.24$$

$h' =$ sum of crumbled depths on both sides of the mortar

From Figure 4.3b, we have

$$2\alpha = \frac{Z}{F/2} \Rightarrow \alpha = \frac{Z}{F} \qquad 4.25$$

We generate the splitting force Z equation 4.24 and 4.25.

$$Z = F.\alpha = F\frac{1}{4}\frac{h'}{d} \qquad 4.26$$

By assuming the stress distribution as shown in Figure 4.3d, we have:

$$\sigma_{st,br} = \frac{Z}{h_{br}/2} \qquad 4.27$$

$$F = \sigma_{xx}\ d \qquad 4.28$$

$\sigma_{st,Br}$ = splitting tensile stress in the brick

From 4.26 and 4.27 and then using 4.28, we have.

$$\sigma_{L2} = \sigma_{st,br} = \frac{Z}{h_{br}/2} = \frac{F}{2h_{br}}\frac{h'}{d} = \frac{1}{2}\frac{d}{h_{br}}\frac{h'}{d}\sigma_{xx} \qquad 4.29$$

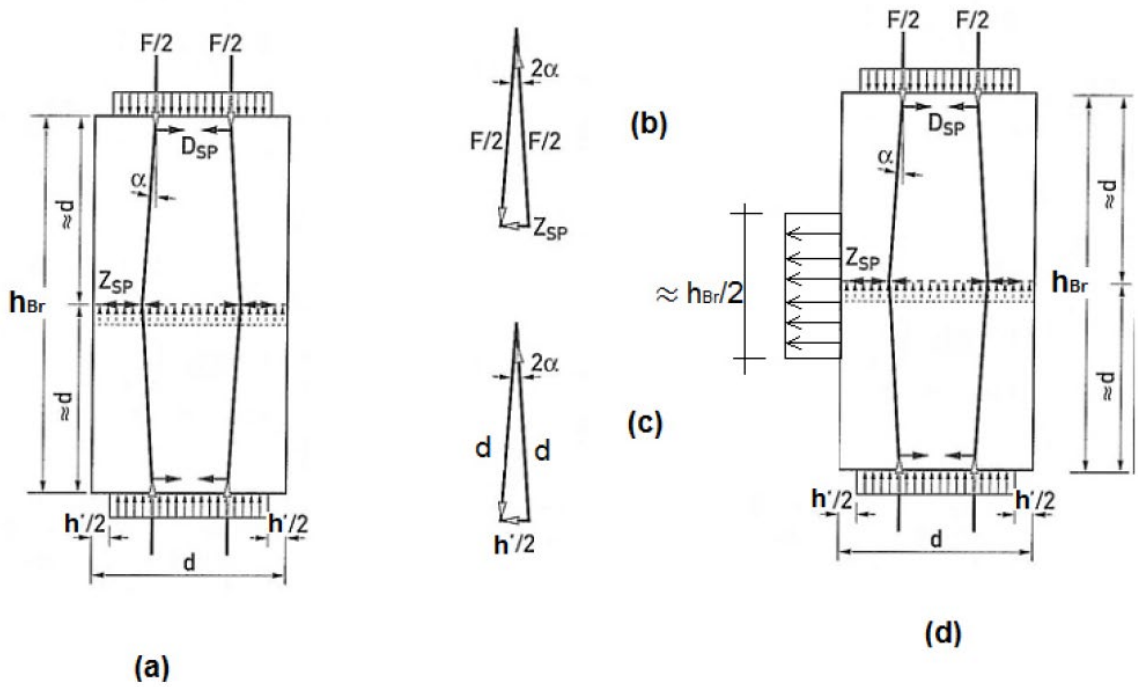

Figure 4.3: Splitting stresses in the brick.

4.3. EMPIRICAL COMPRESSIVE STRENGTH OF MASONRY OF VARIOUS RESEARCH PROJECTS

The first works on failure compression models of units pointed out that the different lateral strains of unit and bed joint mortar, the joint thickness t, and the height of the block h have significant influence on the transverse tensile strength of masonry. (Hilsdorf, 1965) have been derived the stress and deformation state from elasticity equations. The proposed solution was derived by considering a unit-mortar prism subjected to an axial compressive stress σ_{xx}.

4.3.1. FAILURE MODEL OF HILSDORF (HILSDORF, 1965, 1969)

The first works on failure compression models of units pointed out that the different lateral strains of unit and bed joint mortar, the joint thickness t, and the height of the block h have significant influence on the transverse tensile strength of masonry.

Masonry units near the joints are stressed bi-axially. Local failure in the form of vertical cracks can appear when the following failure criterion is reached according to Hilsdorf. Hilsdorf pointed out that the different modulus of elasticity of brick and mortar have an essential influence on the compression strength of

masonry. Different lateral strains of both materials lead to three-axial compression in mortar, and compression-tension in brick. These tensile stresses in the brick are the main reason for cracking and failure of the masonry structure.

Hilsdorf [8, 9] have been derived the stress and deformation state from elasticity equations. The proposed solutions were derived by considering a unit-mortar prism subjected to an axial compressive stress σ_{xx} as shown in Figure 3.10.

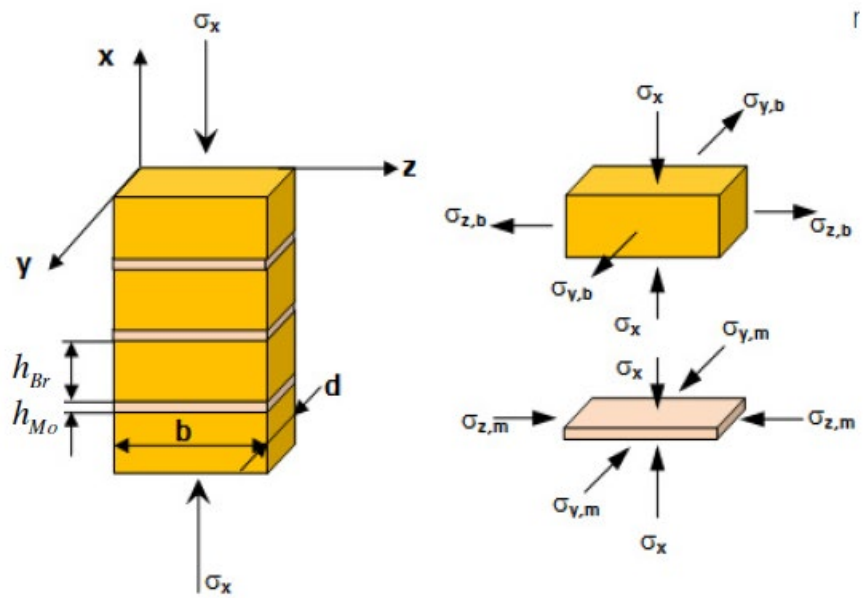

Figure 4.4; Stress state in unit-mortar prism under compression.

In section 3.1 above, Lateral stress in the brick, are calculated by.

$$\sigma_{yy,br} = \sigma_{zz,br} = \sigma_L = \frac{\frac{E_{br}}{E_{mo}}\mu_{mo} - \mu_{br}}{(1-\mu_{br}) + (1-\mu_{mo})\frac{E_{br}}{E_{mo}}\frac{h_{br}}{h_{mo}}}\sigma_{xx} \qquad 4.30$$

where.

μ_{br} Poisson's ratio of the brick

μ_{mo} Poisson's ratio of the mortar

σ_{xx} vertical stress in the brick (compression)

$\sigma_{yy,br}$ lateral y stress in the brick (tension)

$\sigma_{zz,br}$ lateral z stress in the brick (tension)

σ_L lateral stress in the brick (tension)

E_{br} E-modulus of the brick,

E_{mo} E-modulus of the Mortar

h_{mo} height of the bed joint

h_{br} height of the brick

Masonry units near the joints are stressed bi-axially. Local failure in form of vertical cracks can be appeared when the following failure criterion is reached according to Hilsdorf,

$$\frac{\sigma_L}{f_{t,br}} + \frac{\sigma_{xx}}{f_{c,br}} = 1 \qquad 4.31$$

This failure criterion can be represented by line A in Figure 3. Line A like B in Figure 3 represents the development of internal stresses under the increase of external compression.

The intersection point of line A and B refers to developing a local crack. However, this is not the point of failure, the failure according to Hilsdorf can occur when unit can no longer provide the biaxial restraint necessary to prevent failure of the mortar. This will occur when the line defining the tri-axial strength of mortar line C intersects the failure line of the unit. It is well known from studies performed on concrete that the compressive strength can be increased by increasing the confinement stresses. Therefore, the tri-axial strength of mortar could be represented by an equation originally obtained for concrete.

$$\sigma_{xx} = f_{mo} + 4.1\ \sigma_{yy,mo} \qquad 4.32$$

From equation 3.55, we get.

$$\frac{\sigma_L}{f_{t,br}} = 1 - \frac{\sigma_{xx}}{f_{c,br}}$$

$$\sigma_L = f_{t,br}\left(1 - \frac{\sigma_{xx}}{f_{c,br}}\right) \qquad 4.33$$

From section 3.1, $\sigma_{yy,mo} = \sigma_{yy,br}\frac{h_{br}}{h_{mo}} = \sigma_L \frac{.h_{br}}{h_{mo}}$ and substitute it into equation 3.56

$$\sigma_{xx} = f_{mo} + 4.1\ \sigma_L \frac{h_{br}}{h_{mo}}$$

$$\sigma_{xx}\ h_{mo} = f_{mo}\ h_{mo} + 4.1\ \sigma_L\ h_{br}$$

$$\sigma_L = \frac{\sigma_{xx}h_{Mo} - f_m h_{Mo}}{4.1\ h_{Br}}$$

$$\sigma_L = \frac{1}{4.1\ h_{Br.}}(\sigma_{xx} - f_{mo})h_{mo}$$

$$\sigma_L = \frac{h_{Mo}}{4.1\ h_{Br.}}(\sigma_{xx} - f_{mo})$$

with $\alpha = \frac{h_{Mo}}{4.1\ h_{Br}}$.

$$\sigma_L = \alpha(\sigma_{xx} - f_{mo}) \qquad 4.34$$

Equating equations 4.33 and 4.34, we have,

$$\alpha(\sigma_{xx} - f_{c,mo}) = f_{t,br}(1 - \frac{\sigma_{xx}}{f_{c,br}})$$

$$\alpha\ \sigma_{xx} - \alpha f_{c,mo} = f_{t,br} - f_{t,br}\frac{\sigma_{xx}}{f_{c,br}}$$

$$\alpha\ \sigma_{xx}\ f_{c,br} - \alpha\ f_{c,mo}\ f_{c,br} = f_{t,br}f_{c,br} - f_{t,br}\sigma_{xx}$$

$$\alpha\ \sigma_{xx}\ f_{c,br} + \sigma_{xx}\ f_{t,br} = \alpha\ f_{c,mo}\ f_{c,br} + f_{t,br}f_{c,br}$$

$$\sigma_{xx}(\alpha\ f_{c,br} + f_{t,br}) = f_{c,br}\ (\alpha\ f_{c,mo} + f_{t,br})$$

$$\sigma_{xx} = \frac{f_{c,br}\ (\alpha\ f_{c.mo} + f_{t,br})}{(\alpha\ f_{c,br} + f_{t,br})} \qquad 4.35$$

equation 4.35 gives the magnitude of the local stress at failure corresponding to the intersection of lines A and C.

The average masonry stress (compression strength of masonry) at failure is then.

$$F_{c,Ma} = \frac{\sigma_{xx}}{U}$$

$$F_{c,ma} = \frac{f_{c,br}\ (\alpha\ f_{c,mo} + f_{t,br})}{U(\alpha\ f_{c,br} + f_{t,br})} \qquad 4.36$$

where.

$f_{c,br}$ = The uni-axial compressive strength of unit

$f_{t,br}$ = The strength of the unit under biaxial tension

$f_{c,mo}$ = The uni-axial compressive strength of mortar

$F_{c,Ma}$ = compression strength of Masonry

U = coefficient of non-uniformity, this coefficient has been determined by Hilsdorf for different brick-mortar combinations. For example, for cement mortar it is around 1,3 as a mean value in the common strength range.

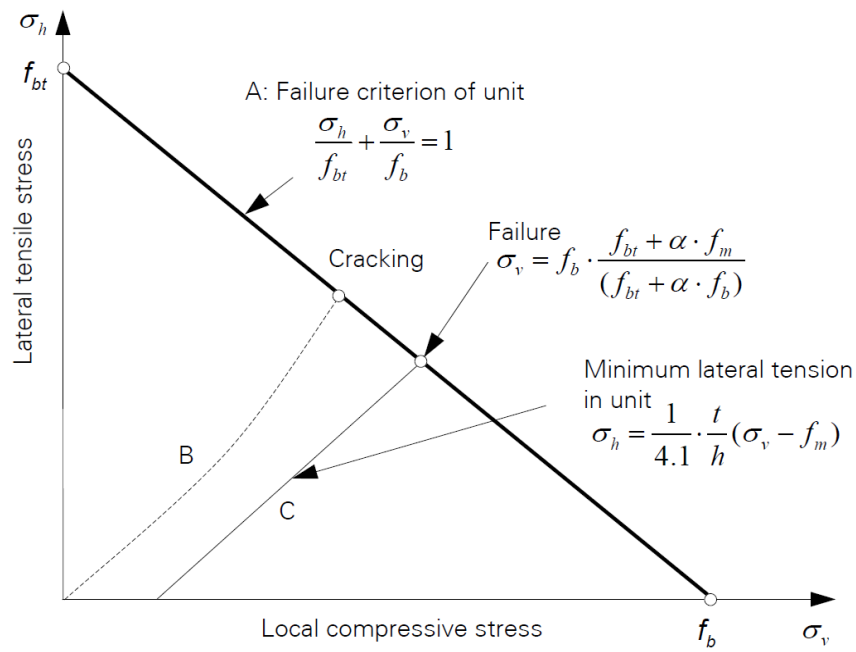

Figure 4.5; Hilsdorf's failure theory of masonry under compression.

Geometry (height,h_{mo}) and mechanical properties (Poisson's ratio h_{mo} and E modulus,h_{Mo}) of mortar affect the lateral tensile stress in the brick σ_L, see equation (4.32), and consequently the cracking stress of masonry. Estimating Masonry Strength Depending on the EC 6 and Different Research Projects Compression strength in masonry $F_{c,Ma}$ is also affected by geometry (height,h_{mo}), compression strength of masonry $f_{c,Mo}$ and coefficient of non-uniformity U, which is mainly dependent on the mortar, see equation (4.36).

In (Hilsdorf, 1969) it is also mentioned that when using the same brick, the masonry strength increases with increased mortar quality, hand work and thinner mortar joints. If the mortar strength is much less than that of the brick, then the masonry strength is only a small percentage of the brick strength; however, it is many times higher than the strength of the mortar alone. Only if the mortar strength is much higher than that of the brick, then the strength of the masonry reaches the strength of the brick.

4.3.2. FAILURE MODEL OF KHOO AND HENDRY

Khoo and Hendry found that the biaxial compression-tension strength envelope for unit can be represented by the relationship.

$$\frac{\sigma_{xx}}{f_{c,br}} + \left(\frac{\sigma_L}{f_{t,br}}\right)^{0.546} = 1 \qquad 4.37$$

This equation is based on large number of test results ranging from 31.63 to 92.66 N/mm^2, see (Figure 4.5). The comparison of the concave shape of this curve with linear relationship assumed by Hilsdorf shows that, the compressive strength of unit is severely reduced by the presence of an orthogonal tensile stress.

Hendry and Khoo have investigated the effect of compressive strength of mortar under confining pressure. Triaxial cell tests were carried out for 1:1/4:3 and 1:1:6 mortars, see (Figure 4.5).

$$\frac{\sigma_{xx}}{f_{mo}} = 1 + 2.91 \left(\frac{\sigma_L}{f_m}\right)^{0.805} \qquad 4.38$$

where

σ_{xx} The major principal stress.

σ_L The minor principal stress.

f_{mo} The uniaxial compressive strength of the mortar

Based on these investigations, a failure theory for masonry was developed (Figure 4.6). Khoo established the failure curves by considering lateral tensile strain in unit material at failure approximately 225 ×10^{-6}. Relating this value to the stress strain curves for mortar obtained from tri-axial tests, a relationship between axial and lateral compressive stresses in mortar is obtained. Introducing the ratio α, between the mortar joint thickness and the unit height, gives the lateral tensile stress in the unit material (Figure 4.6).

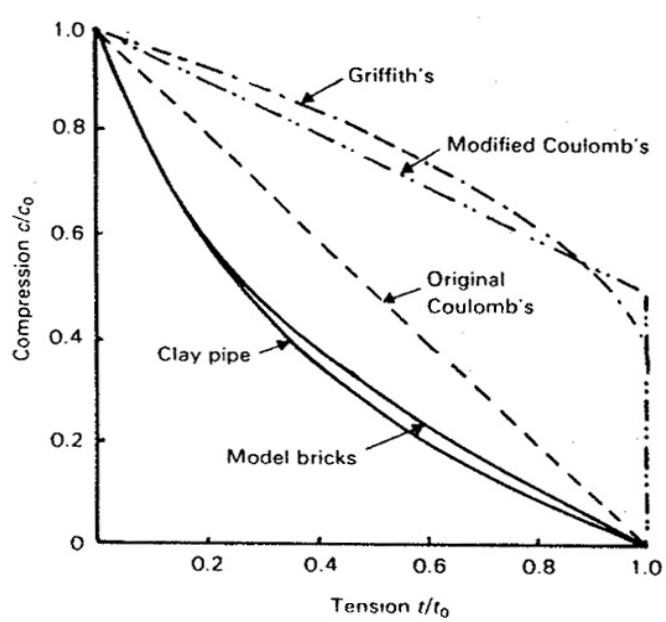

Figure 4.6; Biaxial compression-tension failure envelopes, acc. to Hendry

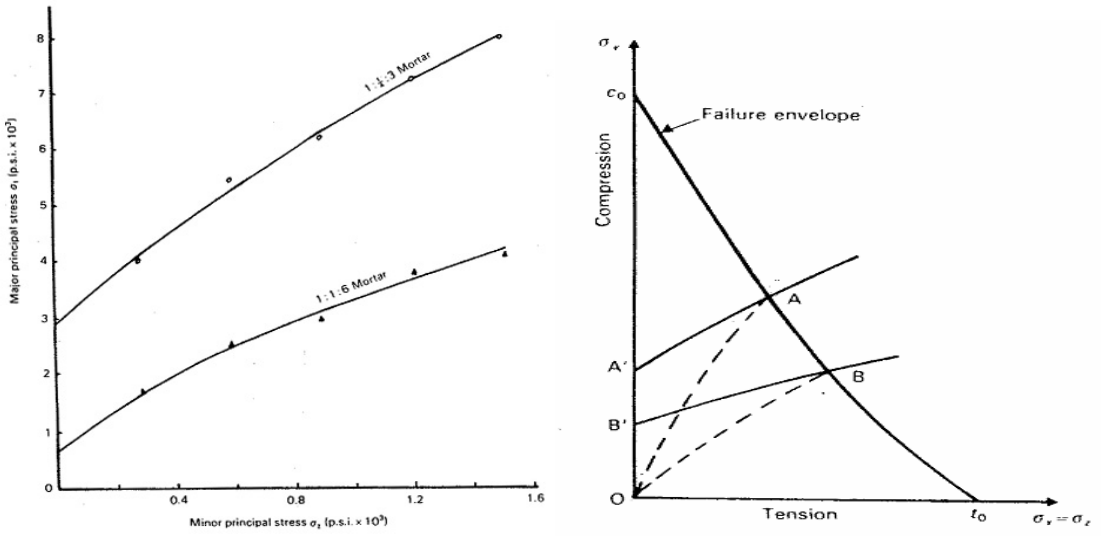

(a) *(b)*

Figure 4.7; (a) Principal stress relationship for mortar in tri-axial compression, (b) failure envelope for unit in biaxial compression-tension, according to Hendry.

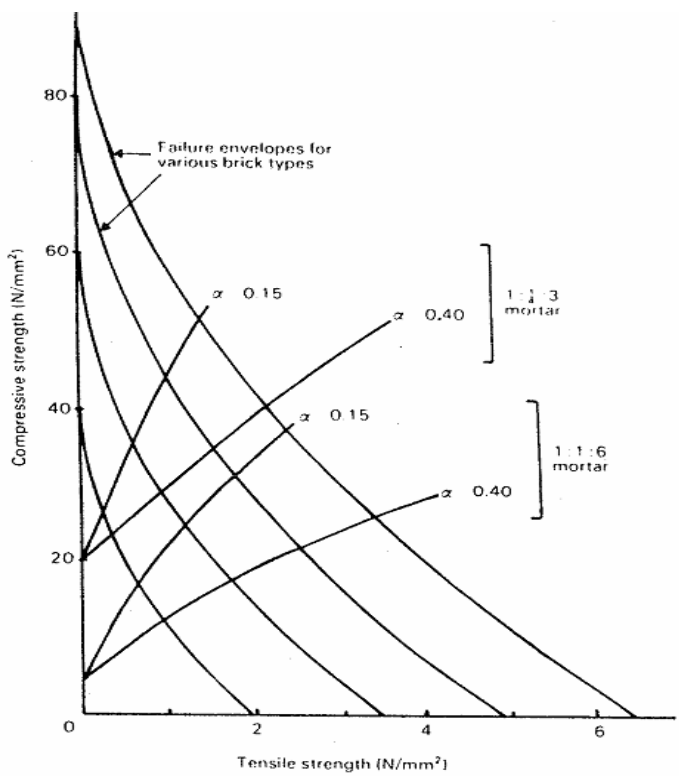

Figure 4.8; Graphical solution for masonry prism compressive strength, Hendry.

4.3.3. FAILURE MODEL OF MANN

The failure model of Mann, which is also addressed in the revised version of DIN 1053 Part 1, is following a completely different way to describe the strength of masonry. The failure model is based on the hypothesis that the failure of the masonry occurs by compression failure of the mortar. The compressive strength of the masonry is thus described by the existing masonry compressive strength of the mortar.

Mann is based on the Mohr's failure hypothesis and describes the mortar strength in masonry as a product of the compressive strength f_m determined on cubes of slenderness t/d = 1 and a form factor. This form factor f considers the increase in strength of the mortar of masonry under multi-axial stress state. The form factor is dependent from uniaxial compressive failure of Rustmeier on mortars of different slenderness t/d.

Mann has introduced further transmission factor ü and form factor f to describe the compression strength of masonry. The compression strength of masonry made from natural brick with inclined mortar is calculated by:

$$f_k = f_m \cdot f \cdot \ddot{u} \qquad 4.39$$

where

f_k = compressive strength of masonry,

f_{mo} = compressive strength of mortar determined for cube t/d =1,

$\ddot{u}$ = the transmission factors given as:

$$\ddot{u} = \frac{A_b}{A}$$

The form factor f is given by the following equation:

$$f = F_{c,Ma} = \frac{8}{9} \cdot \frac{1}{1-\left(1-\frac{2}{3}\cdot\frac{h_{mo}}{d}\right)^2 \cdot \cos^4\alpha} \qquad 4.40$$

where

A_b = the area of the unit

A = the area of the masonry

$F_{c,Ma}$ = compression strength of masonry

h_{mo} = height of the bed joint

d = the width of the mortar joint,

α = inclination angel of the mortar

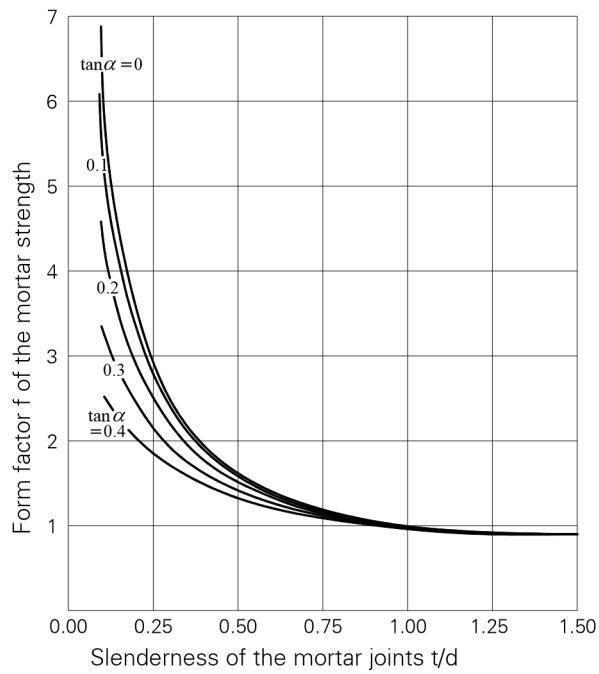

Figure 4.9; Form factor f in relation to the slenderness t/d and the inclination angel α of the mortar.

4.3.4. FAILURE MODEL OF BERNDT

The deformation and fracture process of masonry have been investigated at Dresden University of Technology in time 1989-1994 Berndt [2]. Experimental study was performed together with theoretical interpretation of deformation and fractural process, and significant factors have been found to increase the load bearing capacity of masonry.

It is assumed for most types of masonry that.

$$\frac{E_{Br}}{E_{Mo}}\ \mu_{Mo} \gg \mu_{Br} \qquad 4.41$$

Therefore, Hilsdorf equation (4.7) can be simplified to the following:

$$\sigma_L = \frac{h_{mo} - \mu_{mo}}{h_{br}.1 - \mu_{mo}}\,\sigma_{xx} \qquad 4.42$$

Berndt has explained the phenomena of the spalling of mortar edges at early stage of loading and its influence on the compressive strength (Figure 4.8).

The missing mortar due to spalling will affect the distribution of compressive stresses inside masonry unit. According to principle of Navier and due to the concentration of compressive stresses near the middle of

the unit surface, the height of the unit has an influence on the distribution of stresses at the mid height of the unit (Figure 4.10). This means:

1. If h < 2d, this result in non-uniform stress distribution at the mid of the unit
2. If h > 2d, this result uniform stress distribution at the mid of the unit

Where d is the unit width

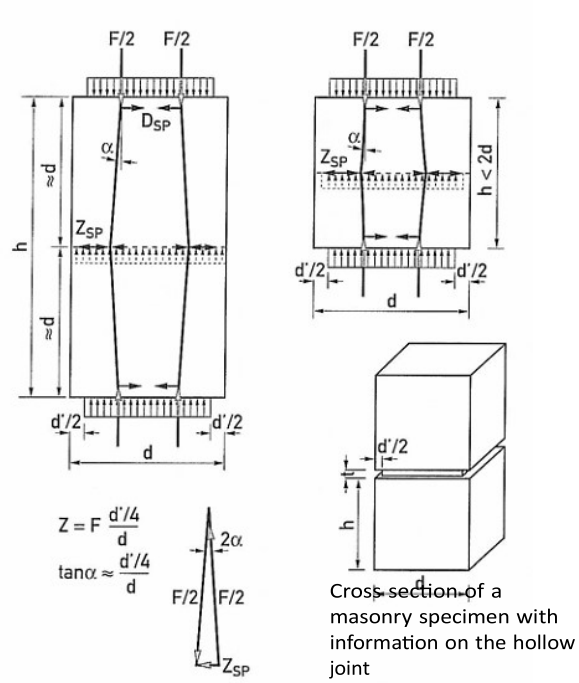

Figure 4.10; The approximate values of tensile splitting forces due to holes in the joints near the edges of the stone

With sufficient accuracy, the tangent of the inclination angel of the stress flow in the unit is

$$\alpha = \frac{1}{4} \cdot \frac{d'}{d} \qquad 4.43$$

where d' is the sum of spalling parts of the mortar from both sides.

Therefore, the splitting forces can be calculated based on the inclination angel:

$$Z_{SP} = F\,\frac{1}{4} \cdot \frac{d'}{d} \qquad 4.44$$

The maximum stress at the mid-height of the unit is then:

$$\sigma_{SP} = \frac{\frac{3}{2} \cdot Z_{SP}}{0.75 \cdot h_{Br}} \qquad 4.45$$

Considering that

$$F_{xx} = \sigma_{xx} \cdot d \qquad 4.46$$

The we get,

$$\text{Max } \sigma_{SP} = 0.5 \frac{d'}{d} \cdot \frac{d}{h_{Br}} \sigma_{xx} \qquad 4.47$$

The elaso-plastic calculation by using Drucker-Prager model for mortar has showed relatively high lateral tensile stresses. The used flow model is based on the linear relationship between the invariant of the stress deviator and the mean pressure and does not consider hardening properties of the mortar. The fully mortared edges of the joint leads to maximum values of transverse tensile stresses at corners and edges, which require the transfer of maximum shear stresses between mortar and unit, Figure 4.10, Elastic calculations can provide the maximum transverse tensile stresses which could also be approximately calculated from the ratio:

$$\frac{\sigma_{L,z}}{\sigma_{xx}} = \frac{h_{Mo}}{h'} \frac{\mu_{Mo}}{1-\mu_{Mo}} \ , \ \mu_{Mo} = 0.2.....0.25 \qquad 4,48$$

Plastic analysis provides, however several times larger transverse stresses than elastic solution, which can be approximated by the following relationship, Figure 4.10-a, b:

$$\frac{\sigma_{L,z}}{\sigma_{xx}} = \frac{h_{Mo}}{h'} \frac{\bar{\mu}_{Mo}}{1-\bar{\mu}_{Mo}} \ , \ \bar{\mu}_{Mo} = 0.5.....0.4 \qquad 4.49$$

It should be taken into consideration that the obtained transverse tensile stresses occur only over a small height range of each unit near the bed joint, and these "calculated contributory block height" for conventional masonry geometry units is not over $h' = 10cm$ when the joint thickness lies between 5... 30 mm.

The high shear stresses on the bearing edge joints release the confinement at depth of $d'/2 = h_{mo} / 2$, which seems partly given by the execution of no-fully mortared joint. In addition, many earlier failures of the mortar edge (spalling) occur before the masonry failure. Elaso-plastic materials have in the failure state of sliding surfaces an angel inclination of:

$$\alpha = 45° + \frac{\rho}{2} \qquad 4.50$$

ρ is the internal friction angle when the influence of low cohesive strength *c* is neglected.

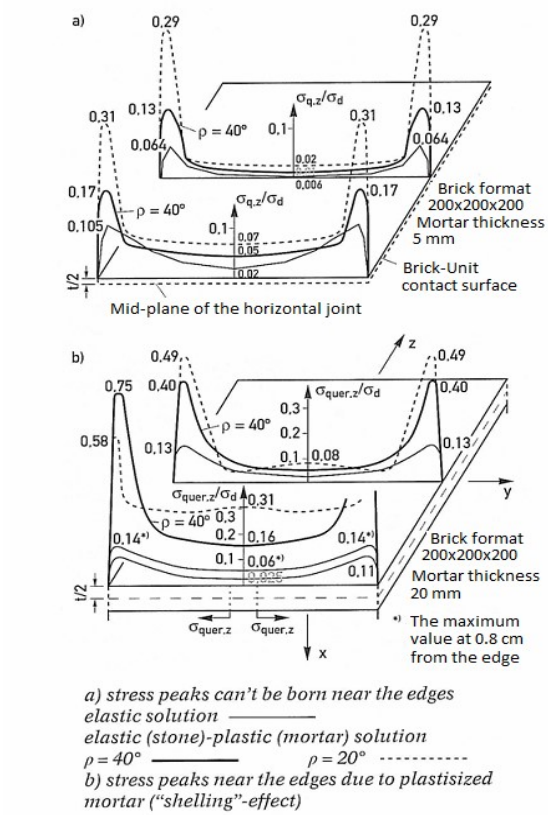

Figure 4.11 Calculated solution for transverse loading with undistributed joints, Schulenberg and Berndt.

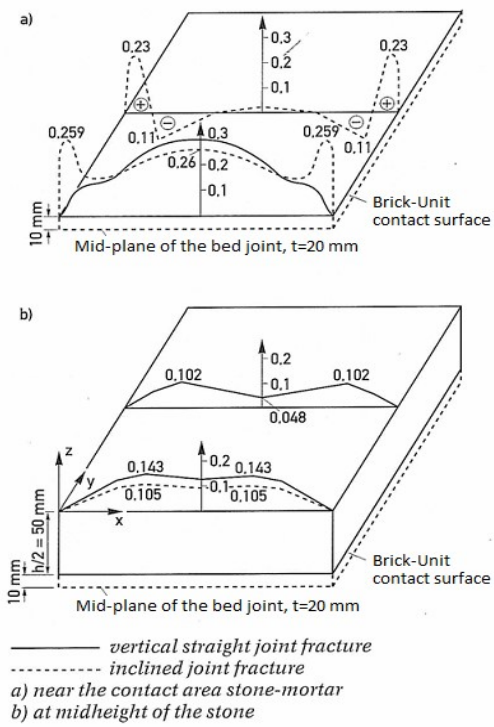

Figure 4.10 Calculated solution for transverse loading with broken joints and plastic mortar in the horizontal joints, Bierwirth et al. and Berndt.

The friction angle ρ was determined from the first test experiments on cylindrical mortar specimens under multiaxial pressure, determined by the Mohr-Coulomb relationship:

$$\sigma_{xx} - \sigma_L = (\sigma_{xx} + \sigma_L) \,.\, \sin\rho \; 2c.\cos\rho \qquad 4.51$$

For this purpose, the two levels of stresses are

$$\frac{1}{3}(\sigma_{xx} + \sigma_L) = \begin{cases} 1.0 \; and \; 2.0 \frac{N}{mm^2} \; for \; MGI \\ 3.0 \; and \; 4.0 \frac{N}{mm^2} \; for \; MGII \end{cases} \qquad 4.52$$

gradually being built up, after which σ_L is increased up to failure. From this, a non-statistically based calculation values were derived:

ρ = 20° *for MGI* (α = 50°.....60° *for* checking the validity)

ρ = 30° *for MGII* (α = 50°.....60°)

Based on test results the value of has been determined:

$$d' = h_{mo} + \frac{h_{mo}}{\tan\left(45+\frac{\rho}{2}\right)} \qquad 4.53$$

The tensile stresses in the transverse direction of the unit can be described by:

$$\sigma_L = \sigma_{yy,br} = \sigma_{zz,br} \approx \left(\frac{h_{mo}}{h'} \cdot \frac{\bar{\mu}_{mo}}{1-\bar{\mu}_{mo}} + 0.3\,\frac{d'}{d} \cdot \frac{d}{h_{br}}\right) \cdot \sigma_{xx} \qquad 4.54$$

where

$$h' = \min\begin{cases} 10cm \\ h \end{cases} \qquad 4.55a$$

$$\bar{\mu}_{Mo} = \begin{cases} 0.5\ for\ MGI \\ 04\ for\ MGI \\ 0.3\ for\ MGI \end{cases} \qquad 4.56b$$

To determine the compressive strength of masonry, Berndt has represented the values $\sigma_{xx}/\ f_{c,Br}$ of $\sigma_L/f_{t,Br}$and the performed experiments in one diagram, Figure 11.

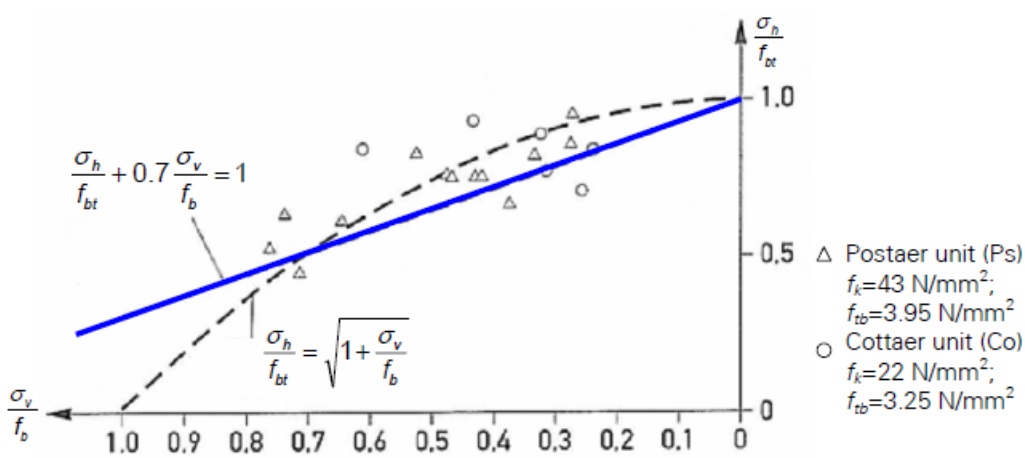

Figure 4.12; Failure envelope for unit in biaxial compression-tension, acc. to Berndt

Although, the recorded test result can be best represented by a non-linear function, it is also can be simplified into the following linear equation, if the cases of high transverse tensile stress in the transverse direction of the static system are excluded.

$$\frac{\sigma_L}{f_{t,Br}} + 0.7\,\frac{\sigma_{xx}}{f_{c,Br}} = 1 \qquad 4.57$$

where

σ_L = is the lateral tensile stress, can be obtained from equation (29)

σ_{xx} = is compressive stress, considering that $E_{br} > E_{mo}$ and $\frac{E_{br}}{E_{mo}} \mu_{mo} >> \mu_{br}$

By replacing the value ofσ_L from equation (29) in equation (31) and considering σ_{xx}= f_k at failure, this gives.

$$f_k = \frac{f_{c,br}}{K_\sigma \frac{f_{c,br}}{f_{bt,br}} 0.7} \approx \frac{f_{bt,br}}{K_\sigma} \qquad 4.58$$

where

$$K_\sigma = \frac{h_{mo}}{h'} \frac{\bar{\mu}_{mo}}{1-\bar{\mu}_{mo}} + 0.3 \frac{d'}{d} \cdot \frac{d}{h_{br}} \qquad 4.59$$

This equation is determined by Bernd to relate the compressive strength of masonry with lateral tensile strength.

4.3.5. FAILURE MODEL OF SABHA

The failure model of Sabha [18, 19] is based on the observation of the failure on the surface joint regions before reaching the ultimate load. The emergence of splitting stresses in units has been taken based on the failure model of Berndt which has the maximum value at the mid-height of the unit, while the tensile stresses due to lateral strain constraints near the joints are the biggest. In contrast to the failure model of Berndt, the stress components here are not combined. The model underlying the failure stress distribution is shown in Figure 4.13.

In the non-failed mortar part of the joints in masonry, a hydrostatic stress state is assumed.

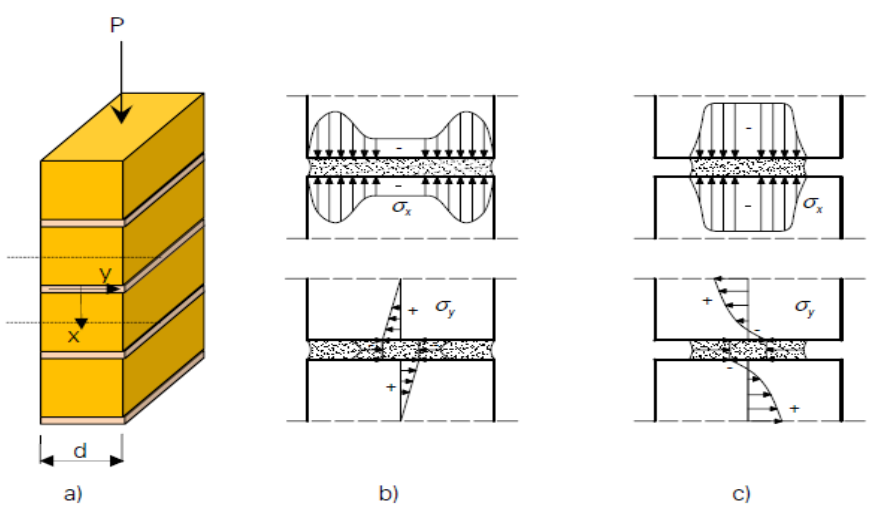

Figure 4.13; Stress distribution in masonry according to Sabha. (a) Masonry specimen under compression, (b) Stress state in elastic stage, (c) stress state in plastic stage.

The validity of the failure model is limited for joint geometries with t < d / 5, because at larger joint heights no multi-axial stress state exists. From FEM studies for the transverse tensile stresses in the unit, the critical spalling depth of the mortar, is determined, and this relationship between the vertical compressive stress in masonry and transversal tensile stresses in unit has been given as following:

$$\sigma_{xx} = \frac{1}{K}\,\sigma_L \qquad 4.60$$

$$K = -\,3.22\left(2.5\,\frac{h_{mo}}{d}\right)^2 + 1.524\,\frac{h_{mo}}{d} \qquad 4.61$$

where

σ_{xx} = the vertical compressive stress in masonry

σ_L = maximum tensile splitting stress in unit

h_{mo}, d = the height and the width of the mortar joint respectively.

This equation represents a linear stress relation for the splitting tensile stress in unit. The splitting tensile stresses arise after exceeding the uniaxial compressive strength of mortar, can be represented by line B in Figure 4.14. The slope of the line corresponds to m=1/k. The compressive strength of the masonry is then the point of intersection with the unit failure curve.

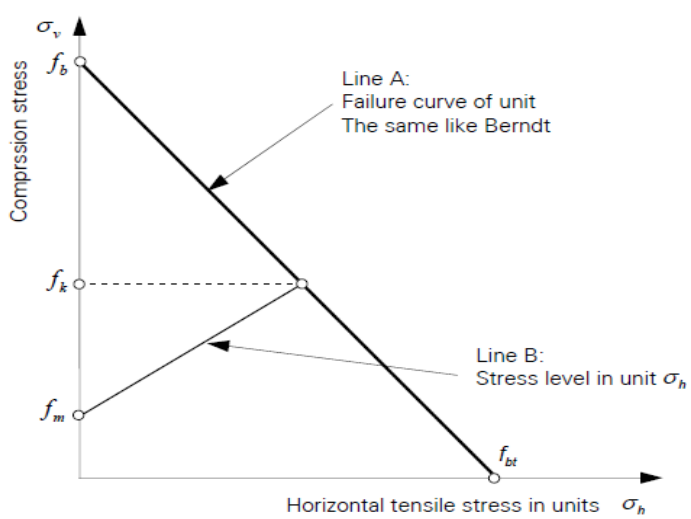

Figure 4.14; Failure model for natural stone masonry according to Sabha.

4.3.6. COMPARISON AND ASSESSMENT OF EXISTING FAILURE MODELS

Reviewing back the failure models in section three, they have one common modelling principle which is based on finding the intersection point between the failure curves of unit and mortar. An exception from that is the failure model of Mann, which is based on the hypothesis that masonry failure occurs by compression failure of the mortar. In all other failure models, namely: Hilsdorf, Khoo and Hendry, Berndt, and Sabha this principle is valid Table 4.1). The failure model of the units is based on the biaxial tension-compression behaviour. All models require for the definition of the failure model two parameters: the normalized mean compressive strength of unit $f_{c,br}$ and the strength of unit under biaxial tension $f_{t,br}$. The failure model of the mortar is based on the triaxial compression behaviour. The models of Berndt and Sabha show a different way for the definition of mortar failure than Hilsdorf and Khoo/Hendry. The models of Hilsdorf and Khoo/Hendry define mortar triaxial failure based on the compressive strength of the mortar f_{mo}, on other hand the models of Berndt and Sabha use the dimensions of mortar joints.

Table 4.1; Summery of the existing failure models of masonry under compression

Failure model	Failure of unit	Failure of mortar
Hilsdorf [8, 9]	$\frac{\sigma_L}{f_{t,Br}} + \frac{\sigma_{xx}}{f_{c,Br}} = 1$ (Eq.3)	$\sigma_L = \frac{h_{Mo}}{4.1\, h_{Br.}}(\sigma_{xx} - f_m)$ (Eq.5)
Khoo and Hendry [12, 13]	$\frac{\sigma_{xx}}{f_{c,Br}} + \left(\frac{\sigma_L}{f_{t,Br}}\right)^{0.546} = 1$ (Eq. 9)	$\frac{\sigma_{xx}}{f_{mo}} = 1 + 2.91\left(\frac{\sigma_L}{f_m}\right)^{0.805}$ (Eq.10)
Berndt [2]	$\frac{\sigma_L}{f_{t,Br}} + 0.7\frac{\sigma_{xx}}{f_{c,Br}} = 1$ (Eq.29)	$\frac{\sigma_L}{\sigma_{xx}} = \frac{h_{Mo}}{h'}\frac{\bar{\mu}_{Mo}}{1-\bar{\mu}_{Mo}} + 0.3\frac{d'}{d}\cdot\frac{d}{h_{Br}}$ (Eq.27)
Sabha [18, 19]	$\frac{\sigma_L}{f_{t,Br}} + 0.7\frac{\sigma_{xx}}{f_{c,Br}} = 1$ (Eq.29)	$\frac{\sigma_L}{\sigma_{xx}} = -3.22\left(2.5\frac{h_{mo}}{d}\right)^2 + 1.524\frac{h_{mo}}{d}$ (Eq.32)

Warnecke et al. [22] have performed a comparison of the failure models with experimental results. The compressive strength values of masonry have been calculated for the failure models of Hilsdorf, Berndt, Sabha, and Mann. The results are summarized in Table 4.2. The compressive strength of masonry has been calculated according to the failure model of Hilsdorf under the assumption of a linear gradient of the unit failure curve. The slope of the failure line of the mortar is taken m = 1.5 which is independent from the mortar class [3]. For regular bonder, the ratio of the unit height to the mortar height has been taken equal to h/t=15 and for random bonder h/t=5. The calculated values of the compressive strength of masonry exceed the experimental values by up to two or three times, Table 4.2. This can be explained due to the

high scattering joint slenderness, which is leading to different restraining degrees at the joints and to sharp stress paths. Masonry is going to lose the ability of load redistribution due to the large differences in inner stiffness after the occurrence of local failure zones. This prevents to achieve the compressive strength as a theoretical point of intersection of unit and mortar failure curves. The failure model of Hilsdorf therefore overestimates the values of compressive strength.

Table 4.2 Comparison of the experimental compression strength of masonry [N/mm^2] with ones calculated from failure models, Warnecke et al. [22].

	Regular bonder sandstone				Irregular bonder limestone	
	Mortar MI f_m=7.5 N/mm^2		Mortar MIII f_m=29.1 N/mm^2		Mortar MI f_m=7.5 N/mm^2	
	h/d=5	h/d=10	h/d=5	h/d=10	h/d=5	h/d=10
Experimental results f_k	**10.0**	**13.0**	**25.2**	**21.2**	**5.1**	**4.5**
f_k acc. to Hilsdorf [9]	45.0		67.5		12.5	
f_k acc. to Berndt [2]	20.3		20.3		5.1	
f_k acc. to Sabha [19]	22.0		40.0		12.5	
with transmission factor ü acc to Mann	18.7		34.0		7.5	
f_k acc. to Mann [15] with f_m h/d=1	(60.8)		(226.5)		16.5	
with f_m acc. to DIN	6.0		(93.9)		1.6	

For the assessment of the failure model of Berndt the Poisson ratio has been taken ν=0.5 for both mortar classes which corresponds to the plastic state. For the regular bonder sandstone, the following parameters were considered, masonry thickness of d=15 cm, the spalling depth of the mortar from both sides d'=3 cm and the height of the unit h=15 cm. The results show that the regular bonder masonry with high quality

mortar has good agreement with the experimental values. However, the comparison of compressive strength for lower mortar quality shows that mortar strength is not well considered to calculate the strength of masonry. The weak point in the failure model lies in the assumption of linear elastic material behavior up to failure but not considering the strength properties of the mortar.

For assessing the failure model of Sabha, linear failure curve for units has been used. For regular bonder, the ratio t/d has been taken equal to 0.07, and for irregular bonder is t/d=0.14. The calculated compressive strength values were proportional to the experimental values. This shows that the influence of mortar strength and unit strength on the compressive strength of masonry has been explained properly but at too high a level of strength. Further comparison has been performed considering the transmission factor of Mann. The transmission factor has been taken ü = 0.85 for regular bonder and ü = 0.6 for the irregular bonder. The results showed satisfactory agreement with the experimental values.

The values of compression strength have been calculated according to the failure model of Mann for t/d=1. For regular bonder, the slenderness of the mortar joint is taken as t/d=0.10 and the transmission factor ü=0.85. For irregular bonder masonry the following parameters were considered t/d=0.23 and ü=0.60. These values are within the limits specified in DIN 1053. The calculated compressive strength values are about three to ten times the experimental values. An additional calculation with mortar strength according to DIN 18555 was performed. The calculated values were clearly below the experimental results. The failure model of Mann is underlying the failure hypothesis that masonry failure occurs due to the compression failure of the mortar which is contrary to many experimental studies. The fracture model of Sabha shows good agreement with the experimental values if the transmission factor of Mann is additionally introduced. Furthermore, the strength properties of units and mortar as well as the geometric parameters should not be estimated by the mean value, but by the characteristic value lying on the safe side. The failure models of Hilsdorf and Mann are however, for the examined masonry by Warnecke et al. are not suitable.

5. CRACKING STRENGTH OF MASONRY USING ENERGY BALANCE CRITERION

The force required for failure in a material depends on the mode of cracking, the fracture surface energy of the material, the geometry and elasticity of the specimen.

The specific fracture surface energy is the fundamental material property dictating cracking strength (compression or tension) and not compressive or tensile strength.

Griffith (1920) demonstrated that cracking is better described by an energy criterion where the surface energy embodied in the crack is created by an expenditure of elastic and mechanical energy in the system. The condition for extension of crack length a on this energy is

$\frac{d}{da}(U$ = surface energy + elastic energy + mechanical energy) = 0.

$$\frac{dU}{da} = 0 \qquad 5.1$$

This energy balance must result in an equation for the cracking force F of the form, $F = f$(fracture surface energy, geometry, elasticity).

Where Fracture surface energy is a material constant best for describing compression cracking strength and it is the same for both tension and compression.

Mode of complexities of compression failure are classified into the following three categories.

- plastic or yielding mode.
- cone failure or cracking mode
- axial splitting

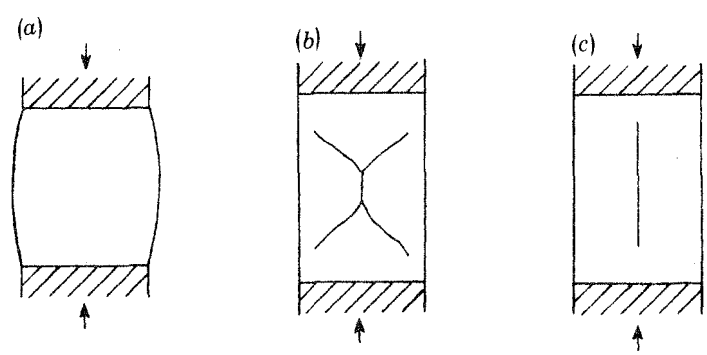

Figures 5.1; Compression failure: (a) plastic yielding, (b) cone failure, (c) axial splitting. (Kendall, 2008)

For the plastic yielding failure in Figure 1a, only the compressive strength is sufficient to describe the failure. The yielding mode is described by stress criterion such that the force yield F_y depends on the area A of the specimen and its yielding stress σ_y. i, e, F_{yield} = f (geometry, yielding stress).

$$\sigma_{yy} = \frac{F_{yy}}{A} \quad 5.2$$

The cracking mode or cone failure are denoted by energy balance criteria in form of energy equilibrium in such a way that the cracking force is a function of $F_{cone} = f$(fracture surface energy, geometry, elasticity), i.e.

$$\frac{dU}{da} = \frac{d}{da} f(\text{surface energy + geometry + elastic energy}) = 0 \quad 5.3$$

The axial splitting is also described by energy criterion. The splitting force is a function of $F_{splitting^g} = f$(fracture surface energy, geometry, elasticity).

In this research work, the mode of cracking and splitting failure is used to derive the compressive or tensile cracking or splitting strength of masonry. We assumed that the masonry composite is uniform though heterogeneous. This is because masonry is a brittle material, and it fails by splitting in the unit (mode 1 failure mechanism with stress intensity factor k_1) and by shear at the edge of the mortar (mode 11 failure mechanism with stress intensity factor k_{11}).

5.1. ANALYSIS OF ENERGY BALANCE OF CRACK PROPAGATION IN BRITTLE MATERIAL

Inglis (1913) derived stress concentration fracture around an elliptical hole as,

$$\sigma_{yy} = \sigma\,(1 + \frac{2a}{b}) \quad 5.4$$

where

2a = larger diameter of ellipse

b = smaller diameter of ellipse

If a = b (a circular hole), then $\sigma_{yy,Ma} = 3\sigma$, which yields the well-known stress concentration factor near a circular hole.

For infinite sharp crack, b → 0, then we have a "line crack," and the stress σ_{yy} increases without limit. Hence $\sigma_{yy} = \infty$

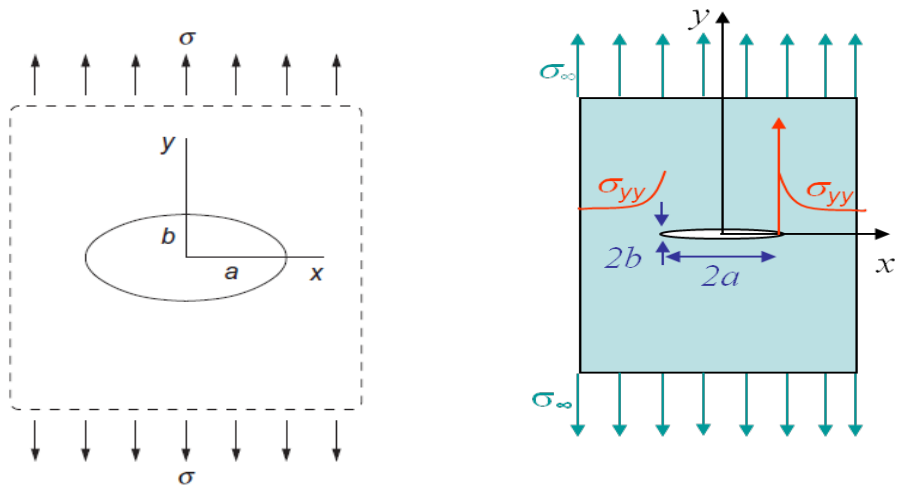

Figure 5.2; An elliptic hole in an infinite plate subjected to tension.

If a stress-based failure criterion is used to predict the extension of such a "crack," one would find the unreasonable answer that any amount of applied stress would cause the crack to grow.

Griffith took an energy balance point of view and reasoned that the unstable propagation of a crack must result in a decrease in the strain energy of the system (for a body with a fixed boundary where no work is done by external forces during the crack extension), and proposed that a crack would advance when the incremental release of strain energy dU_E associated with a crack extension da in a body becomes greater than the incremental increase of surface energy dU_S as new crack surfaces are created also associated with a crack extension da in a body . That is,

$$dU_E \geq dU_S \qquad 5.5$$

The equality sign indicates the critical point for crack propagation. In other words, if the supply of energy from the cracked plate is equal to or greater than the energy required to create new crack surfaces, the crack can extend.

When a crack propagates, elastic energy is released in the volume of the material and two new surfaces are created resulting in surface energy. Crack propagates if the elastic strain energy released is greater than the surface energy.

5.1.1. CRACKING STRENGTH FOR MASONRY SUBJECTED TO UNIAXIAL STRESS

It is already established above that,

$$\frac{dU_T}{da} = \frac{d}{da} f(\text{surface energy + geometry + elastic energy}) = 0$$

U_T = The total potential energy which is the sum of the strain energy in the elastic material and the surface energy of the crack. The energy conservation principle is applied as the crack grows an infinitesimal, da.

$$\frac{dU_T}{da} = 0$$

Elastic strain energy per unit volume or elastic strain energy density U_d is given by,

$$U_d = \frac{1}{2}\,\sigma_{yy,Ma} \cdot \varepsilon_{yy\,Ma} \qquad 5.6$$

This is the energy released on the cracked volume. From Hook's law of elasticity,

$$\varepsilon_{yy,Ma} = \frac{\sigma_{yy,Ma}}{E_{Ma}}$$

Then we put into equation 5.6,

$$U_d = \frac{1}{2}\frac{\sigma_{yy,Ma}^2}{E_{Ma}} \qquad 5.7$$

Elastic strain energy released U_E is given by $\frac{U_E}{V} = U_d$ therefore,

$$U_E = U_d \,.\, V_{Ma}$$

$$U_E = \frac{1}{2}\frac{\sigma_{yy,Ma}^2}{E_{Ma}} V_{Ma} \qquad 5.8$$

Volume of the cracked material is the volume of the cracked ellipse = area multiply by thickness

$$A = \pi\,(2a)a = 2\pi a^2 \qquad 5.9$$

$$V = 2\pi a^2 .\, \mathrm{t} = 2\pi a^2 \mathrm{t} \qquad 5.10$$

Hence elastic strain energy released in the uncrack volume is,

$$U_E = \frac{1}{2}\frac{\sigma_{yy,Ma}^2}{E_{Ma}} \,.\, 2\pi a^2 \mathrm{t}$$

$$U_E = \pi\,\frac{\sigma_{yy,Ma}^2}{E_{Ma}}\, a^2 \mathrm{t} \qquad 5.11$$

Strain energy per unit thickness would be,

$$U_E = \frac{\pi\,\sigma_{yy,Ma}^2\, a^2}{E_{Ma}} \qquad 5.12$$

where

V = volume of the cracked elliptical section.

A = area of the cracked elliptical section.

$\varepsilon_{yy,Ma}$ = strain in the masonry

$\sigma_{yy,Ma}$ = applied cracking stress on the masonry.

E_{Ma} = elastic modulus of the masonry.

$2a$ = crack length.

t = thickness.

U_d = elastic energy density elastic energy per unit volume.

U_E = elastic strain energy per unit thickness.

This is the elastic strain energy released in the volume and it is accompanied by the growth of new crack by the creation of two new surfaces. We now consider this surface energy in creating these two new surfaces.

It is easy to calculate the surface energy for a crack (having two crack tips) with length $2a$, and γ is the surface energy density and the fact that two crack surfaces for a crack have been accounted for. Griffith used Inglis' solution to obtain the total energy released U_T due to the presence of a crack of length $2a$ in an infinite two-dimensional body. His method for calculating energy release was very complicated since he considered the energy change in the body as a whole.

Surface energy density created or surface energy per unit area U_d is given as

$$U_d = \gamma_s \qquad 5.13$$

Then surface energy density created, $\gamma_s = \frac{U_s}{A}$, i.e.

$$U_S = \gamma_s . A \qquad 5.14$$

Area of one cracked surface $A = 2at$ and for two surfaces, we get.

$$A = 4at \qquad 5.15$$

Hence, if we put equation 5.15, into equation 5.14, we would have.

$$U_S = \gamma_s . 4at$$

$$U_S = 4at\gamma_s \qquad 5.16$$

Surface energy per unit thickness

$$U_s = 4a\gamma_s \qquad 5.17$$

where

A = area of the cracked elliptical section

γ_s = Surface energy density or surface energy per unit area

2a = crack length (larger diameter of the ellipse)

t = thickness of cracked elliptical unit

U_s = Surface energy

Total energy in the material is the change in potential energy of the specimen with elliptical crack.

$$U_T = U_{cracked} - U_{uncracked} = \Delta U = U_S - U_E$$

$$U_T = 4a\gamma_s - \frac{\pi\, \sigma_{yy}^2\, a^2}{E_{Ma}} \qquad 5.18$$

Applying the conservation of energy principle when the cracks grow by amount, da. Crack is stable when terms are balanced, and equilibrium condition is maintained.

$$\frac{dU_T}{da} = 0$$

$$\frac{d}{da}\left(4a\gamma_s - \frac{\pi\sigma_{yy,Ma}^2\, a^2}{E_{Ma}}\right) = 0$$

$$\frac{d}{da}(4a\gamma_s) - \frac{d}{da}\left(\frac{\pi\, \sigma_{yy,Ma}^2\, a^2}{E_{Ma}}\right) = 0$$

$$4\gamma_s - \frac{2\,\pi\sigma_{yy,Ma}^2\, a}{E_{Ma}} = 0$$

$$2\gamma_s = \frac{\pi\, \sigma_{yy,Ma}^2\, a}{E_{Ma}} \qquad 5.19$$

$$\therefore\ \sigma_{yy,Ma}^2 = \frac{2\, E_{yy,Ma}\, \gamma_s}{\pi a}$$

$$\sigma_{yy,Ma} = \sqrt{\frac{2\, E_{Ma}\, \gamma_s}{\pi a}} \qquad 5.20$$

From section 3.5,

$\sigma_{yy,Ma} = \sigma_{yy,br} = \sigma_{yy,mo}$ and $\varepsilon_{yy,Ma} = \varepsilon_{yy,br}\frac{h_{br}}{h_{Ma}} + \varepsilon_{yy\,mo}\frac{h_{mo}}{h_{Ma}}$ and $E_{Ma} = \frac{E_{br}.E_{mo}.(h_{br}+h_{mo})}{E_{mo}h_{br} + E_{br}h_{mo}}$

$$\sigma_{yy,Ma} = \sqrt{2\frac{\frac{E_{br}.E_{mo}.(h_{br}+h_{mo})}{E_{mo}h_{br}+\ E_{br}h_{mo}}\ \gamma_s}{\pi a}}$$

$$F_{cr,Ma} = \sigma_{yy,Ma} = \sqrt{\frac{E_{br}.E_{mo}.(h_{br}+h_{mo})}{E_{mo}h_{br}+\ E_{br}h_{mo}}.\frac{2\gamma_s}{\pi a}} \qquad 5.21$$

For N number of cracks. Total cracking strength will be.

$$\text{N}.F_{cr,Ma} \qquad 5.22$$

If $\sigma_{yy,Ma}\ (F_{cr,Ma}) \geq \sigma_c$, or if $\frac{\partial U_E}{\partial a} \geq \frac{\partial U_s}{\partial a}$ then crack propagates.

where,

$\sigma_{yy,Ma}$= tensile stress needed for crack to propagates

$F_{cr,Ma}$ = cracking strength of masonry

σ_c = critical cracking stress

5.2. CRACKING STRENGTH FOR MASONRY SUBJECTED TO SHEAR STRESS

When the stress is shear stress as seen in figure 5.4a, the shear strain energy becomes as computed as shown.

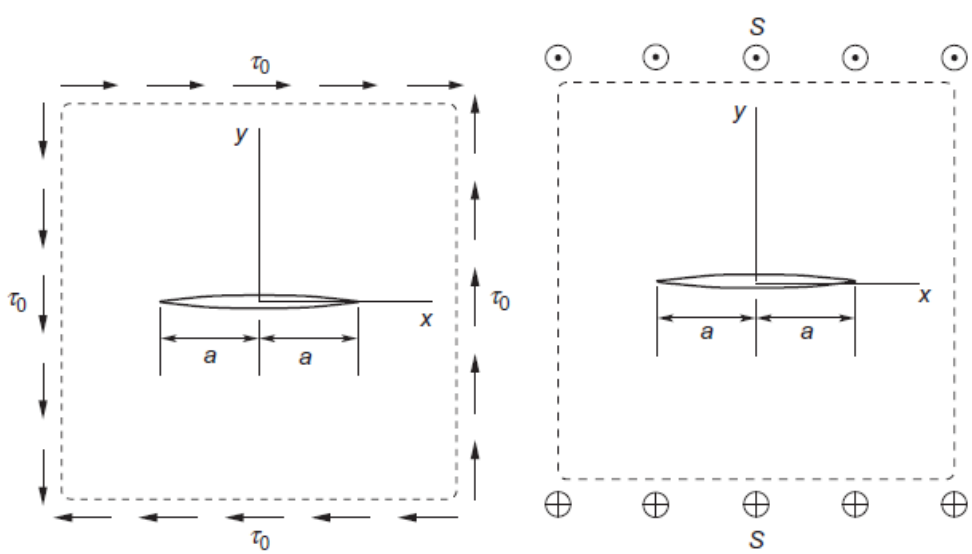

(a). (b)

Figure 5.4; (a) crack in pure in-plane shear and Figure. (b) out of plane shear respectively.

Shear strain energy per unit volume or energy density U_d in terms of shear strain is given by.

$$U_d = \frac{1}{2}\tau_{xy,Ma}.\gamma_{xy,Ma} \qquad 5.23$$

And going through the previous procedures again and from hook's law, shear strain γ_{xy} corresponding to shear stress τ_{xy} in xy plane,

$$\gamma_{xy,Ma} = \frac{\tau_{xy,Ma}}{G_{xy,Ma}}$$

Substituting the shear strain into equation 5.52, we have

$$U_d = \frac{1}{2}\frac{\tau_{xy,Ma}^2}{G_{xy,Ma}} \qquad 5.24$$

Elastic strain energy released due to shear U_E is given by $U_E = U_d\ .V,$ therefore

$$U_E = \frac{1}{2}\frac{\tau_{xy,Ma}^2}{G_{xy,Ma}}.V \qquad 5.25$$

Volume of the cracked material is the volume of the cracked ellipse = area multiply by thickness

$$V\ = 2\pi a^2.\ \mathrm{t} = 2\pi a^2\mathrm{t}$$

Hence elastic strain energy released in the uncrack volume is

$$U_E = \frac{1}{2}\frac{\tau_{xy,Ma}^2}{G_{xy,Ma}}\ .\ 2\pi a^2\mathrm{t}$$

$$U_E = \pi\frac{\tau_{xy,Ma}^2}{G_{xy,Ma}}\ a^2\mathrm{t} \qquad 5.26$$

Strain energy per unit thickness would be,

$$U_E = \frac{\pi\,\tau_{xy,Ma}^2}{G_{xy,Ma}}a^2$$

Total energy in the material is the change in potential energy of the specimen with elliptical crack,

$$U_T = U_{cracked} - U_{uncracked} = \Delta U = U_S - U_E$$

$$U_T = 4a\gamma_s - \frac{\pi\,\tau_{xy}^2\,a^2}{G_{xy,Ma}} \qquad 5.27$$

Applying the conservation of energy principle when the cracks grow by amount, da. Crack is stable when terms are balanced, and equilibrium condition is maintained

$$\frac{dU_T}{da} = 0$$

$$\frac{d}{da}(4a\gamma_s\ - \frac{\pi\,\tau_{xy,Ma}^2\,a^2}{G_{xy,Ma}}) = 0$$

$$\frac{d}{da}(4a\gamma_s) - \frac{d}{da}\left(\frac{\pi\,\tau_{xy,Ma}^2\,a^2}{G_{xy,Ma}}\right) = 0$$

$$4\gamma_s - \frac{2\,\pi\,\tau_{xy,Ma}^2\,a}{G_{xy,Ma}} = 0$$

$$2\gamma_s = \frac{\pi\,\tau_{xy,Ma}^2\,a}{G_{xy,Ma}} \qquad 5.28$$

$$\therefore\ \tau_{xy,Ma}^2 = \frac{2\,G_{xy,Ma}\,\gamma_s}{\pi a}$$

$$\tau_{xy,Ma} = \sqrt{\frac{2\,G_{xy,Ma}\,\gamma_s}{\pi a}} \qquad 5.29$$

$$\tau_{xy,Ma} = \sqrt{\frac{2G_{xy,Ma}\,\gamma_s}{\pi a}} \qquad 5.30$$

From section 3.5,

$G_{xy,Ma} = \frac{G_{xy,br}.G_{xy,mo}.(h_{br}+h_{mo})}{G_{xy,mo}h_{br}+\ G_{xy,br}h_{mo}}$ and $\gamma_{xy,Ma} = \gamma_{xy,br}\frac{h_{br}}{h_{Ma}} + \gamma_{xy,mo}\frac{h_{mo}}{h_{Ma}}$ and $\tau_{xy,Ma} = \tau_{xy,br} = \tau_{xy,mo}$

$$\tau_{xy,Ma} = \sqrt{\frac{2\,\frac{G_{xy,br}.G_{xy,mo}.(h_{br}+h_{mo})}{G_{xy,mo}h_{br}+\ G_{xy,br}h_{mo}}\gamma_s}{\pi a}}$$

$$F_{cr,Ma} = \tau_{xy,Ma} = \sqrt{\frac{G_{x,y\ br}.G_{xy,mo}.(h_{br}+h_{mo})}{G_{xy,mo}h_{br}+\ G_{xy,br}h_{mo}}\cdot\frac{2\gamma_s}{\pi a}} \qquad 5.31$$

where,

$F_{cr,Ma}$ = cracking shear strength of masonry

$\tau_{xy,Ma}$ = in plane shear stress of the masonry in x-y plane

$G_{xy,Ma}$ = in plane shear modulus of the mortar in x-y direction

Plane subjected to pure anti-plane shear: Subsequently, for anti-shear stress (out of plane shear) in y-z or z-x direction and from young modulus.

$$\gamma_{yz,Ma} = \frac{\tau_{yz,Ma}}{G_{yz,Ma}} \text{ and } \gamma_{zx,Ma} = \frac{\tau_{zx,Ma}}{G_{zx,Ma}}$$

$$\tau_{yz,Ma} = \sqrt{\frac{2G_{yz,Ma}\,\gamma_s}{\pi a}} \quad \text{and} \quad \tau_{zx,Ma} = \sqrt{\frac{2G_{zx,Ma}\,\gamma_s}{\pi a}} \qquad 5.32$$

Also, from section 3.5,

$G_{yz,Ma} = \frac{G_{yz,br}.G_{yz,mo}.(h_{br}+h_{mo})}{G_{yz,mo}h_{br}+\ G_{yz,br}h_{mo}}$ and $\gamma_{yz,Ma} = \gamma_{yz,br}\frac{h_{br}}{h_{Ma}} + \gamma_{yz,mo}\frac{h_{mo}}{h_{Ma}}$ and $\tau_{yz,Ma} = \tau_{yz,br} = \tau_{yz,mo}$

$G_{zx,Ma} = \frac{G_{zx,br}.G_{zx,mo}.(h_{br}+h_{mo})}{G_{zx,mo}h_{br}+\ G_{zx,br}h_{mo}}$ and $\gamma_{zx,Ma} = \gamma_{zx,br}\frac{h_{br}}{h_{Ma}} + \gamma_{zx,mo}\frac{h_{mo}}{h_{Ma}}$ and $\tau_{zx,Ma} = \tau_{zx,br} = \tau_{zx,mo}$

$$F_{cr,Ma} = \tau_{yz,Ma} = \sqrt{\frac{G_{yz,br}.G_{yz,mo}.(h_{br}+h_{mo})}{G_{yz,mo}h_{br}+\ G_{yz,br}h_{mo}}.\frac{2\gamma_s}{\pi a}} \quad 5.33$$

$$\text{and } F_{cr,Ma} = \tau_{yz,Ma} = \sqrt{\frac{G_{zx,br}.G_{zx,mo}.(h_{br}+h_{mo})}{G_{zx,mo}h_{br}+\ G_{zx,br}h_{mo}}.\frac{2\gamma_s}{\pi a}} \quad 5.34$$

where

$F_{cr,Ma}$ = shear cracking strength of masonry

$\gamma_{yz,Ma}$ and $\gamma_{zx,Ma}$= anti-plane shear strain caused by shear stress

$\tau_{yz,Ma}$ and $\tau_{zx,Ma}$= anti-plane shear stress in masonry.

$G_{yz,Ma}$ and $G_{zx,Ma}$= out of plane shear modulus of the mortar

5.3. A RELATION AMONG ENERGIES (INCLUDING EXTERNAL ENERGY)

The Griffith theory for fracture of perfectly brittle elastic solids is founded on the principle of energy conservation, that is, energy added to and released from the body must be the same as that dissipated during crack extension. It states that, during crack extension of da, the work done dW_E by external forces, the increment of surface energy, dU_S, and the increment of elastic strain energy dU_E must satisfy,

$$dU_S + dU_E = dW_E \quad 5.35$$

For a conservative force field, the condition can be expressed in the form.

$$\frac{\partial}{\partial a}(U_S + U_E + V_E) = 0 \quad 5.36$$

where

U_S = total crack surface energy associated with the entire crack.

U_E = total elastic strain energy of the cracked body.

V_E = total potential of the external forces.

Note that a negative dV_E implies a positive work dW_E done by external forces.

In order to calculate the criterion for crack propagation, equation 1 is utilized.

6. THE ELASTIC STRESS FIELD AROUND A CRACK TIP, CRACK MODEL AND INTERFACE ELEMENT

Brittle fracture in a solid in the form of crack growth is governed by the stress field around the crack tip and by parameters that describe the resistance of the material to crack growth. Thus, the analysis of stresses near the crack tip constitutes an essential part of fracture mechanics. For brittle materials exhibiting linear elastic behavior, we use methods of elasticity to obtain stresses and displacements in cracked bodies. These methods include analytical ones, such as the complex potential function method and the integral transform method, and numerical ones, the complex potential function method is introduced and used to analyze the stresses and displacements around crack tips. The characteristics of the near-tip asymptotic stress and the crack growth criterion based on the crack tip field are discussed in this section.

6.1. MODES OF FRACTURE AND STRESS INTENSITY FACTOR

A crack in a solid consists of disjoined upper and lower faces. The joint of the two crack faces forms the crack front. The two crack faces are usually assumed to lie on the same surface before deformation. When the cracked body is subjected to external loads (remotely or at the crack surfaces), the two crack faces move with respect to each other and these movements may be described by the differences in displacements u_x, u_y, and u_z between the upper and lower crack surfaces, where (x, y, z) is a local Cartesian coordinate system centered at the crack front with the x-axis perpendicular to the crack front, the y-axis perpendicular to the crack plane, and the z-axis along the crack front.

There are three independent movements corresponding to three fundamental fracture modes as pointed out by Irwin, which are schematically illustrated in Figure 6.1. These basic fracture modes are usually called Mode I, Mode II, and Mode III, respectively, and any fracture mode in a cracked body may be described by one of the three basic modes, or their combinations as described below.

Linear elastic fracture mechanics is only valid for brittle materials e.g., ceramics, concrete, masonry etc. and for ductile materials; the region of plastic deformation is restricted to the vicinity of crack tip.

The failure mechanism is categorized into three modes as shown in the Figure 6.1

1. Mode I (Opening Mode): The two crack surfaces experience a jump only in u_y, that is, they move away symmetrically with respect to the undeformed crack plane (x-z-plane). This type of failure occurs in the unit.

2. Mode II (Sliding Mode): The two crack surfaces experience a jump only in u_x, that is, they slide against each other along directions perpendicular to the crack front but in the same unreformed plane. Crack tearing shear deformation parallel to crack direction. This type of failure occurs in the mortar.

3. Mode III (Tearing Mode): The two crack surfaces experience a jump only in u_z, that is, they tear over each other in the directions parallel to the crack front but in the same undeformed plane. crack tearing shear deformation perpendicular to crack direction.

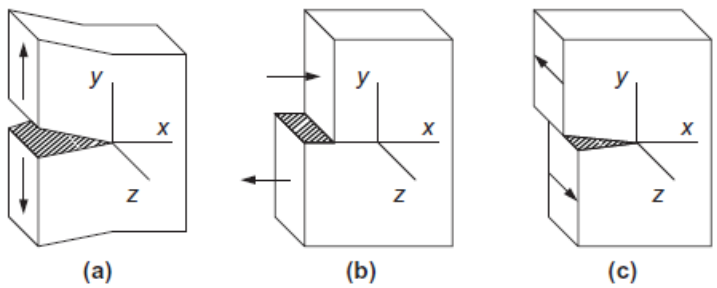

Figure 6.1; Schematic of the basic fracture modes: (a) Mode I (opening), (b) Mode II (sliding), (c) Mode III (tearing) (Z.-H. Jin, C. T. Sun).

The three basic modes of crack deformation can be more precisely defined by the associated stresses ahead of the crack front, which may be considered as the crack tip in two-dimensional problems. It will be seen in the following sections that the near-tip stresses in the crack plane (x-z-plane) for these three modes can be expressed as ($y = 0$, $x \rightarrow 0^+$) respectively,

For mode 'i', $\sigma_{xy} = \sigma_{yz} = 0$ and $\sigma_{yy} \neq 0$

$$\sigma_{yy} = \frac{K_1}{\sqrt{2\pi x}} + 0(\sqrt{x}), \qquad 6.1$$

For mode 'ii', $\sigma_{yy} = \sigma_{yz} = 0$ and $\sigma_{xy} \neq 0$

$$\sigma_{xy} = \frac{K_{II}}{\sqrt{2\pi x}} + 0(\sqrt{x}), \qquad 6.2$$

For mode 'iii', $\sigma_{yy} = \sigma_{xy} = 0$ and $\sigma_{yz} \neq 0$

$$\sigma_{xz} = \frac{K_{III}}{\sqrt{2\pi x}} + 0(\sqrt{x}), \qquad 6.3$$

where the three parameters

K_1 = stress intensity factors corresponding to the opening or splitting mode.

K_{II} = stress intensity factors corresponding to the sliding or shearing mode.

K_{III} = stress intensity factors corresponding to the tearing (anti-plane or out of plane shearing) mode.

These expressions show that the stresses have an inverse square root singularity at the crack tip and the stress intensity factors K_I, K_{II}, and K_{III} measure the intensities of the singular stress fields of opening, in-plane shearing, and anti-plane shearing, respectively.

6.1.1. FAILURE MECHANISM IN MODE I CRACK

One of the most typical crack problems in fracture mechanics is an infinite plane with a line crack of length 2*a* subjected to biaxial stress σ at infinity, as shown in Figure 6.1. In practice, if the crack length is much smaller than any in-plane size of the concerned elastic body, the region may be mathematically treated as an infinite plane with a finite crack. The problem is Mode I since the loads are symmetric with respect to the crack line.

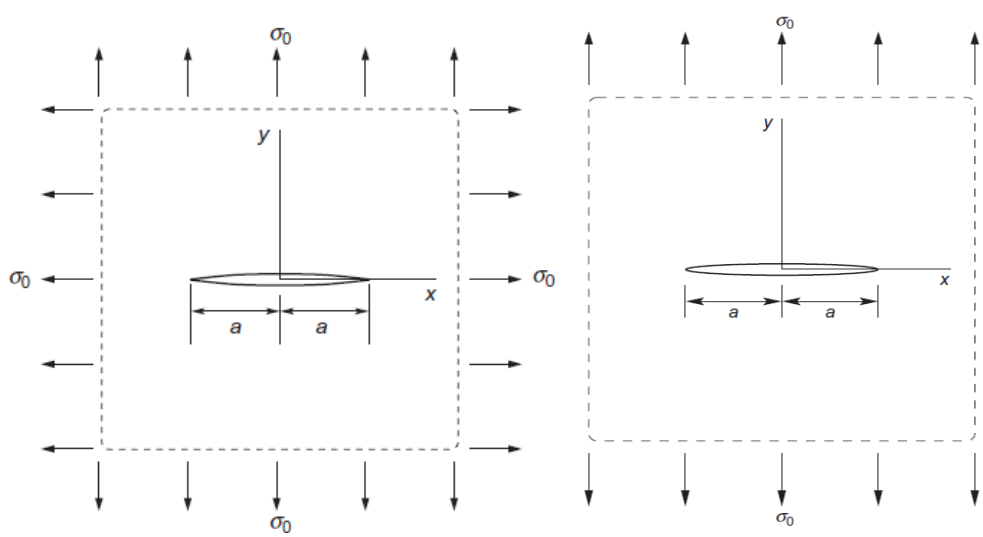

Figure 6.2; A crack in an infinite elastic plane subjected to (a) biaxial and (b) uniaxial tension.

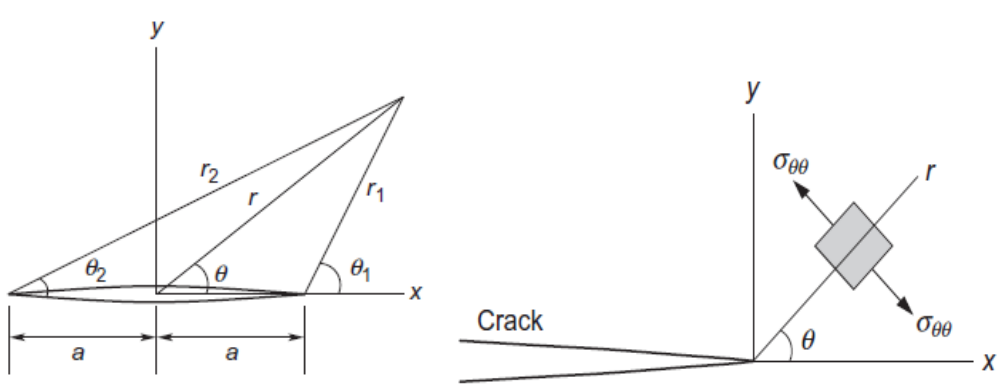

Figure 6.3; Coordinate systems at the crack tip and the circumferential stress σ

Irwin used the polar coordinate to express the stress components near the crack tip. Approximate stress field at the crack tip are obtained as follows,

$$\sigma_{xx} = \frac{\sigma_0\sqrt{a}}{\sqrt{2r_1}} \cos\tfrac{1}{2}\theta_1(1 - \sin\tfrac{1}{2}\theta_1 \sin\tfrac{3}{2}\theta_1) \qquad 6.4$$

$$\sigma_{yy} = \frac{\sigma_0\sqrt{a}}{\sqrt{2r_1}} \cos\tfrac{1}{2}\theta_1(1 + \sin\tfrac{1}{2}\theta_1 \sin\tfrac{3}{2}\theta_1) \qquad 6.5$$

$$\sigma_{xy} = \frac{\sigma_0\sqrt{a}}{\sqrt{2r_1}} \sin\tfrac{1}{2}\theta_1 \cos\tfrac{1}{2}\theta_1 \cos\tfrac{3}{2}\theta_1) \qquad 6.6$$

Along the crack extended line $\theta_1 = \theta = 0$, $\cos 0 = 1$ and inserting π in the numerator and the denominator, hence theses crack tip stresses reduce to,

$$\sigma_{xx} = 0.\ \sigma_{yy} = \frac{\sigma_0\sqrt{\pi a}}{\sqrt{2\pi r_1}}, \text{ and } \sigma_{xy} = 0$$

In the year 1957, G. Irwin found that stresses around a crack in terms of scaling factor. Stress intensity factor K is defined as,

if x = r_1, we then obtain σ_{yy}= $\frac{\sigma_0\sqrt{\pi a}}{\sqrt{2\pi x}}$, and compairing with equation 6.4, σ_{yy}= $\frac{K_1}{\sqrt{2\pi x}}$

$$K_1 = \sigma_0\sqrt{\pi a} \qquad 6.7$$

where σ = the remote stress

This relates the K_1 = with remote stress σ and crack length a. Its S: I unit is mpa$\sqrt{m}$.

K_1 depends on boundary conditions, therefore,

$$K_1 = \mathrm{Y}\sigma_0\sqrt{\pi a} \qquad 6.8$$

where Y is the geometric connection factor or stress intensity modification factor, calibrated by finite element.

Fracture toughness characterizes the resistance of a material to fracture when the stress intensity factor reaches a critical value, crack starts to grow.

$$K_{1c} = \mathrm{Y}\sigma_c\sqrt{\pi a} \qquad 6.9$$

where

K_{1c} = stress intensity factor in mode 1.

K_{1c} = stress intensity factor at critical region or fracture toughness in mode 1.

σ_0 = is the stress in the perpendicular crack direction.

σ_c = the critical stress strength.

If $K_1 > K_{1c}$, or $\sigma_0 > \sigma_{1c}$ failure occurs.

Fracture toughness is the critical stress intensity factor, as a material constant. It is independent of the loading conditions and crack length, and it is measured from experiments.

Note: If the initial notch is aligned with loading direction, no crack will occur

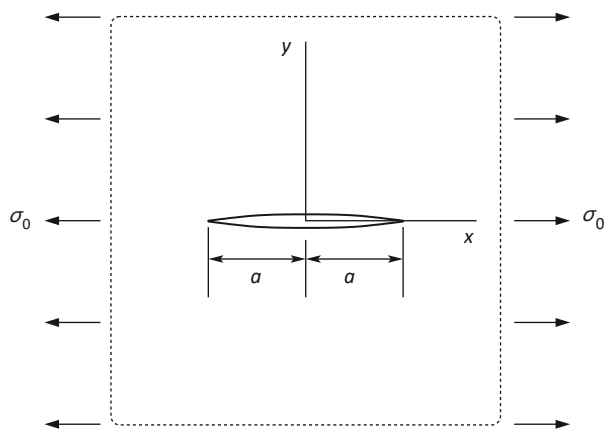

Figure 6.4; A crack in an infinite elastic plane subjected to uniaxial tension aligned to notch direction.

6.1.2. FAILURE MECHANISM IN MODE II CRACK

Consider a cracked plate of infinite extent that is subjected to uniform shear stress τ_0 at infinity as shown in Figure 6.5. This is a basic Mode II problem with the following skew-symmetric boundary conditions:

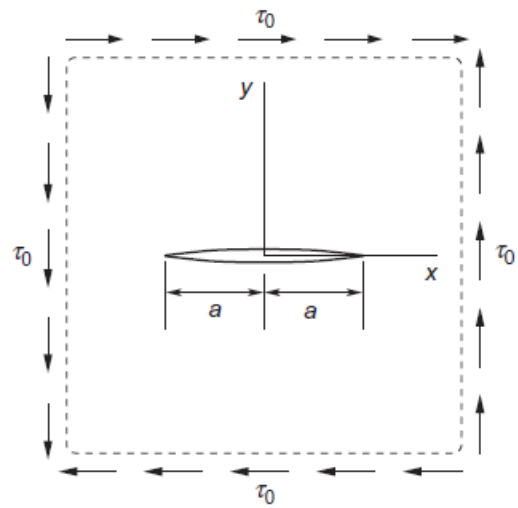

Figure 6.5; A crack in an infinite elastic plane subjected to pure in-plane shear.

Following the analytical solution, we have the complete stress field.

$$\sigma_{xx} = \frac{\tau_0\sqrt{a}}{\sqrt{2r_1}} \sin\tfrac{1}{2}\theta_1(2 + \cos\tfrac{1}{2}\theta_1 \cos\tfrac{3}{2}\theta_1) \qquad 6.10$$

$$\sigma_{yy} = \frac{\tau_0\sqrt{a}}{\sqrt{2r_1}} \sin\tfrac{1}{2}\theta_1 \cos\tfrac{1}{2}\theta_1 \cos\tfrac{3}{2}\theta_1) \qquad 6.11$$

$$\sigma_{xy} = \frac{\tau_0\sqrt{a}}{\sqrt{2r_1}} \cos\tfrac{1}{2}\theta_1(1 - \sin\tfrac{1}{2}\theta_1 \sin\tfrac{3}{2}\theta_1) \qquad 6.12$$

Along the crack extended line (θ_1 = θ = 0) and x = r_1 near the crack tip, the stresses are

$$\sigma_{xx} = 0.\ \sigma_{yy} = 0, \text{ and } \sigma_{xy} = \frac{\tau_0\sqrt{\pi a}}{\sqrt{2\pi x}}$$

Comparing with $\sigma_{xy} = \frac{K_{11}}{\sqrt{2\pi x}}$ from equation 6.5

$$K_{11} = \tau_0\sqrt{\pi a} \qquad 6.13$$

$$K_{11} = \Upsilon\tau_0\sqrt{\pi a} \qquad 6.14$$

where

τ_0 is the shear stress parallel to the direction of crack.

6.1.3. FAILURE MECHANISM IN MODE III CRACK

The Mode III fracture is associated with the anti-plane or out of plane deformation,

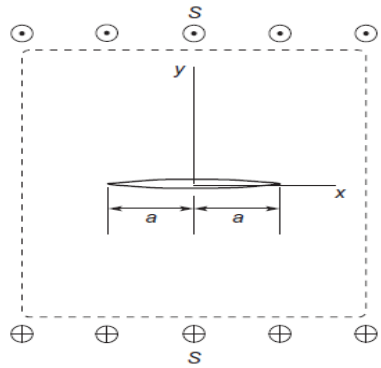

Figure 6.6; A crack in an infinite elastic body subjected to anti-plane shear.

And using the polar coordinates, the stress components can be obtained as

$$\sigma_{xz} = \frac{S\sqrt{a}}{\sqrt{2r_1}} \cos\frac{1}{2}\theta_1 \qquad 6.15$$

$$\sigma_{yz} = \frac{S\sqrt{a}}{\sqrt{2r_1}} \sin\frac{1}{2}\theta_1 \qquad 6.16$$

Again, consider the stress along the crack extended line ($\theta_1 = \theta = 0$) and near the crack tip. It is obtained as

$$\sigma_{yz} = 0, \;\; \sigma_{xz} = \frac{S\sqrt{\pi a}}{\sqrt{2\pi x}}$$

Comparing these stresses with eq. (6.6) $\sigma_{yz} = \frac{K_{III}}{\sqrt{2\pi x}}$, we have the Mode III stress intensity factor K_{III} for the crack problem as.

$$K_{III} = S\sqrt{\pi a} \qquad 6.17$$

Where S is the anti-shear stress (out of plane shear) or shear stress perpendicular to the direction of crack.

6.2. STRAIN ENERGY RELEASE RATE AND PLASTIC DEFORMATION AT THE CRACK TIP

Already established from equation 5.19 that,

$$2\gamma_s = \frac{\pi\sigma^2 a}{E_{Ma}}$$

For a plane stress state. See equation 5.20.

$$\sigma_c = \sqrt{\frac{2E_{Ma}\gamma_s}{\pi a}}$$

For plane strain state i.e., thicker specimen,

$$\sigma_c = \sqrt{\frac{2E_{Ma}\gamma_s}{\pi a(1-\mu^2)}} \qquad 6.18$$

In addition, mechanics of fracture depend on plastic work done γ_p and this γ_p depends on the crack speed, T of the material in brittle material,

If $\gamma_p < 0.1\ \gamma_s$ then we have $\gamma_s + \gamma_p$ instead of γ_s, Critical crack strength in plastic deformation is given by.

$$\sigma_c = \sqrt{\frac{2E_{Ma}(\gamma_s + \gamma_p)}{\pi a}} \qquad 6.19$$

For plastic deformation in plane strain,

$$\sigma_c = \sqrt{\frac{2E_{Ma}(\gamma_s + \gamma_p)}{\pi a(1-\mu^2)}} \qquad 6.20$$

If $\gamma_p >> \gamma_s$, this implies $\gamma_s + \gamma_p = \gamma_p$ for plane stress,

$$\sigma_c = \sqrt{\frac{2E_{Ma}\gamma_p}{\pi a}} \qquad 6.21$$

For plane strain, in plastic deformation,

$$\sigma_c = \sqrt{\frac{2E_{Ma}\gamma_p}{\pi a(1-\mu^2)}} \qquad 6.22$$

Fracture depends on crack extension force. Irwin suggests crack propagates when $\sigma_0 \geq \sigma_c$ (critical value)

Elastic energy in the material is defined from equation 5.10 and 5.15 as,

$$U_E = \frac{\pi\,\sigma_0^2\,a^2}{E_{Ma}} \text{ and } U_S = 4a\gamma_s$$

The half rate of change of elastic energy with respect to crack length is known as energy release rate,

$$G_{Ma} = \frac{1}{2}\frac{\partial U_E}{\partial a} = \frac{1}{2}\frac{\partial}{\partial a}\left(\frac{\pi\,\sigma_0^2\,a^2}{E_{Ma}}\right)$$

$$G_{Ma} = \frac{\pi\,\sigma_0^2\,a}{E_{Ma}} \qquad 6.23$$

Where G = strain energy release rate, the energy per newly created surface J/m^2. It is also called crack extension force, the force acting on crack, normalized by crack length (N/m)

Similarly, energy release rate in terms of surface energy

$$G_{Ma} = \frac{1}{2}\frac{\partial U_S}{\partial a} = \frac{1}{2}\frac{\partial(4a\gamma_s)}{\partial a}$$

$$G_{Ma} = 2\gamma_s \qquad 6.24$$

Where a is the crack length and da is the crack extension. If the elastic body is free from external tractions, the potential energy becomes the strain energy. The energy release rate is then equivalent to the strain energy release rate.

$$G_{Ma} = G_{c,Ma} \qquad 6.25$$

Where G_c is the critical value of G. G_c is two times surface energy γ_c, which applies to perfectly brittle solids. Irwin and Orowan extended the preceding criterion to metals experiencing small-scale yielding by lumping the surface energy and the plastic energy dissipation into G_c.

6.3. THE RELATIONSHIP BETWEEN ENERGY RELEASE RATE AND STRESS INTENSITY FACTOR

The energy and the near-tip stress field approaches for the fracture of elastic bodies are equivalent, that is, there exists a unique relation between the energy release rate and the stress intensity factor. This relationship can be established by the so-called crack closure method.

From equation 6.9

$$\sigma_c\sqrt{\pi a} = \sqrt{2E_{Ma}\gamma_s} \qquad 6.26$$

This is the critical stress intensity factor $K_{1c} = \sigma_c\sqrt{\pi a} = \sqrt{2E_{br}\gamma_s}$ the fracture toughness which depends on the material constants.

From the equation 6.23

$$G_{Ma} = \frac{\pi\,\sigma_0^2\,a}{E_{Ma}} \text{ for plane stress}$$

$$GE_{Ma} = \pi\sigma_0^2 a \qquad 6.27$$

Squaring both sides of the equation

$$\sqrt{G_{Ma}E_{Ma}} = \mathrm{Y}\sigma_0\sqrt{\pi a} = K_1$$

Assuming Y = 1

$$\sqrt{E_{Ma}G_{1,Ma}} = \sigma_0\sqrt{\pi a} = K_1$$

$$\Rightarrow G_{1,Ma} = \frac{K_1^2}{E_{Ma}} \text{ for plane stress} \qquad 6.28$$

Similarly, for plane strain

$$G_{Ma} = \frac{\pi\, \sigma_0^2\, a\, (1-\mu^2)}{E_{br}} \text{ for plane strain}$$

$$GE_{Ma} = \pi\sigma_0^2 a\, (1 - \mu^2)$$

Squaring both sides

$$\sqrt{E_{Ma} G_{1,Ma}} = \sigma_0 \sqrt{\pi a} \sqrt{(1 - \mu^2)} = K_1 \sqrt{(1 - \mu^2)}$$

$$G_{1,Ma} = \frac{K_1^2}{E_{Ma}} (1 - \mu^2) \text{ for plane strain} \qquad 6.29$$

For Mode II and Mode III problems, if the crack is assumed to grow in its original direction (a Mode II crack generally deflects from the original crack direction; we can obtain similar relations between G and K as

$$G_{11,Ma} = \frac{K+1}{8\mu} K_{II}^2 \qquad 6.30$$

$$G_{111,,Ma} = \frac{1}{2\mu} K_{III}^2 \qquad 6.31$$

where k is the number of unit shear stress.

6.4. STRESS INTENSITY FACTOR AT AN INCLINED CRACK NOTCH (MIXED MODE FRACTURE)

Combined Mode I and Mode II tests are usually carried out on a tension panel with an oblique crack as shown in Figure 5.1. The in-plane sizes of the panel are much larger than the crack length so that the panel can be theoretically treated as an infinite one.

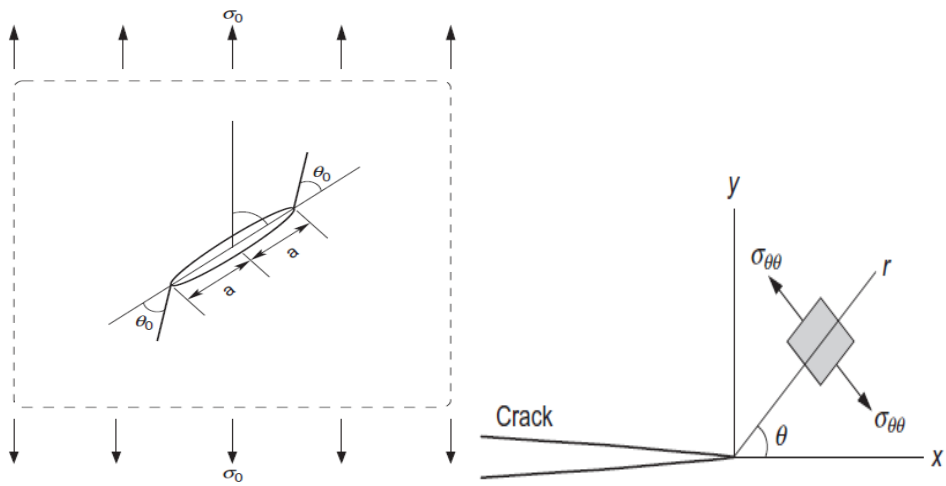

a b

Figure 6.7a; A tension panel with an oblique crack. The in-plane sizes of the panel are much larger than the crack length. Figure 6.7b Coordinate systems at the crack tip and the circumferential stress.

Where (r, θ) are the polar coordinates centered at the crack tip as shown in Figure 5.10. Using the coordinate transformation relations of stress tensor, the transformation matrix is deduced as

$$\begin{bmatrix} \cos^2\theta & \sin^2\theta & 2\sin\theta cos\theta \\ \sin^2\theta & \cos^2\theta & -2\sin\theta cos\theta \\ -\sin\theta cos\theta & \sin\theta cos\theta & \cos^2\theta - \sin^2\theta \end{bmatrix}$$

Let the old stress field be $\begin{bmatrix} \sigma_{xx} \\ \sigma_{yy} \\ \tau_{xy} \end{bmatrix}$ and new stress field be $\begin{bmatrix} \sigma_{xx^1} \\ \sigma_{yy^1} \\ \tau_{xy1} \end{bmatrix}$

Then we evaluate the new stress field, this is resolved by applying stress transformation.

$$\begin{bmatrix} \sigma_{xx^1} \\ \sigma_{yy^1} \\ \tau_{xy1} \end{bmatrix} = \begin{bmatrix} \cos^2\theta & \sin^2\theta & 2\sin\theta cos\theta \\ \sin^2\theta & \cos^2\theta & -2\sin\theta cos\theta \\ -\sin\theta cos\theta & \sin\theta cos\theta & \cos^2\theta - \sin^2\theta \end{bmatrix} \begin{bmatrix} \sigma_{xx} \\ \sigma_{yy} \\ \tau_{xy} \end{bmatrix} \qquad 6.32$$

Solving for σ_{x^1}, σ_{y^1} and $\tau_{x^1y^1}$

$$\sigma_{xx^1} = \sigma_{xx}\cos^2\theta + \sigma_{yy}\sin^2\theta + 2\tau_{xy}\sin\theta cos\theta$$

$$\sigma_{yy^1} = \sigma_{xx}\sin^2\theta + \sigma_{yy}\cos^2\theta - 2\tau_{xy}\sin\theta cos\theta$$

$$\tau_{xy1} = (\sigma_{yy} - \sigma_{xx})\sin\theta cos\theta + 2\tau_{xy}(\cos^2\theta - \sin^2\theta)$$

Loading condition: $\begin{pmatrix}\sigma_{xx}\\ \sigma_{yy}\\ \tau_{xy}\end{pmatrix} = \begin{pmatrix}0\\ \sigma\\ 0\end{pmatrix}$

$$\sigma_{xx^1} = \sigma_{yy}\sin^2\theta \qquad 6.33$$

$$\sigma_{yy^1} = \sigma_{yy}\cos^2\theta \qquad 6.34$$

$$\tau_{xy1} = \sigma_{yy}\sin\theta cos\theta \qquad 6.35$$

Therefore, the combined or mixed stress intensity factor is given as, for splitting, mode 1

$$K_1 = \mathrm{Y}\sigma_{yy^1}\sqrt{\pi a} = \mathrm{Y}\sigma_{yy}\cos^2\theta\sqrt{\pi a} \qquad 6.36$$

And shearing, mode 11

$$K_{11} = \mathrm{Y}\tau_{xy1}\sqrt{\pi a} = \mathrm{Y}\sigma_{yy}\sin\theta cos\theta\ \sqrt{\pi a} \qquad 6.37$$

Hence the mixed modes would be $K_1 + K_{11}$ for x and y direction loading respectively.

$$K_1 + K_{11} = \mathrm{Y}\sigma_{yy}\cos^2\theta\sqrt{\pi a} + \mathrm{Y}\sigma_{yy}\sin\theta cos\theta\sqrt{\pi a} \qquad 6.38$$

Summary

With these analytical expressions, we can deduce that,

- Tension loading: the total cracking strength of masonry occurs in the unit (because the failure is occurring in the unit, hence we assumed that the mortar is stronger) and loading is mode 1.

$$F_{cr,Ma} = \sigma_{yy,Ma} = \sqrt{\frac{E_{yy,br}.E_{mo}.(h_{br}+h_{mo})}{E_{yy,mo}h_{br} + E_{yy,br}h_{mo}}.\frac{2\gamma_s}{\pi a}} \qquad 6.39$$

- Shear loading: the mortar is weaker: here the cracking of the mortar is best described as shear failure, i.e., loading and cracking in mode 11.

$$F_{cr,Ma} = \tau_{xy,Ma} = \sqrt{\frac{G_{x,y\ br}.G_{xy,mo}.(h_{br}+h_{mo})}{G_{xy,mo}h_{br} + G_{xy,br}h_{mo}}.\frac{2\gamma_s}{\pi a}} \qquad 6.40$$

- In case of out of plane loading (mode III).

$$F_{cr,Ma} = \tau_{yz,Ma} = \sqrt{\frac{G_{yz,br}.G_{yz,mo}.(h_{br}+h_{mo})}{G_{yz,mo}h_{br} + G_{yz,br}h_{mo}}.\frac{2\gamma_s}{\pi a}} \qquad 6.41$$

- Inclined notch: If the masonry has an inclined notch, the shear failure is distributed along the edges, and this causes a split in the unit. Hence

$$F_{cr,Ma} = \sigma_{yy,Ma} + \tau_{xy.Ma}$$

$$F_{cr,Ma} = \sqrt{\frac{E_{yy,br}.E_{mo}.(h_{br}+h_{mo})}{E_{yy,mo}h_{br}+\ E_{yy,br}h_{mo}}.\frac{2\gamma_s}{\pi a}} + \sqrt{\frac{G_{x,y\ br}.G_{xy,mo}.(h_{br}+h_{mo})}{G_{xy,mo}h_{br}+\ G_{xy,br}h_{mo}}.\frac{2\gamma_s}{\pi a}} \qquad 6.42$$

6.5. COHESIVE CRACK MODEL

The cohesive crack model is generally accepted as a realistic simplification of the fracture of brittle or quasi-brittle materials. This model was proposed by Hillerborg, Modéer and Petersson in the late seventies (Hillerborg et al., n.d.), and initially called the fictitious crack model. In this model, the entire fracture process is lumped into a line, which makes it possible to treat the whole bulk of the body as elastic.

Besides the description of crack development, the cohesive crack models also describe the performance of uncracked material. Main features in the formulation of the relevant relationships of the cohesion crack model are:

1. The uncrack material can be described by a linear-elastic, isotropic, stress strain relationships using Young's modulus E and Poisson's ratio μ.

2 A cohesive crack initiates at the point where the maximum principal stress σ_1 first reaches a critical value called the cohesive strength σ_t. This cohesive crack forms normal to the direction of the major principal stress and given that this stress is induced by the notch, the cohesive crack forms ahead of the notch itself.

3 After its formation, the cohesive crack opens while transferring stress from one face to another. Once the crack has been initiated, the stress transferred (the cohesive stress) is a function of the crack opening displacement history. For monotonic mode (I) opening, the stress transferred, r, is normal to the crack faces and is a unique function of the crack opening w.

$$\sigma = f(w) \qquad 6.43$$

The function f(w) is termed the softening function or softening curve.

Two properties of the softening function are worth noting: the cohesive strength σ_1 and the cohesive fracture energy G_f.

The cohesive strength is the stress at which the crack is created and starts to open, i.e.

$$\sigma_1 = f(0) \qquad 6.44$$

The cohesive fracture energy G_F is the external energy supply required to create and fully break a unit surface area of the cohesive crack, and is given by the area under the softening function, i.e.

$$G_f = \int_0^{wc} f(w)dw$$

where w_c is the critical crack opening, after which the cohesive stress becomes zero.

σ

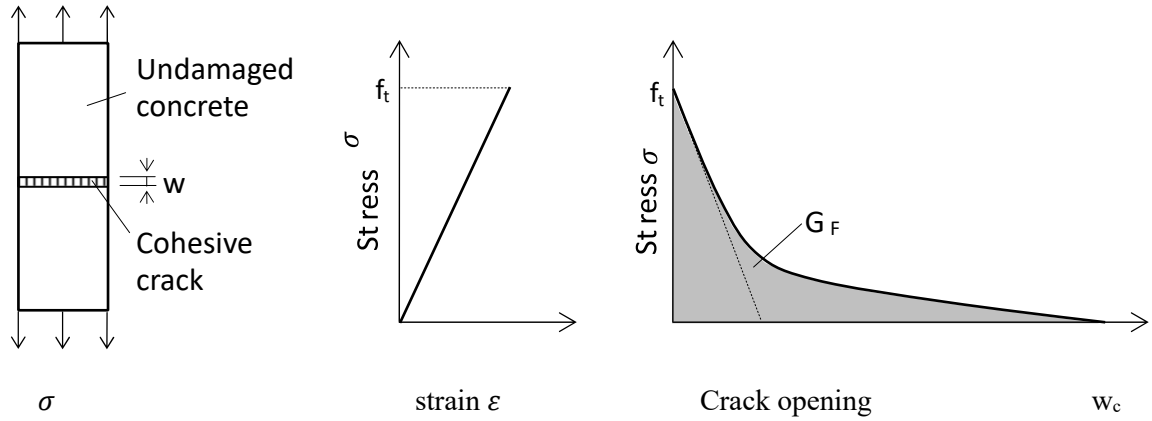

Figure. 6.8; The cohesive zone model loading and corresponding stress-strain graph.

The characteristic features of the softening function 3(w) are:

a) The stress σ which is transmitted when the crack is initiated (w = 0) is equal the tensile strength σ_t of the material.

b) The area under complete stress-crack opening curve corresponds to the fracture energy GF. This energy is defined as the energy needed for a complete separation of the material ($w > w_c$).

c) The critical crack opening w_c is defined as a crack opening at which no tension stresses can be transmitted across the crack anymore.

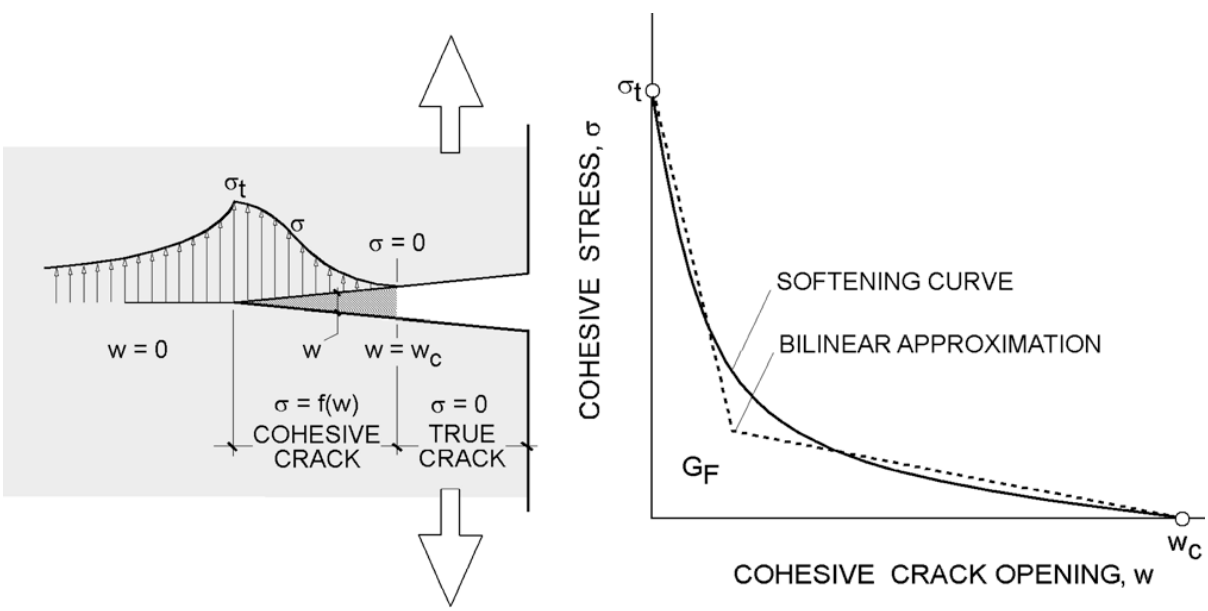

Figure 6.9; The cohesive zone model; notation used and sketches of two softening functions (Rocco & Roselló, 2008).

6.5.1. CONCEPT OF THE CHARACTERISTIC LENGTH AND FRACTURE ENERGY

A further parameter, important in the structural behavior, is the characteristic length: The characteristic length l_{ch} equals a half-length of the specimen, in which the accumulated elastic energy is equal to the energy needed for a complete separation of the material (energy consumed during the cracking process).

From Hook's law of elasticity,

$$\varepsilon_{yy,Ma} = \frac{\sigma_{yy,Ma}}{E_{Ma}}$$

Elastic strain energy per unit volume or elastic strain energy density U_d is given by.

$$U_d = \frac{1}{2}\sigma_{yy,Ma} \cdot \varepsilon_{yy,Ma} \qquad 6.45$$

Substituting into equation 6.45, we get

$$U_d = \frac{1}{2}\frac{\sigma_{yy,Ma}^2}{E_{br}} \qquad 6.46$$

Elastic strain energy released U_E is given by $\frac{U_E}{V} = U_d$ therefore,

$$U_E = U_d \,.\, V \qquad 6.47$$

$$U_E = \frac{1}{2}\frac{\sigma_{yy,Ma}^2}{E_{Ma}} \,.\, V \qquad 6.48$$

Volume of the specimen $V = AL$

$$U_E = \frac{1}{2}\sigma_{yy,Ma}^2 \cdot \frac{AL}{E_{Ma}} \qquad 6.49$$

Energy for complete fracture per unit area $\frac{U_E}{A} = G_F$

$$G_F = \frac{1}{2}\frac{\sigma_{yy,ma}^2}{A}\frac{AL}{E_{ma}} \qquad 6.50$$

$$G_F = \frac{1}{2}\sigma_{yy,ma}^2\frac{L}{E_{ma}} \qquad 6.51$$

$$\frac{L}{2} = \frac{G_F E_{ma}}{\sigma_{yy,ma}^2}$$

$$l_{ch} = \frac{G_F E_{ma}}{\sigma_{yy,ma}^2} \qquad 6.52$$

For plain strain

$$l_{ch} = \frac{G_F}{\sigma_{yy,ma}^2} \frac{E_{ma}}{1-\mu^2} \qquad 6.53$$

$$\text{Hence } F_{c,Ma} = \sigma_{yy,Ma} = \sqrt{\frac{G_F E_{ma}}{l_{ch}}} \qquad 6.54$$

It can be observed that there is no clear correlation between both quantities, but with increasing bond strength, the fracture energy also tends to increase. This is only logical when the definition of the fracture energy is considered. From its definition, it is obvious that the fracture energy must be zero, when the tensile strength is zero and must be infinite, when the tensile strength is infinite. For analytical purposes, strength is directly proportional to the square root of fracture energy.

With an increase of l_{ch} the brittleness decreases. The average of all masonry prisms was 110 mm with a CV of l20%o and of the units 230 mm with a CV of 55%. in terms of brittleness the joint interface is twice as brittle as the units (Petersson, 1981).

This simple formulation of the cohesive crack model is able to capture the main aspects of the fracture of brittle materials, particularly of components with blunted notches that do not exhibit a pre-crack or singularity. This model can be generalized in different ways:

1. The material outside the process zone – considered initially as isotropic linear elastic – can behave in a more complex manner,

2. The softening function may depend on triaxiality or on a previous loading history, and

3. The uniaxial model formulation can be generalized to a mixed-mode one.

(Van der Pluijm, 1999) carried out deformation-controlled tests in small masonry specimens of solid clay and calcium-silicate units. These tests resulted in an exponential tension softening curve with a mode I fracture energy G_F ranging from 0.005 to 0.02 [N/mm] for a tensile bond strength ranging from 0.3 to 0.9 [$N/mm2$], He also found values ranging from 0. 06 to 0. 13 N/mm for tensile strength values ranging from 1. 5 to 3. 5 N/mm^2. According to the unit-mortar combination. This fracture energy is defined as the amount of energy to create a unitary area of a crack along the unit-mortar interface.

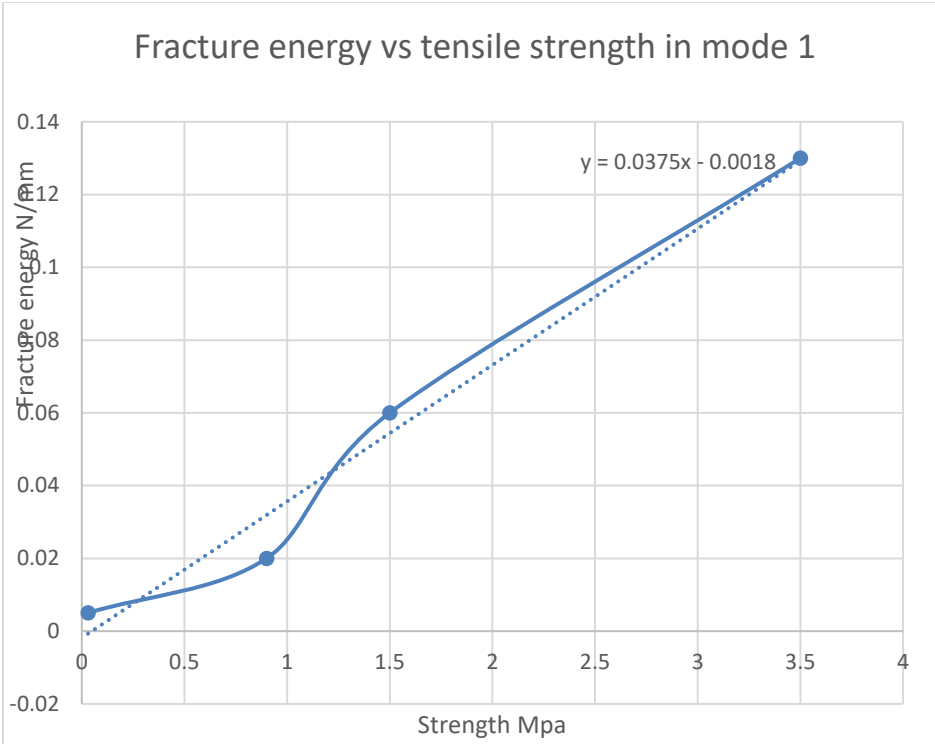

Figure 6.10; Tensile bond strength versus mode I fracture energy for all types of tested masonry.

6.5.2. THE BILINEAR SOFTENING CURVE

In concrete-like materials, the softening curve can be approximated by a bilinear function, as depicted in Figure 6.11 below. This simple diagram captures the essential facts: Large-scale debonding, or fracture, of aggregates in the steepest part, and frictional pull-out of aggregates and crack face bridging in the shallow tail of the diagram. This function is completely characterized.

When the following four parameters are known, as shown in Fig. 6.11, The tensile strength, the specific fracture energy G_F, the abscissa of the centroid of the softening area $\overline{w}$, and the initial slope, measured as the horizontal intercept w_1 of the initial segment.

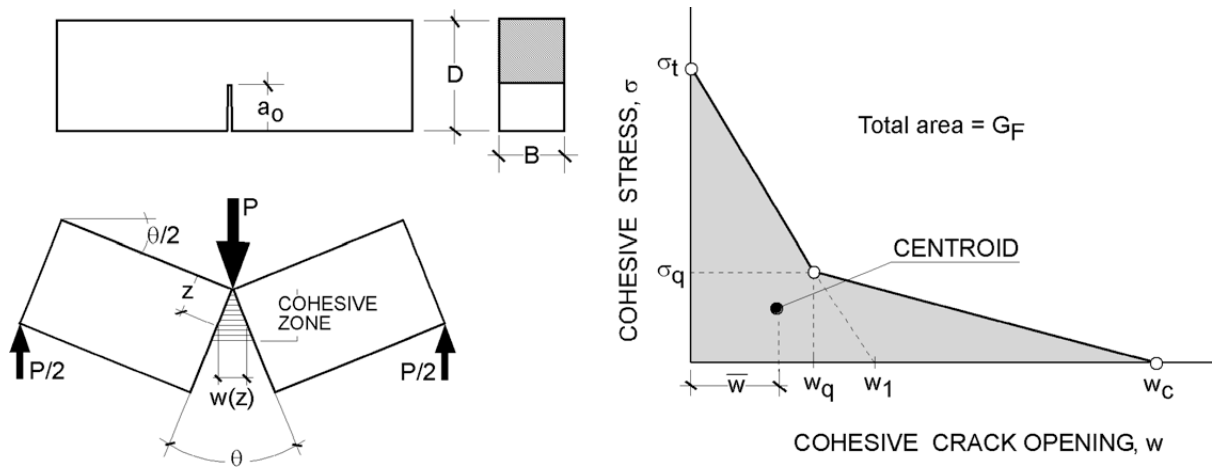

Figure 6.11; Sample geometry and rigid-body kinematics at the end of the bending test Simplified softening curve.

6.6. INTERFACIAL CRACKS BETWEEN TWO DISSIMILAR SOLIDS (E.G., BRICK AND MORTAR)

Engineering structures may be made of two or more dissimilar materials. Examples include structural composites, coating-substrate systems, and multilayered electronic devices. In a medium consisting of two or more materials with distinct properties, failure often initiates at the interfaces. Thus, the behavior of interface cracks is of interest.

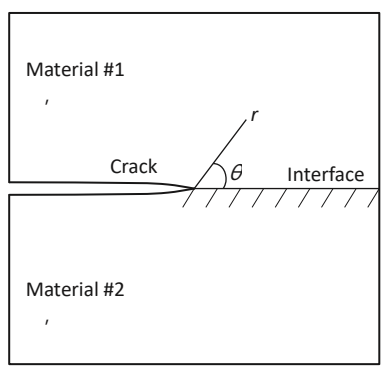

Figure 6.12; A crack at the interface between two dissimilar homogeneous materials.

6.6.1. INTERFACE MODEL

The interface cohesive model which combines damage and friction is described in this section. The interface model, developed based on the mechanical model proposed by Alfano and Sacco and by Alfano et al.,

adopts a micromechanical approach. In fact, with reference to a typical interface zone between brick and mortar, represented in Figure 7.4, a micromechanical analysis of the damaging process is analyzed. Three different states can be recognized at the brick-mortar interface:

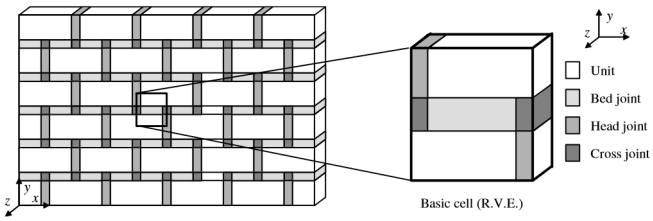

Figure 6.13a; Basic cell for masonry and homogenization process.

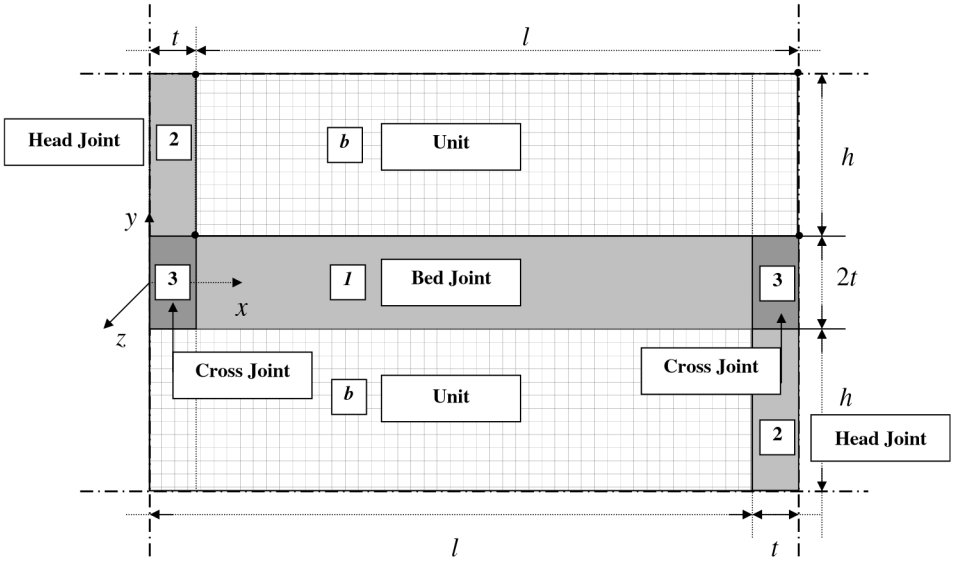

Figure. 6.13b; Definition of masonry axes and masonry components considered in the adopted formulation: unit, head joint, bed joint and cross joint.

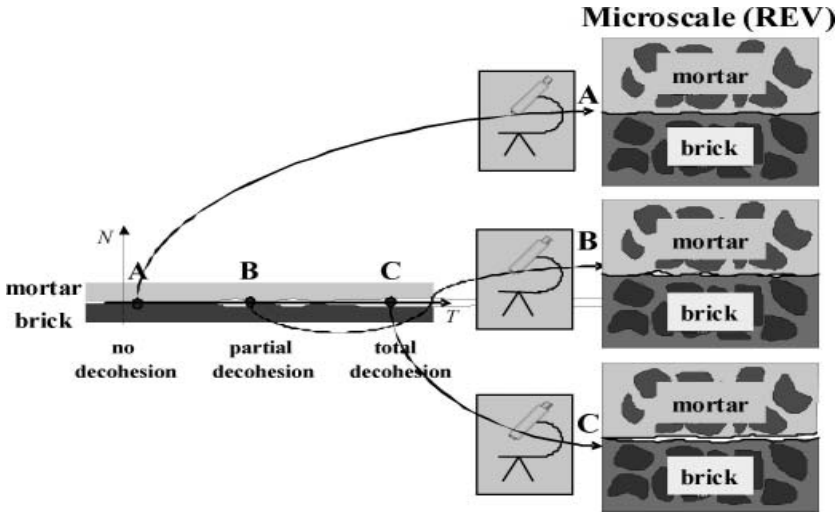

Figure 6.13c; Kinematics of the representative elementary volume.(Sacco & Toti, 2010).

- At interface point A, the mortar-brick connection is undamaged.
- At interface point B, partial decohesion between the two contact surfaces of the different materials occurred.
- At the interface point C, the decohesion phenomenon is complete.

The representative elementary volume (REV) of the interface is introduced; it is characterized by the height h, obtained as the sum of the thicknesses of the mortar and brick involved in the degradation phenomenon at interface, the length *b*, determined as the characteristic distance between the micro cracks, and the width *w*, which depends on the size of the mortar-brick. It can be remarked that the decohesion phenomenon of the two materials occurs with a physical degradation of thin layers in the adherents, where micro cracks and micro-voids arise. The thickness of the layers involved in the damage process of the adherent materials can be considered as a mechanical property of the mortar and brick. Thus, the height *h* of the REV depends on the specific materials in adhesion; the two layers involved in the damage process are often characterized by different thicknesses. Typically, a mortar layer of 1–3 mm and a brick layer of 0.5–2mm can be considered implicated in interface degradation.

Considering the REV of interface at point *A*, the contact surfaces do not present any detachment. The REV of interface associated to point *B* contains partial decohesion due to the presence of micro cracks, so that the representative area can be split in two parts: an undamaged part and a damaged one. In the REV corresponding to point *C* the coalescence of micro cracks occurred and a total decohesion is present, so that the REV results completely damaged.

Summarizing, the total area *A* at the brick-mortar material discontinuity in the REV, obtained as,

$$A = b \,.\, w \qquad 6.55$$

This can be decomposed into an undamaged part.

$$A_u = (b - a) \cdot w \qquad 6.56$$

And a completely damaged part

$$A_d = a \cdot w$$

Such that

$$A = A_u + A_d. \qquad 6.57$$

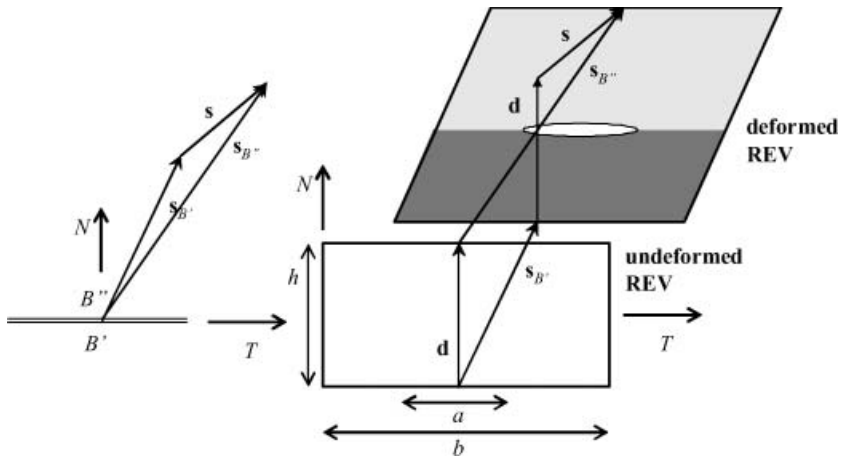

Figure 6.14. Kinematics of the representative elementary volume

Following standard arguments of continuous damage mechanics, the damage parameter D is introduced as the ratio between the damaged part and the whole area:

$$D = \frac{A_d}{A} = \frac{a}{b} \qquad 6.58$$

The two parts $A_u + A_d$. Can be recovered as $A_u = (1 - D)A$ and $A_d = AD$

Geometrical vector analysis, we have $S = S_{B^{\#}} - S_{B'}$

$$S_{B^{\#}} = S + S_{B'} \qquad 6.58$$

And the total length is.

$$d + S_{B^{\#}} = d + S + S_{B'} \qquad 6.59$$

Figure 5.14, the relative displacement S can be written as a function of

$$S = \{S_N \quad S_T\}^T \qquad 6.60$$

The relative displacement vector at the typical point of the mortar-block interface is denoted by s. Accordingly, the REV associated to the point is subjected to an overall relative displacement equal to S. In particular, the vector s represents in the REV the relative displacement between the two edges parallel to the micro crack direction, i.e., to the line of material discontinuity, as schematically illustrated in Figure 6.15.

Note that the relative displacement **s** induces in the REV only the average strain components.

$$\varepsilon_N = \frac{S_N}{h} \text{ and } \gamma_{NT} = \frac{S_T}{h} \qquad 6.61$$

According to the scheme illustrated in Figure 6.14, where only a half of the REV is reported, the overall behavior of the REV can be obtained as the superposition of three schemes: the first scheme considers the REV subjected to a relative displacement **s***e*, assuming the relative displacement of the crack mouths equal to zero; in the second scheme, a relative displacement **c**, able to account for the crack opening, is prescribed at the crack mouths, leading to the overall relative displacement S_c; in the third scheme, the REV is subjected to a relative displacement **p** at the crack mouths, due to the frictional sliding, which induces an overall relative displacement **s***p*. In such a way, the overall relative displacement **s** is obtained as:

$$S = S_e + S_c + S_p \qquad 6.62$$

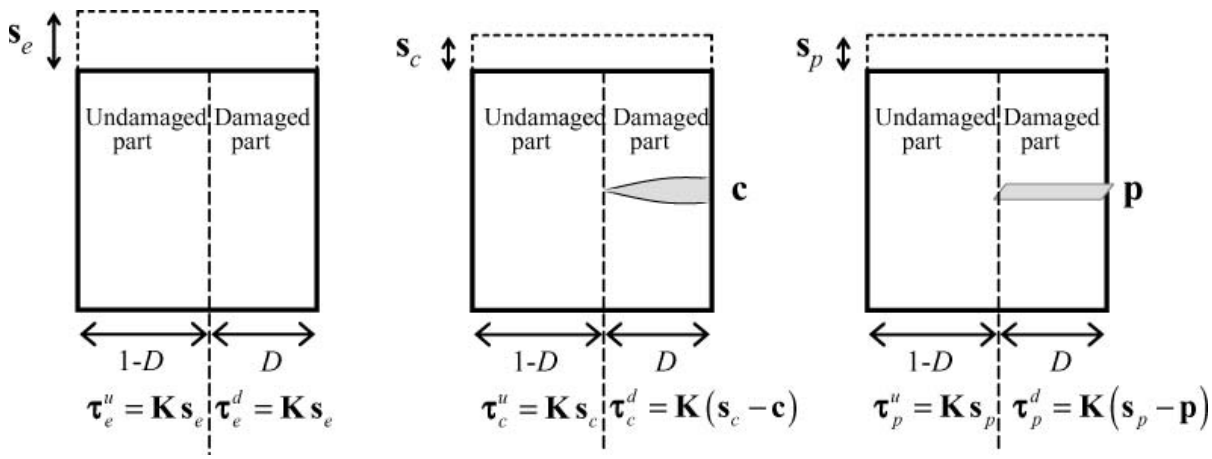

Figure 6.15 Mechanical scheme for the response of a half of the REV.

6.7. INTRODUCTION TO PHASE FIELD MODEL FOR FRACTURE

The variational formulation of brittle fracture as formulated where the total energy is minimized with respect to any admissible crack set and displacement field, allows the identification of crack paths, according to (C. Kuhn and R. Muller), branching of preexisting cracks and even crack initiation without additional criteria. For its numerical treatment a continuous approximation of the model in the sense of Γ-convergence has been presented by Bourdin in [2]. In the regularized Francfort- Marigo model, cracks are represented by a field variable (secondary variable) $s \in [0, 1]$ which is 0 if the material is cracked and 1 if it is undamaged.

In this work, we reinterpret the crack variable as a phase field order parameter and address cracking as a phase transition problem. The crack growth is governed by the evolution equation of the order parameter

which resembles the Ginzburg- Landau equation. The numerical treatment is done by finite elements combined with an implicit Euler scheme for the time integration.

6.7.1. THEORY OF A PHASE FIELD MODEL FOR FRACTURE

- Phase field models are mathematical models for solving interfacial problems.
- The method replaces boundary conditions at the interface by a PDE for an auxiliary field, called the phase field that takes the role of an order parameter.
- Values of the phase field are used to identify regions of the domain.
- As the phase field is evolved in time, the geometry of the interface (or crack) is likewise evolved.

7. NUMERICAL SIMULATION OF MASONRY (ANSYS MODEL)

The model is defined using different types of elements to reproduce the structural behaviour of a masonry wall consisting of two bricks and mortar between them. All elements are defined according to existing elements in ANSYS (ANSYS, 2009b). In this case, the elements considered to constitute the model are of type "plane finite element", "nonlinear spring element" and "contact element".

In this model, for every type of element, a different type of material (linear or nonlinear) and failure criteria or stress-strain relationship was considered. An important detail is that the model needs as input the mechanical properties of every structural component (bricks, mortar, bond and, eventually, concrete and steel i.e., for reinforced masonry).

The main properties of the materials are (Grabowski, 2005a) and (Van der Pluijm & Vullings, 2006):
Brick maximum compression strength: f_{br}=26900 KN/m^2 =$26.9 N/mm^2$.
Brick initial elasticity module: E_{br}= $4865 * 10^6\ kN/m^2 = 4865 N/mm^2$.
Mortar maximum compression strength: f_{mo}=$22000\ kN/m^2$ = $22 N/mm^2$.
Mortar initial elasticity module: $E_{mo} = 1.1178 * 10^6\ kN/m^2$ = $1178 N/mm^2$.
From Mauerwerk-Kalender (Irmschler, Schubert, & Jäger, 2004)
Poisson's coefficient for bricks: $\mu_{br} = 0{,}20$.
Poisson's coefficient for mortar: μ_{mo}= 0,15.
Length of brick = 150mm, Height of brick h_{br} = 100mm, Thickness of brick = 100mm, Height of mortar h_{mo} = 20mm.

7.1. DEFINING ENGINEERING DATA

The material parameters were taken directly from the standard masonry test modeling presented in the previous section of the thesis. However, as mentioned in the previous section most of the parameters that characterize behavior of masonry under tensile loads do not play any major significant role in the standard compression test. Therefore, at this stage there is no conclusive or complete set of material parameters to define masonry materials under tension.

The same approach is made to find the values for material parameters that will characterize masonry behaviour under tension without changing its compressive parameters in order to overcome this problem. The model underwent further iterations to first find out which material parameters affect it the most and what its values should be to obtain the optimal material.

Table 7.1; Stress – strain relationship in compression

strain	stress
0.00093	8,745
0.004	22,525
0.006	26,500
0.007	26,500
0.01	5,300
0.012	5,300

(a) brick

Strain	Stress
0	0
0.00165	4,059
0.005	9,225
0.01	12,300
0.012	12,300
0	0

(b) mortar

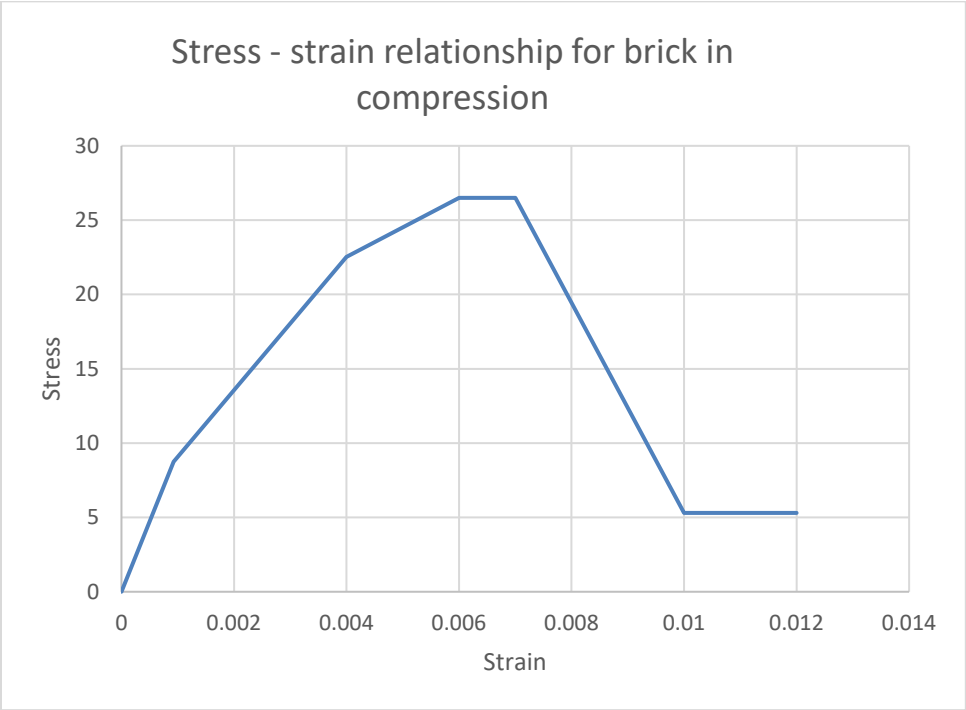

Figure 7.1; Stress-Strain relationship input for Drucker-Prager Brick in compression

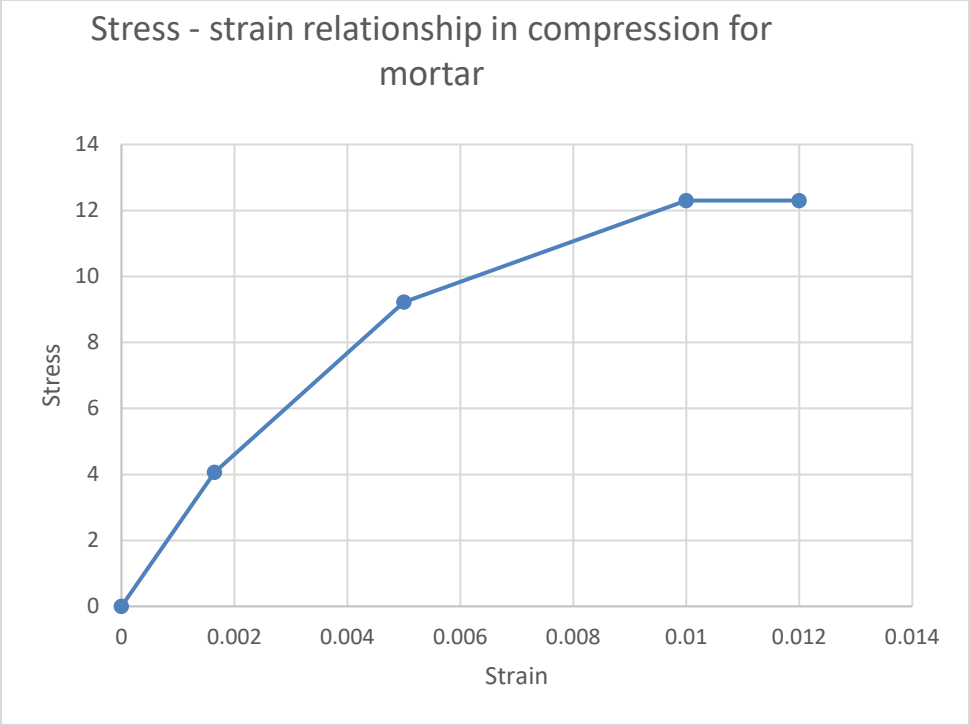

Figure 7.2; Stress-Strain relationship input for Drucker-Prager mortar in compression

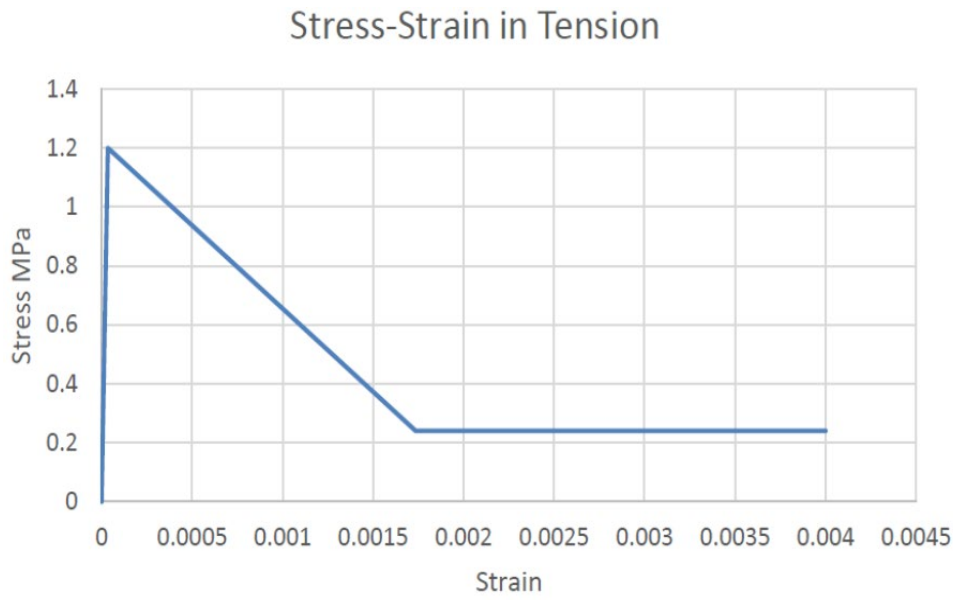

Figure 7.3; Stress-Strain relationship input for Drucker-Prager masonry in compression.

7.1.1. DEFINE ELASTIC MATERIAL PROPERTIES

The base elastic modulus and density of the material account for its self-weight are defined. The isotropic or anisotropic elastic behavior are also defined. The element type used is plane element 182.

Table 7.2; Elastic material parameters and density.

Constant	Notation	Property	Brick value	Mortar Value	Units
$C1$	ρ	Density	2100	1300	Kg/m^3
$C2$	E	Young modulus	4865	1178	MPa
$C3$	μ	Poisson's ratio	0,2	0,15	----

7.1.2. DEFINING EXTENDED DRUCKER-PRAGER CAP

The EDP Cap material model has a yield criterion similar to the other extended Drucker-Prager yield criteria with the addition of two cap surfaces that truncate the yield surface in tension and compression regions. It is used for modeling the geomaterial plasticity that results from compaction at low mean stresses, followed by significant pre-failure dilation, but before shear failure occurs. The following table lists the coefficients that are addressed for the cap model.

Table 7.3; Extended Drucker-Prager Cap Yield Function Values of the Parameters

Constant	Notation	property	Brick Values	Mortar Values
$C1$	R_c	Compaction cap parameter	7	7
$C2$	R_t	Expansion cap parameter	1	1
$C3$	X_i	Compaction cap yield pressure	-7,5	-7.5
$C4$	σ_c	Cohesion yield parameter	0,0005	1
$C5$	B	Shear envelope exponent	0,000007	0.931

$C6$	A	Shear envelope exponential coefficient	0,0001	0.0001
$C7$	α	Shear envelope linear coefficient	0,057704	0.058
$C8$	ω	Ratio extension to compression strength	0,9	0.9
$C9$	W_1^c	Limiting value of volumetric plastic strain	0.143	0.052
$C10$	D_1^c	Hardening parameter	0,03	0.076
$C11$	D_1^c	Hardening parameter	-0,00005	-0.0000

7.1.3. DEFINING THE DRUCKER-PRAGER YIELD-STRENGTH PARAMETERS

In Drucker-Prager material model, we define the Drucker – Prager Brick and Mortar yield strength, dilatancy and softening properties model. These values are gotten from the stress-strain relationship below.

Table 7.4; Drucker-Prager non-linear material parameters values.

Constant	Notation	Property	Brick value	Mortar Value	Units
$C1$	R_c	Uniaxial Compressive Strength	26,9	22	MPa
$C2$	R_t	Uniaxial Tensile Strength	3,7	1.9	MPa
$C3$	R_b	Biaxial Compressive Strength	30	24	MPa
$C4$	δ_t	Tensile Dilatancy Parameter	0,25	0,25	
$C5$	δ_t	Compressive Dilatancy Parameter	1,0	1,0	
$C6$	k_{cm}	Plastic strain at uniaxial compressive strength	0,007	0,005	

$C7$	k_{cr}	Ultimate effective plastic strain in compression	0,01	0,012	
$C8$	Ω_{ci}	Relative stress at start of nonlinear hardening	0,33	0,33	
$C9$	Ω_{cr}	Residual compressive relative stress	0,2	0,1	
$C10$	k_{tr}	Plastic strain limit in tension	0,002	0,002	
$C11$	Ω_{tr}	Residual tensile relative stress	0,2	0,2	

7.1.4. DEFINING THE MENETREY-WILLAM MODEL

To define the Menetrey-Willam yield strength parameters, the hardening-softening behavior of the yield surfaces is defined by the hardening-softening functions, the dilatancy angle is also defined.

Table 7.5; Menetery-Willam non-linear material parameters.

Constant	Notation	Property	Brick value	Mortar Value	Units
$C1$	R_c	Uniaxial Compressive Strength	42.3	28.1	MPa
$C2$	R_t	Uniaxial Tensile Strength	1.2	0,9	MPa
$C3$	R_b	Biaxial Compressive Strength	50,6	38	MPa
$C4$	w	Dilatancy angle	10	10	
$C5$	k_{cm}	Plastic strain at uniaxial compressive strength	0,007	0,005	
$C6$	k_{cr}	Ultimate effective plastic strain in compression	0,01	0,012	
$C7$	Ω_{ci}	Relative stress at start of nonlinear hardening	0,33	0,33	
$C8$	Ω_{cr}	Residual compressive relative stress	0,2	0,1	

$C9$	k_{tr}	Plastic strain limit in tension	0,002	0,002	
$C10$	Ω_{tr}	Residual tensile relative stress	0,2	0,2	

7.2. MODEL GEOMETRY, CONTACT, MESHING, AND BOUNDARY CONDITIONS

Model: A 2D surface body is created in ANSYS design modular as shown below

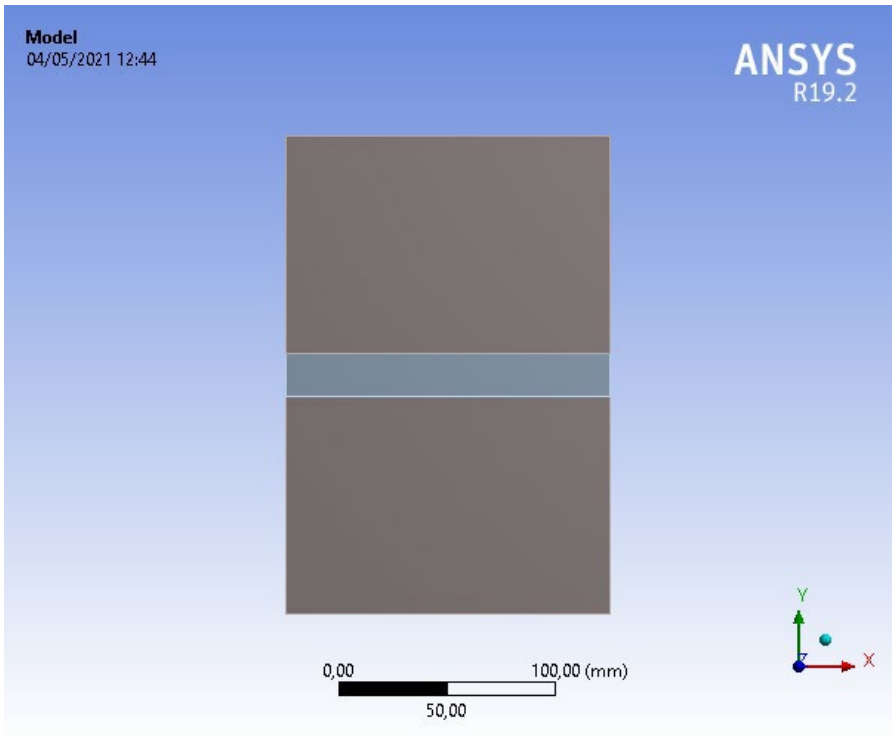

Figure 7.4; A 2D masonry model

Geometry: A 2D surface body in ANSYS workbench is created by first setting the analysis type to 2D, then proceeded by creating the three surface bodies as shown below. The surface body in between is the mortar. The dimension of the brick is 150x100mm and that of the mortar is 150x20mm.

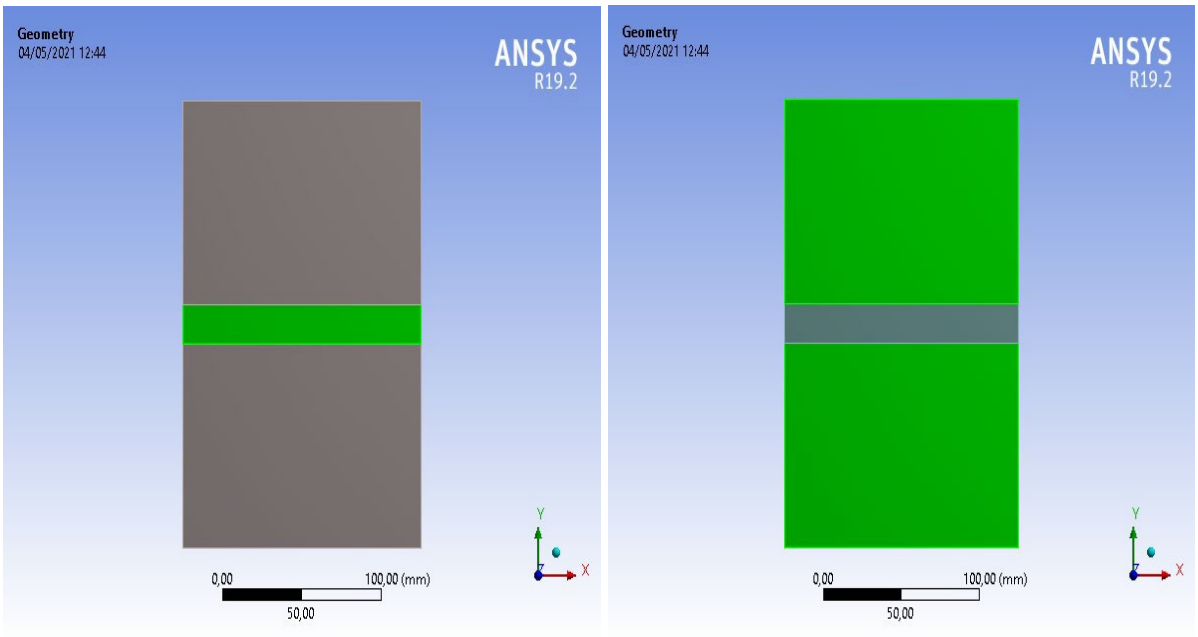

Figure 7.5; Geometry for 2D masonry structure.

Contact: The contact pair is created introducing a bonded region. In the first diagram, contact body is the bottom body (brick) and the second body (mortar) is target body. In the second figure, the contact body is the mortar while the target body is top brick.

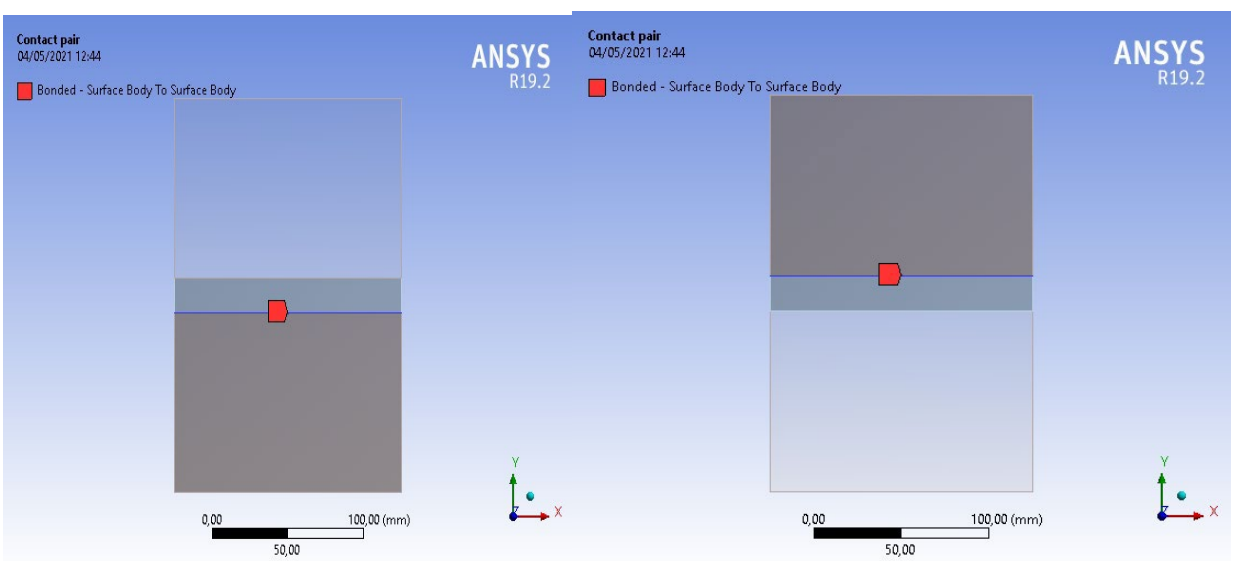

Figure 7.6; Bonded contact pair for 2D masonry composite.

Meshing formulation: A general meshing is used by setting the element size to 10mm and the element order is set as 'Linear' since a 2D surface body is applied. All other settings are left as default.

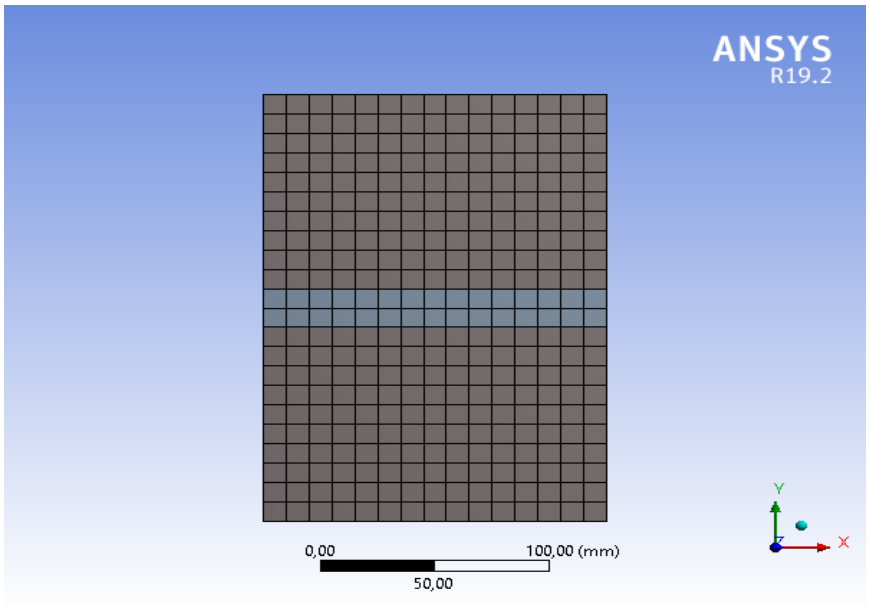

Figure 7.7; 2Dmeshing formulation

Boundary condition: The surface body is loaded at the bottom and at the top with a maximum pressure of 9Mpa. This loading condition enables the model to produce a symmetrical result.

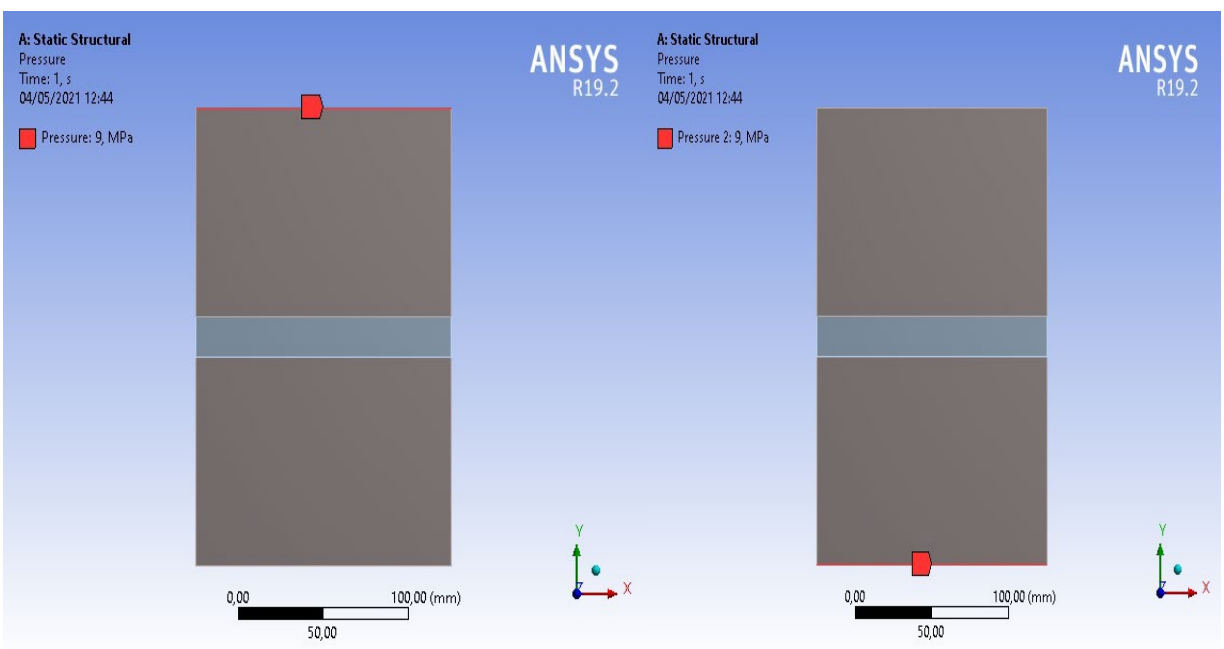

Figure 7.8; Boundary condition and loading.

7.2.1. POST PROCESSING FOR EXTENDED DRUCKER-PRAGER CAP WITH DRUCKER PRAGER SOFTENING RESULTS

The images visualization of the results is presented in this section. The main objective is to visualize deformation, stress, and plastic strains inside the model. The plastic strains results will suggest the crack formation and its location. The normal stresses will display the anisotropic nature of the masonry.

Directional deformation: the result of the deformations in y and x directions are shown below. The deformation at the top is the same as the deformation at the bottom because the plate is symmetrically loaded.

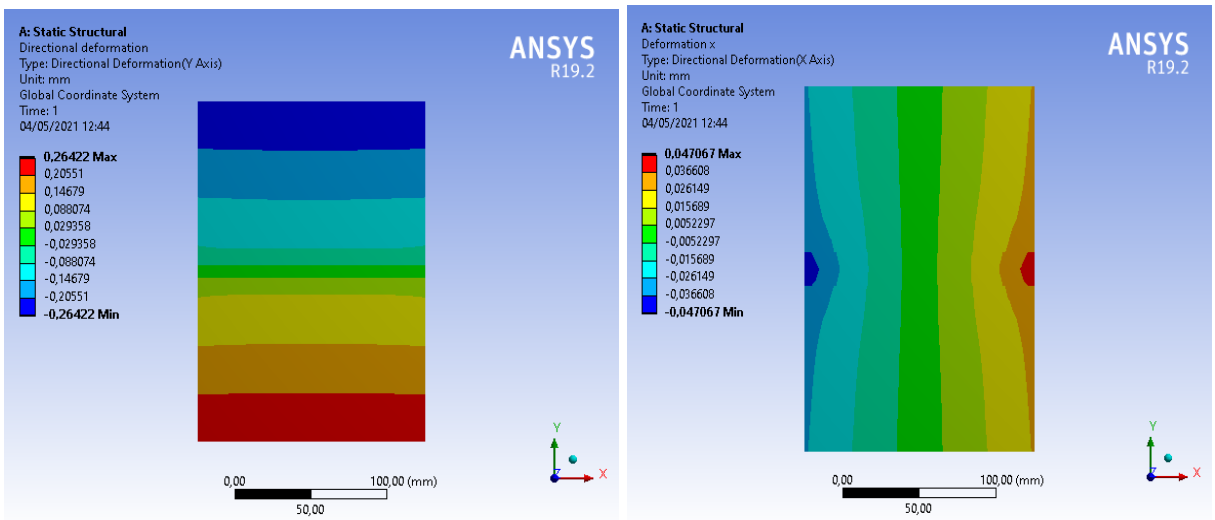

Figure 7.9 Drucker Prager Directional deformation in x and y directions.

Maximum and minimum principal stresses: This shows the anisotropic behavior of the masonry composite material as the compressive values are a lot higher than the tensile values. The maximum stress is 10Mpa.

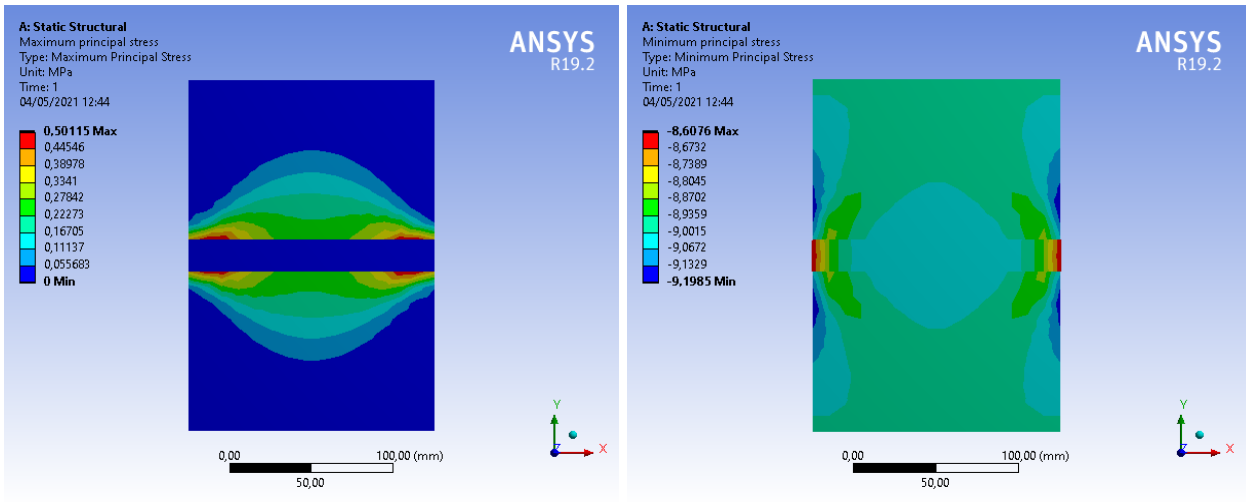

Figure 7.10; Drucker Prager Principal stresses.

Equivalent plastic strain: This is a measure of how cracks are distributed in the deformed body. The plastic strain location is exactly where they are expected to appear with the largest values right at the center (mortar) and at the interface between the brick and mortar, i.e., the joint. The interface is the region of the weakest part of masonry, the crack distribution around this zone is maximum.

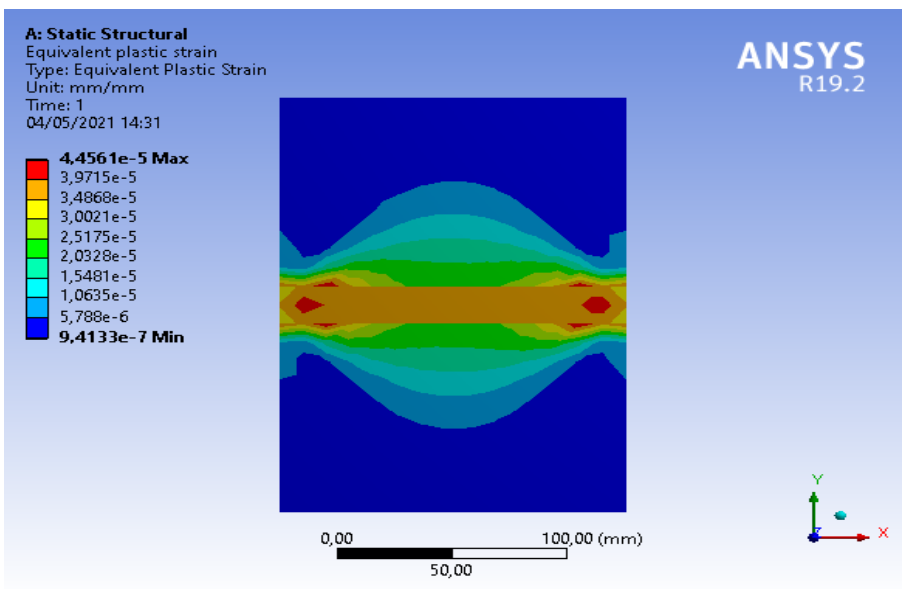

Figure 7.11; Drucker Prager Equivalent Plastic Strain

7.2.2. POST PROCESSING FOR EXTENDED DRUCKER-PRAGER CAP WITH MENETERY-WILLAM SOFTENING RESULTS

Directional deformation: this indicates that the deformation at the top is much more than the deformation at the bottom because the bottom is constrained.

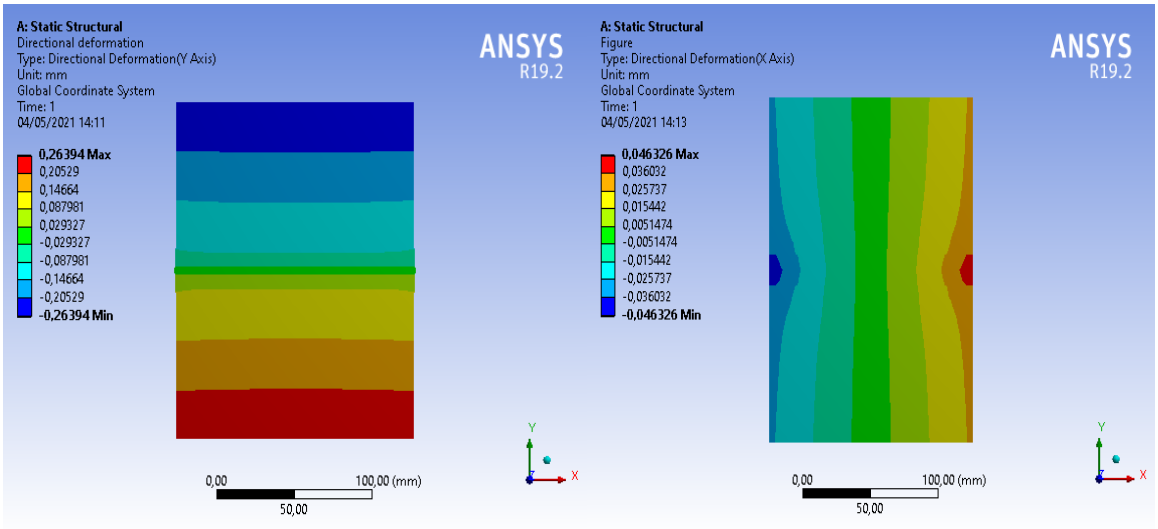

Figure 7.12; Menetery-Willam Directional deformation.

Principal stresses: This shows the anisotropic behavior of the masonry composite material as the compressive values are a lot higher than the tensile values.

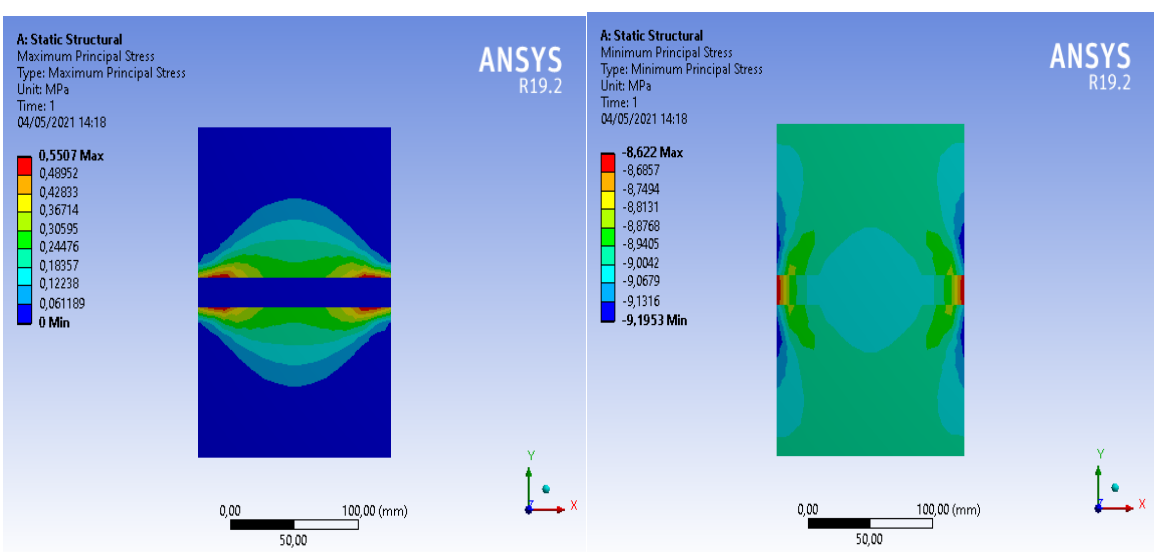

Figure 7.13; Menetery-Willam principal stresses

Equivalent plastic strain: This is a measure of how cracks are distributed in the deformed body. The plastic strain location is exactly where they are expected to appear with the largest values right at the center (mortar) and at the interface between the brick and mortar, i.e., the joint. The interface is the region of the weakest part of masonry, the crack distribution around this zone is maximum.

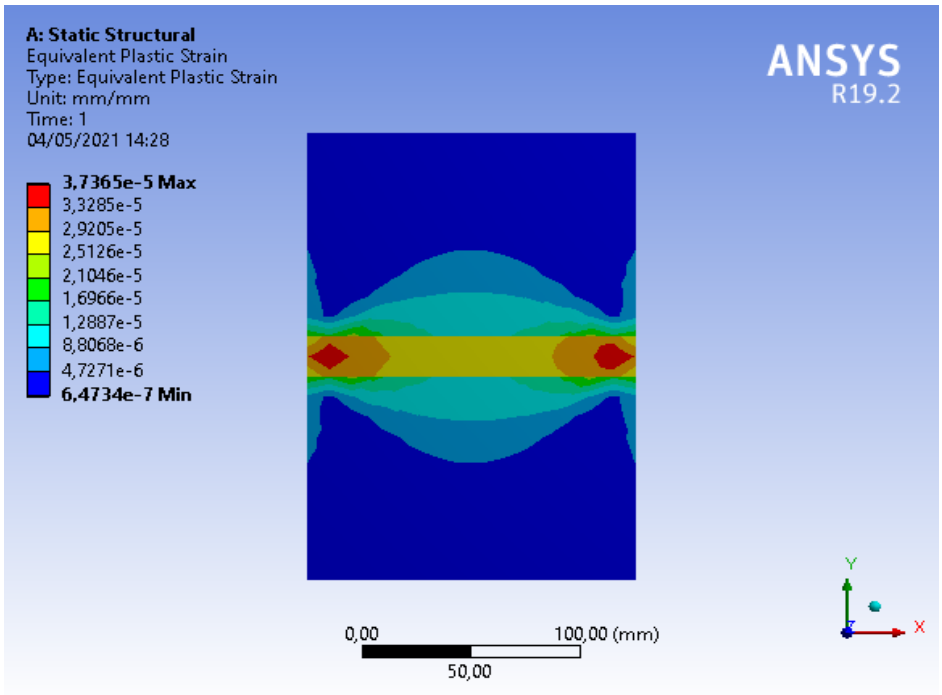

Figure 7.14; Menetery-Willam Equivalent Plastic Strain

7.2.3. COMPARISON OF CRACKING STRENGTH OF MASONRY WITH VARYING DIMENSIONS

- Length of brick = 200mm, Height of brick h_{br} = 250mm, Thickness of brick = 200mm, Height of mortar h_{mo} = 20m.

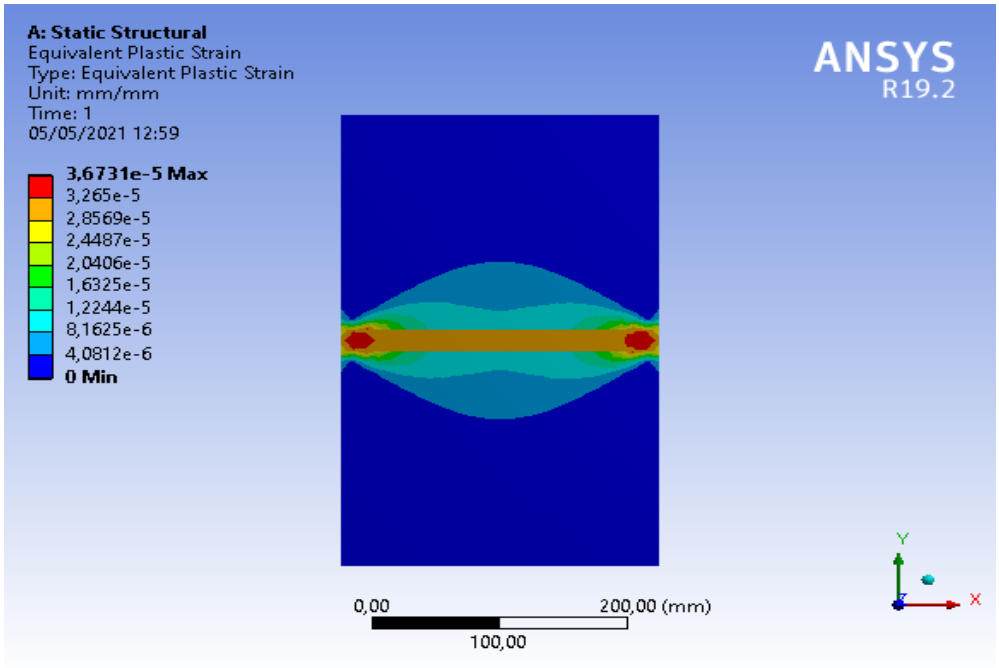

Figure 7.15; Drucker Prager Equivalent plastic strain for 250mmx200mm brick.

From this result, it can be observed that the higher the height of brick, lesser the compressive strength and then the higher crack distribution.

- Length of brick = 150mm, Height of brick h_{br} = 200mm, Thickness of brick = 150mm, Height of mortar h_{mo} = 15mm.

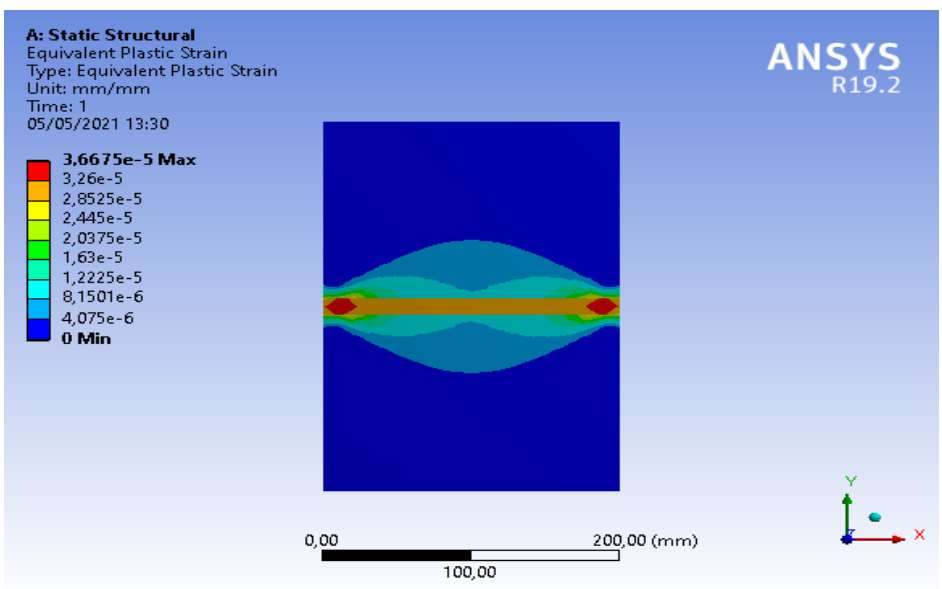

Figure 7.16; Drucker Prager Equivalent plastic strain for 200mmx150mm brick.

From this result, it can be observed that the higher the height of brick, the higher the compressive strength and then less crack distribution. The compressive strength however is lower than the first case above.

- Length of brick = 150mm, Height of brick h_{br} = 100mm, Thickness of brick = 100mm,

Height of mortar h_{mo} = 10mm.

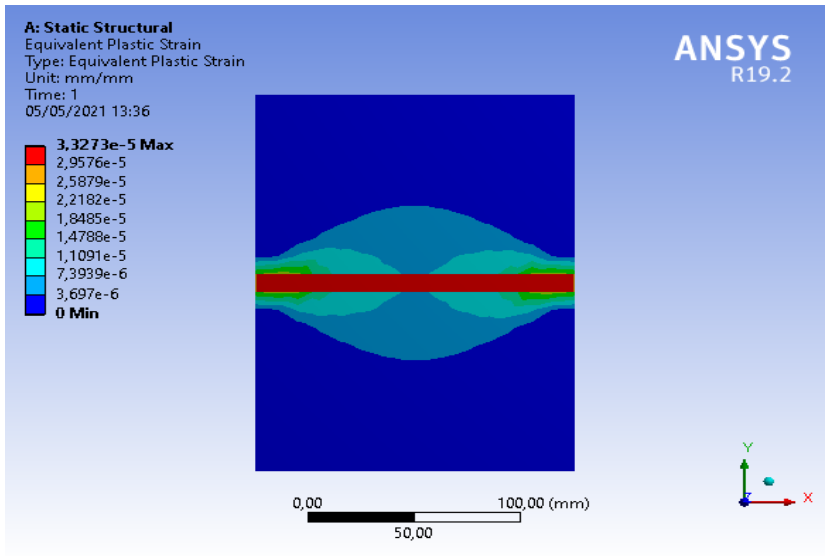

Figure 7.17; Drucker Prager Equivalent plastic strain for 150mmx100mm brick.

From this result, it can be observed that the lower the height of brick, the higher the compressive strength and then smaller the crack distribution. The compressive strength however is higher than the first two cases above because of the thin mortar and shorter brick.

7.3. VALIDATION OF MODEL RESULTS WITH EXPERIMENTAL RESULTS

In (Binda, Fontana, & Frigerio, 1988) experiments were performed on three masonry prisms with three different types of mortars. The prism dimensions were 500x250x600 mm and the bricks are length x width x height = 250 x 120 x 55 mm, mortar thickness was 12 mm. The mechanical properties of the units and mortars are listed in Table 6.2.

Table 7.6: Mechanical properties of masonry components and prisms

Specimen type	Compressive strength [N/mm2]	Tensile strength [N/mm2]	Elastic Modulus [N/mm2]	Poisson ratio [-]

Brick	26,9	3,7	4865	0,094
Mortar 1 MGr I1	1.2	0,9	1178	0,057

Table 7.7: Properties of masonry components, test results and calculated values.

Test ((Reference)	h_{mo} cm	Mortar group	p	h' cm	h'_{br} cm	$\bar{\mu}_{mo}$	$k1$	h''_{br} cm	d_{br} cm	$f_{c,br}$ [N/mm2]	$f_{t,br}$ [N/mm2]	$f_{c,Ma}$ [N/mm2]
MU1 (Binda)	1.2	II	30	1.89	5.5	0.4	0.3	5.5	12	26.9	3.7	11
Sample 1 (Warnecke)	2	I	20	3.40	10	0.5	0.3	15	15	99.6	3	11.4
Sample 2 (Warnecke)	2	III	40	2.93	10	0.3	0.3	15	15	99.6	3	23.8
Sample 3 (Warnecke)	3.75	I	20	6.38	10	0.5	0.3	15	17.5	22	1.6	4.7

This applies on mortar 1 and prism MU1. We use equation (3.36)

With Berndt equation,

$$f_{c,Ma} = \frac{f_{c,br}}{\left(\frac{h_{mo}}{h'_{br}} \frac{\bar{\mu}_{mo}}{1-\ \mu_{mo}} + k1 \frac{h'}{h''_{br}}\right)\left(\frac{15}{d_{br}}\right)^{(15/d_{br})} \frac{f_{c,br}}{f_{t,br}} +\ 0.7}$$

h' = sum of crumbled depths on both sides of the brick, could be calculated by equation (3.28):

$$h' = h_{mo} + \frac{h_{mo}}{\tan\left(45° + \frac{p}{2}\right)}$$

$$h' = 1.2 + \frac{1.2}{\tan\left(45° + \frac{30°}{2}\right)} = 1{,}89 \text{ cm}$$

By putting it in equation (3.36) we get,

$$f_{c,Ma} = \frac{26.9}{\left(\frac{1.2}{5.51} \frac{0.4}{1-\ 0.4} + 0.3 \frac{1.89}{5.5}\right)\left(\frac{15}{12}\right)^{(15/12)} \frac{26.9}{3.7} + 0.7} = 8{,}7\ N/mm^2$$

With Hilsdorf equation

$$\alpha = \frac{h_{Mo}}{4.1\ h_{Br.}} = \frac{12}{4.1 * 55} = 0.0532$$

$$F_{c,ma} = \frac{f_{c,br}\,(\alpha\, f_{c,mo} + f_{t,br})}{U(\alpha\, f_{c,br} + f_{t,br})} = \frac{26.9(0.0532*3.2+3.7)}{1.3(0.0532*26.9+3.7)} = 15.\,607 N/mm^2$$

Berndt is 26% less than test results on the safe side. Hilsdorf is 41.88% more than the test result.

Eurocode 6:1-1, 2013) gives a characteristic value of 5,19, this gives a difference of more than 52%.

Drucker Prager Model result is given below.

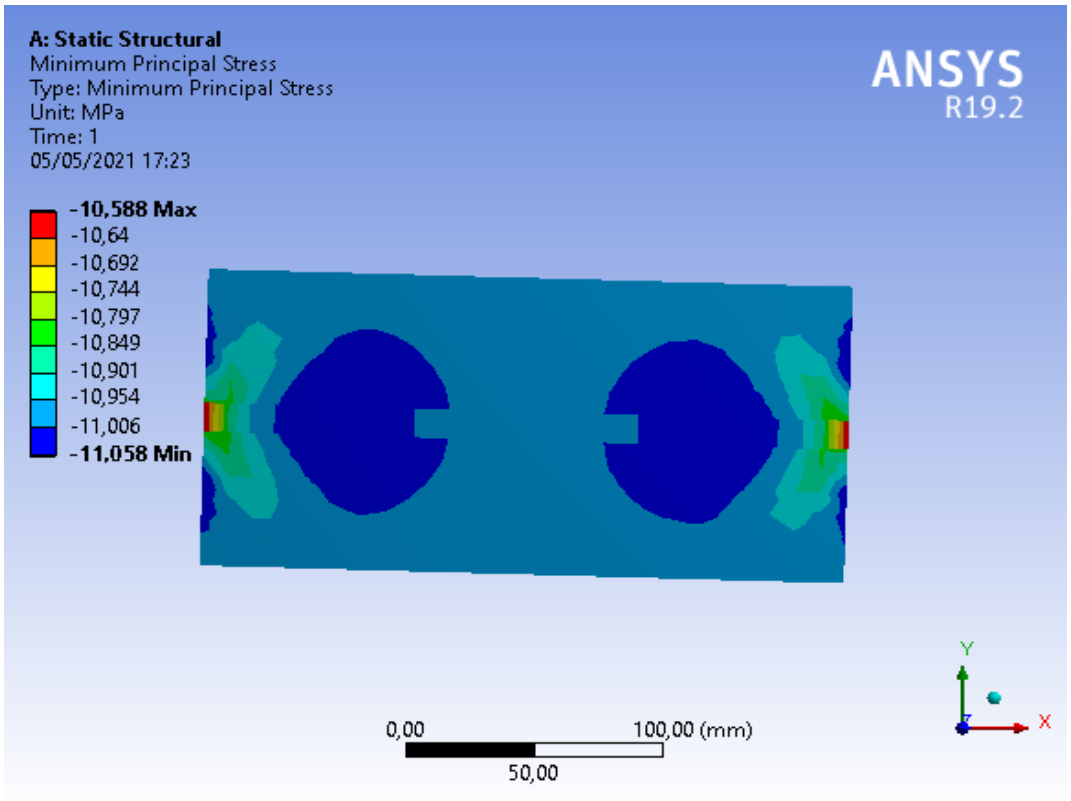

Figure 7.18; Compressive strength of DP masonry model

Comparing the DP values, Berndt values and the defined design values of Eurocode 6 with the test results are in the Table 7.6:

Table 7.8; Results of compressive strength of masonry compared to Drucker Prager model.

Test [Reference	Test 1	DP model 2	Berndt 3	Euro code 4	% error 1 &2	% error 2&3	% error 2 &4
MU1 [Binda]	11	11.058	8.7	5.19	0.525	20.363	53.066

Menetery-William Model result is given below.

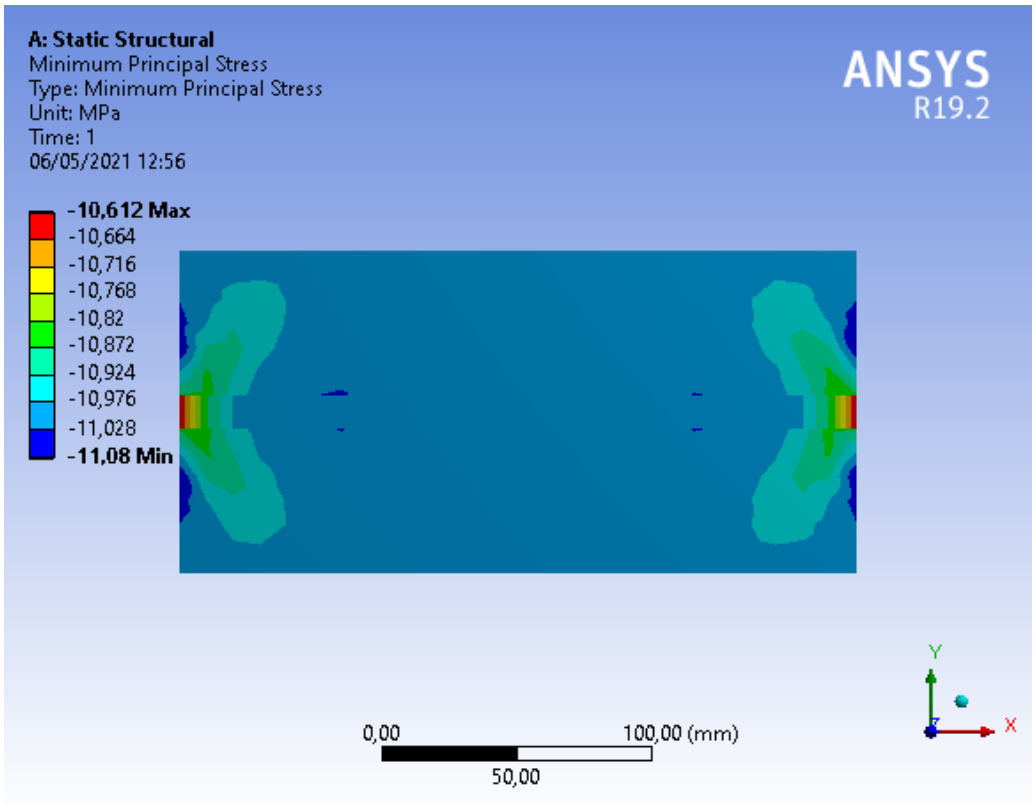

Figure 7.18: Compressive strength of MW masonry model

Comparing the MW values, Berndt values and the defined design values of Eurocode 6 with the test results are in the Table 7.6.

Table 7.8; Results of compressive strength of masonry compared to Menetery William model.

Test [Reference	Test 1	MW model 2	Berndt 3	Euro code 4	% error 1 &2	% error 2 &3	% error 2 &4
MU1 [Binda]	11	11.08	8.7	5.19	0.722	21.48	53.159

Here, we can observe that the model results are very close to the experimental result, only 0.525% error in extended Drucker Prager yield cap model and 0.722% error in Menetery Willian therefore the model is validated since the error are very small.

8. CONCLUSION AND RECOMMENDATION

The change in mechanical behavior of mortar from a brittle material in simple uniaxial compression to an elasto-plastic structure in triaxial compression has been demonstrated experimentally and analytically. Additionally, the adhering change of failure mechanism from the occurrence of diagonal shear bands, attributed to the formation of many interacting vertical cracks forming the shear bands, to a mere pore collapse of the internal structure is observed as well. A theoretical approach, based upon the initiation of the network of vertical cracks within the shear bands, tends to confirm the observed value of κ at which the change in failure mechanism is observed experimentally.

The initial presence of a shear failure mechanism puts forward the use of a non-associated Mohr-Coulomb or Drucker-Prager failure criterion, while the changes in pore structure could probably be modelled with an alteration of the parameters, due to an increase in damage, of the description of the mortar as a cohesive-frictional material. The elaboration of such a material model is foreseen in the near future. The confrontation of such a material model within a FEM-model of the composite masonry structure with a series of test results on the development of the strains and stresses within single leaf masonry walls, which are currently being processed, will be useful to understand the development of the elastic and plastic deformation of the composite structure. Hence, a better understanding of the mechanical behavior of historic masonry structures will be gained.

In this study, energy criteria method has been developed to calculate the cracking strength and the failure mode of masonry under compression and tension. It starts with reviewing and comparing available codes and research approaches dealing with compression behavior of masonry. All these approaches assume deformation properties of mortar higher than that of brick. In the numerical example, we can notice that the formula for cracking strength tends to give an accurate result better than research previous models.

The discontinuous method, extended Finite Element Method, could show how the failure occurs in its components and how stresses are redistributed in them after cracking. This method has been used to show the crack growth in the components of the masonry during the failure. The description of the compressive strength of masonry structure depends on the mechanical and geometrical properties of its components, the units, and the mortar. The more precise the description of the masonry component, the more precise is the result of the compression strength of masonry. Axial compression of masonry leads to three axial compression stress states in the mortar when the deformation properties of mortar are greater than those of the unit. Until now the used function to describe the mortar behavior is the classical Drucker-Prager yield function. A new model, the Extended

Recommending for further research is to verify the proposed formula in chapter 6 with further experimental tests, and numerical modeling with different mechanical and geometrical parameters of masonry components. This is additional to tests studying the three axial material behavior of porous masonry under compression-tensile-tensile stress state. The effect of long-term behavior of masonry components, like creep, could also be a subject for further research, since it may lead to reduce the transversal tensile stress peaks in the unit, leading to higher compression strength of masonry structure as a whole. The future research is to study Numerical implementation of phase field model for fracture.

A.1. Appendix

Drucker Prager cap function with Drucker-Prager yield-strength parameters for ANSYS APDL

```
/COM, Structural       !Preferences
/PREP7
!Stress in MPa
!Elastic modulus !MPa
!pressure !MPa
!distance !mm

!  Define the material properties !Material 1
!element defination
ET,1,182
!Element behavior
KEYOPT,1,3,3 !plane stress with thickness
!Real constant
R,1,100,

!  Define the material model(Modified drucker Prager Cap model)
mp,EX,1,4865
mp,PRXY,1,0.2

! Cap yield function
tb,edp ,1,1,,cyfun        !Material 1, Temperature 1
tbdata,1,7                        ! Rc
tbdata,2,1                        ! Rt
tbdata,3,-7.5                     ! Xi
tbdata,4,0.0005                   ! SIGMA
tbdata,5,0.000007                 ! B
tbdata,6,0.0001                   ! A
tbdata,7,0.057704                 ! ALPHA
tbdata,8,0.9                      !PSI

! Define hardening for cap-compaction portion.
```

```
tbdata,9,0.143                    !W1c
tbdata,10,0.03                    !D1c
tbdata,11,-0.00005                !D2c

! Cap plastic flow potential function
tb,edp ,1,1,,cfpot
tbdata,1,2                        ! RC
tbdata,2,1.5                      ! RT
tbdata,3,0.001                    ! B
tbdata,4,0.05                     ! ALPHA

! Base Drucker-Prager concrete  !Material 1
Rc=26.9          ! uniaxial compressive strength
Rt=3.7           ! uniaxial tensile strength
Rb=32            ! biaxial compressive strength
delta_t=0.25     ! dilatancy factor tension
delta_c=1.0      ! dilatancy factor compression

! Linear hardening/softening  !Material 1
kappa_cm=0.007
kappa_cr=0.01
omega_ci=0.33
omega_cr=0.2
kappa_tr=0.002
omega_tr=0.2
TB,CONCR,1,,,DP
TBDATA,1,Rc,Rt,Rb
TB,CONCR,1,,,DILA
TBDATA,1,delta_t,delta_c
TB,CONCR,1,,,HSD6
TBDATA,1,kappa_cm,kappa_cr,omega_ci,omega_cr,kappa_tr,omega_tr

!  Define the material properties !Material 2
!element defination
```

```
ET,2,182
!Element behavior
KEYOPT,2,3,3 !plane stress with thickness
!Real constant
R,2,100,

!  Define the material model(Modified drucker Prager Cap model)
mp,EX,2,1178
mp,PRXY,2,0.15

! Cap yield function
tb,edp ,2,1,,cyfun        !Material 2, Temperature 1
tbdata,1,7                !Rc
tbdata,2,1                !Rt
tbdata,3,-7.5             !Xi
tbdata,4,1                !SIGMA
tbdata,5,0.931            !B
tbdata,6,0.0001           !A
tbdata,7,0.0578           !ALPHA
tbdata,8,0.9              !PSI

! Define hardening for cap-compaction portion.
tbdata,9,0.052            !W1c
tbdata,10,0.076           !D1c
tbdata,11,-0.0000         !D2c

! Cap plastic flow potential function
tb,edp ,2,1,,cfpot
tbdata,1,2                ! RC
tbdata,2,1.5              ! RT
tbdata,3,0.001            ! B
tbdata,4,0.05             ! ALPHA

! Base Drucker-Prager concrete !Material 2
```

```
Rc=22                    ! uniaxial compressive strength
Rt=1.9                   ! uniaxial tensile strength
Rb=24                    ! biaxial compressive strength
delta_t=0.25            ! dilatancy factor tension
delta_c=1.0             ! dilatancy factor compression

! Linear hardening/softening  !Material 2
kappa_cm=0.0005
kappa_cr=0.012
omega_ci=0.33
omega_cr=0.1
kappa_tr=0.002
omega_tr=0.2
TB,CONCR,2,,,DP
TBDATA,1,Rc,Rt,Rb
TB,CONCR,2,,,DILA
TBDATA,1,delta_t,delta_c
TB,CONCR,2,,,HSD6
TBDATA,1,kappa_cm,kappa_cr,omega_ci,omega_cr,kappa_tr,omega_tr

!  Define the material properties !Material 3
!element defination
ET,3,182
!Element behavior
KEYOPT,3,3,3 !plane stress with thickness
!Real constant
R,3,100,

!  Define the material model (Modified drucker Prager Cap model)
mp,EX,3,4865
mp,PRXY,3,0.2
! Cap yield function
tb,edp ,3,1,,cyfun        !Material 3, Temperature 1
tbdata,1,7                  ! Rc
```

```
tbdata,2,1                !Rt
tbdata,3,-7.5             !Xi
tbdata,4,0.0005           !SIGMA
tbdata,5,0.000007         !B
tbdata,6,0.0001           !A
tbdata,7,0.057704         !ALPHA
tbdata,8,0.9 !PSI
! Define hardening for cap-compaction portion.
tbdata,9,0.143            !W1c
tbdata,10,0.03            !D1c
tbdata,11,-0.00005        !D2c

! Cap plastic flow potential function
tb,edp ,3,1,,cfpot
tbdata,1,2                ! RC
tbdata,2,1.5              ! RT
tbdata,3,0.001            ! B
tbdata,4,0.05             ! ALPHA

! Base Drucker-Prager concrete  !Material 3
Rc=26.9                   ! uniaxial compressive strength
Rt=3.7                    ! uniaxial tensile strength
Rb=32                     ! biaxial compressive strength
delta_t=0.25              ! dilatancy factor tension
delta_c=1.0               ! dilatancy factor compression

! Linear hardening/softening  !Material 3
kappa_cm=0.007
kappa_cr=0.01
omega_ci=0.33
omega_cr=0.2
kappa_tr=0.002
omega_tr=0.2
TB,CONCR,3,,,DP
```

```
TBDATA,1,Rc,Rt,Rb

TB,CONCR,3,,,DILA
TBDATA,1,delta_t,delta_c
TB,CONCR,3,,,HSD6
TBDATA,1,kappa_cm,kappa_cr,omega_ci,omega_cr,kappa_tr,omega_tr

!Create area
BLC4,0,0,150,100
BLC4,0,100,150,20
BLC4,0,120,150,100
!Merge items    !keypoints
NUMMRG,KP, , , ,LOW

!  Generate Mesh
ESIZE,10
TYPE,1
MAT,1,2,3
AMESH,1
AMESH,2
AMESH,3
ALLSEL
FINISH

!solution mode
/solu
!Boundary conditions
DL,1,1,ALL,0
EPLOT
ALLSEL

/SOLU
!Boundary conditions
DL,1,1,ALL,0
```

```
EPLOT
ALLSEL
pressure1=10
SFL,11,PRES,pressure1
ANTYPE,0                ! 0 is for static analysis
NROPT,AUTO
outres,all,all          ! Write all output
ALLSEL
TIME,1
SOLVE
FINISH
/POST1
```

Menetrey-Willam brick Formulation for ANSYS APDL

```
! base Menetrey-Willam concrete !Material 1

Rc=26.9! uniaxial compressive strength

Rt=3.7! uniaxial tensile strength

Rb=30.6! biaxial compressive strength

psi=10! dilatancy angle

! linear hardening softening

kappa_cm=0.007

kappa_cr=0.01

omega_ci=0.33

omega_cr=0.1

kappa_tr=0.002

omega_tr=0.2

TB,CONCRETE,1,,,MW

TBDATA,1,Rc,Rt,Rb

TB,CONCRETE,1,,,DILA
```

```
TBDATA,1,psi

TB,CONCRETE,1,,,HSD6

TBDATA,1,kappa_cm,kappa_cr,omega_ci,omega_cr,kappa_tr,omega_tr
```

Menetrey-Willam mortar Formulation for ANSYS APDL

```
! base Menetrey-Willam concrete! Material 2

Rc=22! uniaxial compressive strength

Rt=1.9! uniaxial tensile strength

Rb=24! biaxial compressive strength

psi=10! dilatancy angle

! linear hardening softening

kappa_cm=0.005

kappa_cr=0.012

omega_ci=0.33

omega_cr=0.1

kappa_tr=0.002

omega_tr=0.2

TB,CONCRETE,2,,,MW

TBDATA,1,Rc,Rt,Rb

TB,CONCRETE,2,,,DILA

TBDATA,1,psi

TB,CONCRETE,2,,,HSD6

TBDATA,1,kappa_cm,kappa_cr,omega_ci,omega_cr,kappa_tr,omega_tr
```

Reference

ACI 530.1-02. (2004). ACI 530.1-02, in ACI 530.1-02: Commentary on specification for masonry structures, Manual of concrete practice:

American Society for Testing and Materials. Part 12: "Chemical-Resistant Nonmetallic Materials; Clay and Concrete Pipe and Tile; Masonry Mortars and Units; Abestos-Cement Products; Natural Building Stones," Book of ASTM Standards, 1967.

American Society for Testing and Materials. Part 9: "Cement; Lime; Gypsum," Book of ASTM Standards, 1967.

American Society for Testing and Materials. Part 10: "Concrete and Mineral Aggreg ates," Book of ASTM Standards, 1967.

Backes. (1985). On the behavior of masonry under tension in the direction of the bed joints (in German). Dissertation, Aachen University of Technology.

Barbosa, C. S., Lourenço, P. B., Mohamad, G., & Hanai, J. B. (2007). Triaxial compression tests on bedding mortar samples looking at confinement effect analysis. http://repositorium.sdum.uminho.pt/

Basha, S., & Kaushik, H. (2014). Non-linear Behavior of Weak Brick-Strong Mortar Masonry in Compression (p. 2433).

Bazant, Z. P. (2014). Fracture Mechanics of Concrete Structures: Proceedings of the First International Conference on Fracture Mechanics of Concrete Structures (FraMCoS1), held at Beaver Run Resort, Breckenridge, Colorado, USA, 1-5 June 1992. (1st ed.). CRC Press. https://doi.org/10.1201/9781482286847

Berndt. (1996). Zur Druck- und Schubfestigkeit von Mauerwerk—Experimentell nachgewiesen an Strukturen aus Elbsandstein. Bautechnik, 73 (1996), Heft 4, pp. 222-234. (pp. 222-234.).

Binda, Fontana, & Frigerio. (1988). Mechanical Behaviour of Brick Masonries Derived from Unit and Mortar Characteristics. In 8th IBMaC.

Brencich, A, A., & Gambarotta, L. (2005). Mechanical response of solid clay brickwork under eccentric loading. Part I: unreinforced masonry. Materials and Structures, RILEM, 38 (pp. 257-266.).

Campbell, J., & Durán, M. (2017). Numerical model for nonlinear analysis of masonry walls. Revista de La Construcción, 16, 189–201. https://doi.org/10.7764/RDLC.16.2.189.

Carol, I., López, C., M., & Roa, O. (2001). Micromechanical analysis of quasibrittle materials using fracture-based interface elements. International Journal of Numerical Methods in Engineering, 52, pp. (pp. 193-215.).

Cundall, P. (1971). A computer model for simulating progressive, large-scale movements in blocky rock systems. In Symposium International Society Rock Mechanics.

DIN 1053-1. (1996). DIN 1053-1, in Mauerwerk—Teil 1: Berechnung und Ausführung. DIN Deutsches Institut für Normung e. V.

DIN 1053-3. (1990). DIN 1053-3, in Mauerwerk; Bewehrtes Mauerwerk; Berechnung und Ausführung. DIN Deutsches Institut für Normung e. V.

DIN 1053-100. (2007). DIN 1053-100, in Mauerwerk—Teil 100: Berechnung auf der Grundlage des semiprobabilistischen Sicherheitskonzepts. DIN Deutsches Institut für Normung e. V.

DIN EN 1996-1-1, Eurocode 6:1-1. (2013). DIN EN 1996-1-1, Eurocode 6:1-1, in Eurocode 6: Design of masonry structures – Part 1-1: General rules for reinforced and unreinforced masonry structures; German version EN 1996-1-1:2005+A1:2012. DIN Deutsches Institut für Normung e. V.:

Diihrkop, Saretok, Sneck, and Svendsen: "Bruk-Murning-Putsning." (Mortar-Masonry-Plastering.) National Swedish Council for Building Research, Stockholm, 1966.

Hayen, R., Balen, K. V., & Gemert, D. (2003). The mechanical behaviour of mortars in triaxial compression. Undefined. /paper/The-mechanical-behaviour-of-mortars-in-triaxial-Hayen-Balen/27a06fdc3ee80f28b2aee2a86cbf0e1a9cf8825b

Hayen, R., Balen, K. V., & Gemert, D. V. (n.d.). THE MECHANICAL BEHAVIOUR OF MORTARS IN TRIAXIAL COMPRESSION. 10.

Hayen, R.; Van Balen, K. & Van Gemert, D.: (2004). The mechanical behaviour of mortars in triaxial compression in cimne, Barcelona, 2004, Arch Bridges.

Hendrickx, R. L. (2010). Observation of the failure mechanism of brick masonry doublets with cement and lime mortars by microfocus X-ray computed tomography. In: Proc. Of 8th International Masonry Conference, eds. W. Jäger, B. Haseltine, and A. Fried, ARGE 8IMC Dresden 2010 Prof. Wolfram Jäger & International Masonry Society.

Hillerborg, A., Modéer, M., & Petersson, P.-E. (n.d.). Analysis of crack formation and crack growth in concrete by means of fracture mechanics and finite elements. Cement and Concrete Research, 6(6), 773–781.

Hilsdorf. (1965). Untersuchungen über die Grundlagen der Mauerwerksfestigkeit. Materialprüfungsamt für das Bauwesen der Technischen Hochschule München:

Hilsdorf, H. K. (1969). Investigation into the Failure Mechanism of Brick Masonry Loaded in Axial Compression. 34–41.

Hogberg, Erik: "Mortar Bond." National Swedish Institute for Building Research, Report No. 40, Stockholm, 1967.

Huster. (2000). Tragverhalten von einschaligem Natursteinmauerwerk unter zentrischer Druckbeanspruchung. Dissertation, Fachbereich Bauingenieurwesen der Universität Gesamthochschule Kassel:

Ingraffea, A., R., & Saouma, V. E. (1985). Numerical modelling of discrete crack propagation in reinforced and plain concrete. Fracture Mechanics of Concrete, eds.,

Kaushik, H. B., Rai, D. C., & Jain, S. K. (2007). Stress-Strain Characteristics of Clay Brick Masonry under Uniaxial Compression. Journal of Materials in Civil Engineering, 19(9), 728–739. https://doi.org/10.1061/(ASCE)0899-1561(2007)19:9(728)

Kenan, M. M. (2012). Faiilure behaviior of masonry under compressiion based on numeriical and analytiical modeliing; phd thesis.

Kendall, K. (2008). Complexities of Compression Failure. 20.

Kohees, M., Sanjayan, J., & Rajeev, P. (2019). Stress-strain relationship of cement mortar under triaxial compression. Construction and Building Materials, 220, 456–463. https://doi.org/10.1016/j.conbuildmat.2019.05.146.

Lotfi, H., & Shing, P. (1994). Interface model applied to fracture of masonry structures. Journal of Structural Engineering, ASCE, 120 (1994), (pp. 63-80.).

Lourenco. (2004). Structural masonry analysis: Recent developments and prospects.

Lourenco, P. (1996). Computational Strategy for Masonry Structures.

Lourenco, P.B., P. B., & Rots, J. G. (1997). &: A multi-surface interface model for the analysis of masonry structures. Journal of Engineering Mechanics, ASCE, 123 (1997), pp. 660-668.

Mohamad, G., Fonseca, F. S., Vermeltfoort, A. T., & Lubeck, A. (2018). Stiffness plasticity degradation of masonry mortar under compression: Preliminar results. Revista IBRACON de Estruturas e Materiais, 11(2), 279–295. https://doi.org/10.1590/s1983-4195201800020004

Murphy, Glenn: "Properties of Engineering Materials," 2nd edition. International Textbook Company, Scranton, Pennsylvania, 1947.

NELISSEN, L. J. M. (1972). Biaxial testing of normal concrete. Heron, 18, p. (pp. 3–90).

Neville, Alan M.: "Properties of Concrete." John Wiley & Sons, New York, 1963

Palmer, L. A., and Parsons, D. A.: "Permeability Tests of 8-in. Brick Wallettes." ASTM Proceedings, Vol. 34, Part II,

p. 419, Washington, 1934.

Petersson. (1981). Crack growth and development of fracture zones in plain concrete and similar nTaterials, Report TVBM-1007, Lund Institute of Technology, 17 4 pp.

Rocco, C. & Roselló. (2008). Cohesive crack modelling of a simple concrete: Experimental and numerical results.

Roman, H., R., & Gomes, I., R. (2004). Numerical modeling of blockwork prisms tested in compression using the finite element method with interface behaviour. In 13th International Brick/Block Masonry Conference. 2004. Amsterdam, The Netherlands.

Rots, J. G. (1988). in Computational Modelling of Concrete Fracture, PhD thesis. Delft University of Technology, The Netherlands.

Sacco, E., & Toti, J. (2010). Interface Elements for the Analysis of Masonry Structures. International Journal for Computational Methods in Engineering Science and Mechanics, 11(6), 354–373. https://doi.org/10.1080/15502287.2010.516793

Sahlin, S. (1971). Structural masonry. Prentice-Hall.

Shi, G. (1988). Discontinuous Deformation Analysis—A New Numerical Model for the Statics and Dynamics of Block Systems, PhD thesis. University of California: Berkeley, USA 1988.

Sotirios, V.-T., & Dimitris, T. (n.d.). Failure Mechanisms and Analysis for Historic Masonry. 1.

Tammam, B. (2012). Failure models of Masonry under compression.

Van der Pluijm, R. (1999). Out-of-Plane Bending of Masonry—Behaviour and Strength." 1999.

Zucchini, A., & Lourenço, P. B. (2007). Mechanics of masonry in compression: Results from a homogenisation approach. Computers & Structures, 85(3–4), 193–204. https://doi.org/10.1016/j.compstruc.2006.08.054